Universitat Autònoma de Barcelona

Computer Graphics and Vision Techniques for the Study of the Muscular Fiber Architecture of the Myocardium

A dissertation submitted by **Fernando Poveda Abansés** at Universitat Autònoma de Barcelona to fulfil the degree of **Doctor en Informàtica**.

Bellaterra, September 2013

Director: **Dr. Enric Martí-Godia**
Universitat Autònoma de Barcelona
Dep. Ciències de la Computació
Co-director: **Dra. Debora Gil Alsina**
Universitat Autònoma de Barcelona
Dep. Ciències de la Computació & Computer Vision Center

Universitat Autònoma de Barcelona

This document was typeset by the author using LaTeX 2_ε.

The research described in this book was carried out at the Dept. Ciències de la Computació, Universitat Autònoma de Barcelona.

ISBN TBD

Printed by TBD

"The last ever dolphin message was misinterpreted as a surprisingly sophisticated attempt to do a double-backwards-somersault through a hoop whilst whistling the 'Star Spangled Banner', but in fact the message was this: So long and thanks for all the fish."

The Hitchhiker's Guide to the Galaxy
Douglas Adams

Acknowledgment

At some unspecified time in the vicinity of 2008 a group of 5 people kickstarted an interesting change in my live. Abraham Martín, Carlos Martinez, Xavier Jurado, Gerard Suades, and Enric Martí where my four new colleagues and professor of the Computer Graphics course of my Engineering degree studies. Plunged in their endless enthusiasm I decided to target my life towards a PhD degree in CG. Thank you all for that unexpected twist. Later on, Enric Martí himself was the person who made possible my will to enter in this postgraduate. Without him I would likely not be here. And I would certainly have not had such a good time. No much later on this journey, Debora Gil joined Enric as my co-director. She brought invaluable help, knowledge and guidance. Really. Invaluable. Even though I might have looked a little bit rebel to her, I admire all her talent and passion. Thank you for sharing all that with me, and for your patience! And I will not forget to thank all my contributors and coauthors Jaume Garcia, Albert Andaluz, Francesc Carreras, and Manel Ballester. My most sincere gratitude to you. More people have participated in this adventure (incredible right?). First, my office mate Antoni Gurguí. Almost from the beginning of my PhD we shared a lot priceless time drinking coffees and beers, embroiled in the most interesting philosophical and philotechnical disquisitions, research questions, creative wednesdays, unreadable codes, doctorate fears and desperations, and endless Internet randomness. Ending this degree means leaving him behind, but I ll be there for him even if I am right in the other end of the world ;) Hope we meet again soon. Otherwise, tota la culpa és del Toni . Second, I also would like to remember a lot of amazing people I had the opportunity to met and share time with during this period. Inside or outside the academia... Jorge, Cesc, Jon, Pil, Monti, Javi, Mena, Roger, Xen, Miki, Edu, Patu, Frans, Marta, Nadia, Mercè, Marta, Chema, Willy, Arnau, Carmen, Carlos, Charlie... well, I cannot name them all. I would need another dissertation. Anyway, Thank You. Third, another important piece of everything I do will always be my parents. You are always there, always supportive, always loving. If there is an axiomatic root of all this... it is you. And last, not another reason of me finishing this work... just The Reason. Without Helena Vilaplana I think I would have lost my patience many times in the unceasing visits to the valley of shit [1]. However, she always gave me the best guidance, she cheered me no matter how hard I got locked. Although I might have seen constantly in distress, you made me enjoy every minute of this venture with your irreplaceable company.

[1] Mandatory reading for PhD students:
http://thesiswhisperer.com/2012/05/08/the-valley-of-shit/

Abstract

Deep understanding of myocardial structure linking morphology and function of the heart would unravel crucial knowledge for medical and surgical clinical procedures and studies. Several clinically procured conceptual models of myocardial fiber organization have been proposed, but the lack of an automatic and objective methodology prevented an agreement. Even with the use of objective measures from modern imaging techniques as Diffusion Tensor Magnetic Resonance Imaging (DT-MRI) no consensus about myocardial architecture has been achieved so far. Reconstruction of this data by means of streamlining has been established as a reference technique for representing cardiac architecture. It provides automatic and objective reconstructions at low level of detail, but falls short to give abstract global interpretations. In this thesis, we present a set of novel multi-resolution techniques applied as a methodology able to produce simplified representations of cardiac architecture in combination with improved streamlining techniques tailored for this environment. Besides, we have contributed a complete validation framework that goes from local analysis of pre-processing methods applied to DT-MRI data, to global analysis of tractographic reconstructions in the multi-resolution framework. This validation is both based on the quantification of anatomical coherence of muscular tissues and reconstruction confidence based on the same principle. We performed experiments of reconstruction of unsegmented DT-MRI canine heart datasets coming from the public database of the Johns Hopkins University. Our approach produces reduced set of tracts that are representative of the main geometric features of myocardial anatomical structure. This methodology and evaluation allowed the obtention of validated representations of the main geometric features of the fiber tracts, making easier to decipher the main properties of the architectural organization of the heart. Fiber geometry is preserved along reductions, which validates the simplified model for interpretation of cardiac architecture. On the analysis of the output from our graphic representations we found correlation with low-level details of myocardial architecture, but also with the more abstract conceptualization of a continuous helical ventricular myocardial fiber array. Objective analysis of myocardial architecture by an automated method, including the entire myocardium and using several 3D levels of complexity, reveals a continuous helical myocardial fiber arrangement of both right and left ventricles, supporting the anatomical model of the helical ventricular myocardial band (HVMB) described by Dr. F. Torrent-Guasp.

Contents

List of Tables

List of Figures

Chapter 1

Motivation

It is the pervading law of all things organic and inorganic, of all things physical and metaphysical, of all things human and all things superhuman, of all true manifestations of the head, of the heart, of the soul, that the life is recognizable in its expression, that form ever follows function. This is the law.

Louis H. Sullivan
The tall office building artistically considered.
Lippincott's Magazine. 1896.

Both heart s form and function have raised interest and curiosity from a wide range of disciplines along the human history, apart from medicine or natural sciences. The etymology of the word in most languages leads us predominantly to a synonymy with center , essence , and even source of emotions . Renaissance artist and intellectual Leonardo da Vinci also succumbed to the fascination of this barely unknown organ, and provided physiological interpretation [63] as well as several illustrations that were the first naturalistic representations of the heart (Fig. 1.1). Even the father of modern philosophy , René Descartes, wrote about the action of the heart and its relation to blood and circulation (and to its ceasing at death) following and giving prominence to the theses of the renowned physician William Harvey [45].

All this fascination lies in its real complexity and importance. The heart is the vital muscular organ in charge of pumping blood to the whole body of all animals with circulatory system. It is in charge of moving approximately 7000 liters of blood to all the tissues in an average human body per day. That is the result of about 120 thousand contractions in a normal day. Only about 300 grams of muscle are *the heart* of the cardiovascular system, responsible of the distribution of nutrients, oxygen, hormones, etc. These supplies account for all the necessary elements for cellular metabolism and therefore, maintain the whole organism alive. But more surprisingly, all this work is performed by *myogenic* function (independent and involuntary activation).

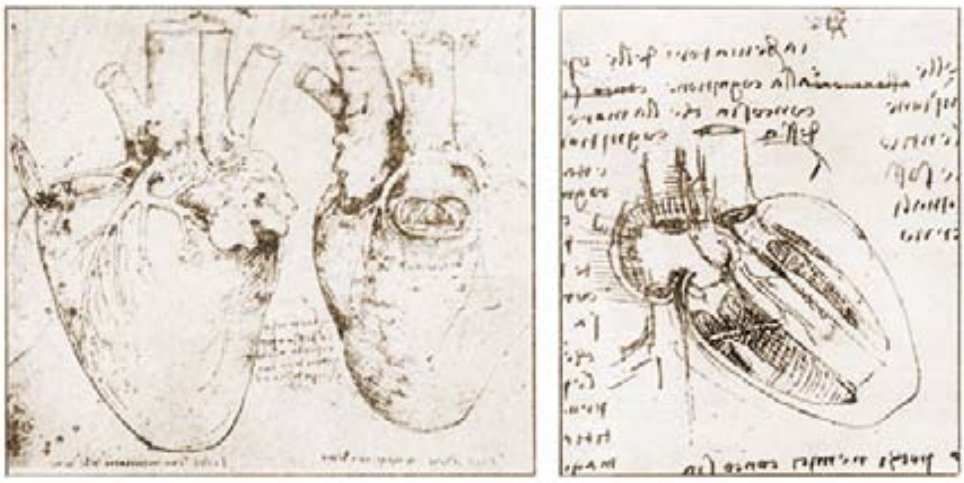

Figure 1.1: Naturalistic drawings of the external anatomy of the heart including coronary arteries and its relation to the pulmonary artery (left). Anterior view of a heart dissection showing ventricular cavities with full detail (right). Both drawn by Leonardo DaVinci on his manuscripts of anatomical exploration. Images adapted from [63].

Everything must work properly at any time to assure the correct function to meet the cardiovascular system needs. The smallest error can lead to serious problems all over the body, and even cause death.

1.1 Relevance of cardiovascular diseases

Recent studies from the Spanish Statistical Institute [57] point that 31,2% of 2009's mortality rate was directly related to cardiovascular diseases. This index is worrying taking into account that it is a yearly increasing index. But it can be even more significant with an European contextualization. A study of the Eurostat (European Statistics Office) [26] indicates that Spain has one of the lowest mortality indexes related to cardiovascular diseases in Europe. In addition to that, it is necessary to point that these studies also show that approximately 65% are directly derived from heart conditions rather than conditions on the rest of circulatory system. From a wider point of view, according to the World Health Organization (WHO), the first leading cause of death is the ischaemic heart disease, affecting both high-income and low-income countries [1]. It is important to the extreme that every year more people die from a cardiovascular related disease than for any other reason. The WHO also estimates that 23 million people will die every day from cardio vascular diseases by 2030.

Moreover, heart failure[1] is known to lead to more frequent hospitalizations, whose causes are often non-cardiac [49]. Heart failure leads to impaired quality of life and shortened life expectancy [101]. Besides, it is noteworthy that an increasing inability to meet the metabolic requirements of end organs or muscles has recently been associated to a greater risk of cancer [49].

Clinically speaking, cardiovascular study is an important area to focus further research in order to reduce the mortality risk among the population.

1.2 Myocardial architecture

It is widely accepted that myocardial muscular architecture plays a critical role in key functional aspects such as the electrical propagation [97, 112] and force production [68], as well as in other important cardiac requirements as perfusion[2] and oxygen consumption of myocardial tissues [54].

It is also a well known fact that the myocardium may undergo **architectural alterations in many heart diseases**. For example, in *dilated cardiomyopathy* (DCM) the heart suffers an hypertrophic remodelling of its muscle and losses its characteristic hemielliptic shape, which leads to reduced ejection fraction[3], an inefficient blood pumping. *Cardiac ischemia* is also known to cause muscular modifications. In this situation, cardiac tissues receive insufficient (up to deprivation) blood flow causing a deficiency of oxygen and glucose necessary for the cellular metabolism. As a result of a significative blood restriction, tissue cannot be kept alive, resulting in muscular degeneration. In order to address some myocardial conditions that imply these muscular alterations, surgical restorative procedures were proposed as a non-transplant option in the past [8]. However, they are currently in the doldrums, criticised for neglecting biological principles of the muscular tissue, and above all, its architecture, leading to a known impairing of heart pumping performance [118]. Better knowledge of the cardiac muscle anatomy could prompt new options [116] (or reinforce already proposed ones) for surgical ventricular restorative procedures and deeper knowledge of these affections.

Efficient cardiac pumping also depends on **rhythmic and coordinated contraction and relaxation of myocardium**. Several heart conditions are tightly related to *arrythmogenesis*. Muscular disposition is accepted to be important in electrical propagation an thus to its function. In fact, muscular cells are known to be in charge of the initiation and propagation of electrical impulse through the tissue. Hence, the understanding of this phenomenon and its disorders must be coupled to muscular architecture [17, 106]. Similarly, *ventricular dyssynchrony* -in which the heart presents differences in contraction timings of ventricles- can also make the heart less effec-

[1] *Heart failure:* General term to cover several heart conditions that end up disabling or limiting the heart to procure blood to the body and satisfy its metabolic needs.

[2] *Perfusion:* Process of delivery and circulation of blood through biological tissues, allowing the necessary supply of oxygen and nutrients.

[3] *Ejection fraction:* Measure of volumetric fraction of blood pumped by either heart ventricles.

tive as a blood pump [76]. This condition highlights that electromechanical coupling could also be key for the particular and sensitive contraction patterns of the heart. Basic agreement of myocardial architecture could help to improve comprehension of electromechanical coupling for future diagnose and treatment of these myocardial conditions.

Defining, understanding, and treating **diastolic heart failure** is another open discussion for cardiologists. The heart pumps blood to the circulatory system, but it is known to produce suction force for blood intake. This cardiac period is generally described as a muscular relaxation that produces depression favouring (or simply accepting) refill by the momentum of blood from previous systole. However, some studies argue that diastolic function must be an active process to achieve efficient filling of the ventricles [115, 28, 118]. Taking into account that this principle has been correlated to an specific heart architecture, it is clear that a better architectural comprehension could bring key information for this open discussion as well.

1.3 Controversy

At this point, it is clear that knowledge about heart s structure would help to set the axioms that could help to better understand cardiac function in health and disease. Further, decoding functional and mechanical knowledge may even offer solutions to some ongoing clinical controversies as well as helping future diagnosis, therapy, and surgery planning. In fact, the study of muscular architecture of the heart has been a topic of special interest during almost 300 years. Uncountable thinkers and researchers have presented and discussed several conceptual models of cardiac architecture and function from a medical point of view. However, as we will discuss in detail in Chapter 2, the heart presents a distinctly complex architecture compared to the rest of the voluntary muscles, and so far, this inherent complexity have hindered an agreement about its form. With that in mind, the need to do this basic research on cardiology becames more clear since, so far, such an essential aspect of the specialty as the knowledge of the architectural formation of this organ can not be considered mature enough.

The architectural complexity of the myocardium comes not only at the macrostructural level, where scientists and doctors have appreciated notable tangling of the muscular mass. Somehow, it has its roots at the microscopical level where its heterogeneous distribution is prone to hinder the comprehension and interpretation of higher level morphologic patterns. These facts have led to an historical lack of consensus in the scientific community about the spatial distribution of myocardial cells that end up constituting the muscular anatomy of the heart. Further than that, the discussion about heart anatomy is still alive [22, 75, 12, 74, 2] due to the still existent difficulty to procure robust information to univocally interpret its structure. This difficulty has in turn prevented to find a universal definition of heart s muscular architecture that represents an agreement among all the researchers and experts in the field.

1.4 From dissection to computer aided modelling

Despite the thorough work in research to achieve a universally accepted myocardial anatomy model, major theories about this muscular architecture have been subject to criticism for its procedures. Some key anatomists on heart anatomy study have remarked their observation that the cardiac muscle is organized in a *syncytial* fashion[4] [93, 22, 5]. This leads to the conclusion that this complex microscopical architecture can probably difficult or even mislead the interpretation of visible muscular tracts used to define the muscular structure of the myocardium in most of the of the aforementioned clinical observations. Given this heterogeneity, many researchers like Lev and Simkins [70] and Grant [42] pointed that the interpretation of these tracts would be subjective to the surgeon on the dissection procedure, and could be done on several ways, leading to distinct interpretations. As a result, researchers could not univocally demonstrate the architecture of the myocardium. Grant [42] also proposed histologic[5] analysis as an objective alternative. This was rapidly and widely accepted, but it also presented strong drawbacks. Histology is a destructive technique. Sections of the analyzed hearts (slices of no more than 3 µm) have to be treated for further analysis. Its reconstruction is not possible because this slices acquire different properties (size, color, texture, etc.). In addition, this is usually a time-consuming and laborious task which may lead to instrumentalitation.

In conclusion, some researchers have shown their concerns on the definition of a myocardial model. Crisicione *et al.* mentioned that *"Like statistics and statisticians, one must be skeptical of models and their makers. Models have the potential to lead reasoning, and they have the potential to mislead it as well"* [22].

However, during the last decade, a new modality of Magnetic Resonance Imaging (MRI) called Diffusion Weighted MRI (DW-MRI) has enabled computational validation of biological structures including the myocardium (Fig. 1.2). This technique can provide a discrete measurement of the three-dimensional (3D) arrangement of myocytes [105] by the observation of local anisotropic diffusion of water molecules caused by biological structures such as cell membranes [85, 31].

There are several alternatives for water diffusion characterization techniques derived from DW-MRI. Among them, Diffusion Tensor MRI (DT-MRI) has been established as the reference imaging modality for the rapid measurement of the whole cardiac architecture (Fig. 1.2). It has brought the possibility to achieve objective representations of the heart muscle. To date, most research has focused on the reconstruction and representation of this tensor data through *tractography* (also known as *fiber tracking* in this area, or *streamlining* in its use for general description of vector fields) [7, 125, 51, 92, 99].(Fig. 1.2) *A grosso modo*, this technique represents spatial coherence of the tensor field information through the representation of curves defined by trajectories of particles dropped in this field (Fig. 1.2). The points where the particle is dropped are known as seed points. Tracking strategies may vary but in general

[4] *Syncytium*: A single biological mass with several nuclei result of cell fusion or subdivision of its nuclei.

[5] *Histology*: The study of the microscopic architecture of cells and tissues.

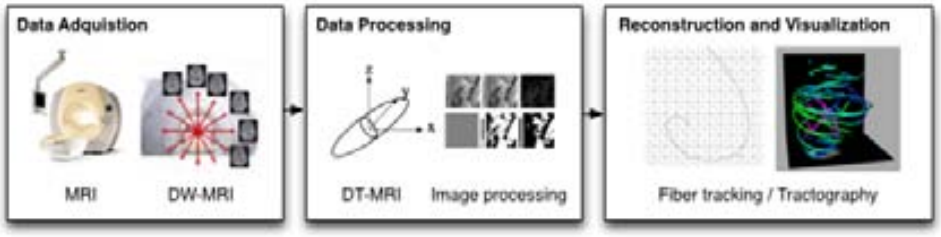

Figure 1.2: *From magnetic resonance to the computational representation of biological structures*: Magnetic resonance allows image adqusition modalities like DW-MRI that are able to measure diffusion of water in tissues like brain white matter or heart muscle. This data can be numerically characterized by a big variety of methods, among them DT-MRI that allows rapid and simple representation of principal structure. This information could in turn be processed by a variety of image processing methodologies. An straightforward example is its use for noise reduction. Finally, fiber tracking offers the possibility to represent complex structures underlying in biological tissues conforming organs like the heart and brain.

come from mathematical integration of loci[6] determined by DT-MRI most significant directions of water diffusion (denoted by the homologous eigenvector of the diffusion tensor).

Nevertheless, the use of tractographies has already presented general shortcomings for the anatomic study of the myocardium. Due to the high level of detail and entanglement of the myocardial anatomy, extraction of the global architecture of the heart is not feasible with an straightforward visual analysis. Proposed tractographic reconstructions present fully detailed representation of the anatomic formation of the heart and have proved their validity for low-level descriptions, but might fail on a higher level of analysis because of their inherent complexity. As a consequence, interpretation may still be biased. Besides, many techniques still face the challenges of having limited certainty of reconstruction, resulting from noise and assumptions introduced in the steps needed to get a final representation from data acquisition. In the case of DT-MRI, this includes some well known limitations to represent low level fiber singularities as crossing, concentration (flow sinks), and dispersion (flow sources). In consequence, streamline representations may generate false impression of precision that needs to be faced in order to obtain reliable reconstructions for anatomical interpretations of the heart.

1.5 Overview of this Thesis

Further than this introduction to the motivations of this work, the thesis is organized as follows:

[6] *Locus (pl. Loci):* Set of points whose coordinates satisfy certain algebraic conditions.

- In **Chapter 2** we provide a brief background on heart anatomy required for deeper comprehension of the problematic around the study and current controversy around anatomical formation of the myocardium. Besides, we provide an overview of the state of the art techniques that are the foundation for our research. This wide review will in turn set the perfect ground to present which are the main contributions of this work.

- **Chapters 3 and 4** include main theoretical contributions of this work. Firstly, focusing on the description of the multi-resolution tools proposed for reconstruction of DT-MRI. Secondly, centered on the definition of the necessary tools for validation of all processing of tensor volumes and tractographic reconstruction of myocardial architecture in the former multi-resolution framework.

- **Chapter 5** aggregates results from the main tools and techniques developed in this PhD. Moreover, we will present a thorough study of anatomical architecture that proves utility and applicability of our methodologies to the study of myocardial architecture.

- Finally, **Chapter 6** concludes this dissertation summarizing the achievements and limitations of our work as well as presenting new ideas and lines of research that may flourish from the foundation of this work.

Chapter 2

Architectural models of the myocardium

No man-made structure is designed like a heart. Considering the highly sophisticated engineering evidenced in the heart, it is not surprising that our understanding of it comes so slowly.

D. D. Streeter,
Gross morphology and fiber geometry of the heart.
Handbook of Physiology Volume 1: the Heart.
Am Physiol Soc. 1979

In this chapter we provide a brief background on heart anatomy (Section 2.1) required for deeper comprehension of the issues around the study and current controversies of the anatomical formation of the myocardium. In addition, we provide an overview of the state of the art computational techniques on the reconstruction and interpretations of the heart structure (Section 2.2) that are the foundation for our research. Finally, after reviewing current challenges in the former computational applications (Section 2.3) the main contributions of this thesis will be contextualized in Section 2.4.

2.1 Heart anatomy

In order to provide a useful guide of heart anatomy for the purpose of this PhD thesis, we will introduce a basic reference of concepts in three main points: We are going to start by defining the grosser anatomy, parts, and functions of the heart (2.1.1) necessary for further reference. After that, we will provide a closer look at microscopical anatomy of the ventricles (2.1.2). Finally, this section will close with an overview form the historical to contemporary interpretations of muscular architecture of the ventricles (2.1.3), which is the main motivation of our thesis.

2.1.1 Auricoventricular anatomy and function

The mammal heart is constituted by four cavities as shown in figure 2.1(a). These cavities are the *right atrium*, *left atrium*, *right ventricle* and *left ventricle*. Each atrium is separated of the homonymous ventricle by a valve which lets the blood in the auricle flow to the ventricle, but also forbids the inverse flow.

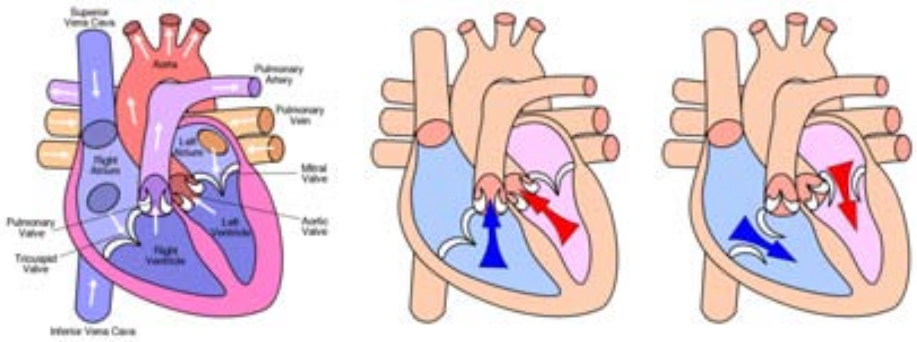

(a) (b) (c)

Figure 2.1: Structure diagram of the parts of the human heart (a). Diagram of systolic (b), and diastolic functions (c). Diagrams under CC BY-SA 3.0, Yaddah Wapcaplet.

The heart is divided on the called *left* and *right* sides because each of these sides works on a different circulation. The left side takes care of the *systemic circulation* which transports oxygenated blood arriving to the left atrium from the lungs via the *pulmonary veins*. Blood transfers to the left ventricle to be expelled through the *aorta* to the body. Separately, the right side deals with the *pulmonary circulation*. It transports the hypoxic blood flow coming from the *vena cava* to the left atrium, and expels it from the left ventricle to the lungs to be re-oxygenated. On both arteries (aorta and pulmonary) there are two valves to obstruct the blood return to the ventricles. The aforementioned circulation is completed with heart contractions (*systole* and *diastole* phases represented in the figures 2.1(b) and 2.1(c)) activated by complex and delicate electrical sequences organized to move the muscular tissue.

2.1.2 Microscopic anatomy of the myocardium

At a lower level, the myocardium is made by millions of muscular cells (cardiomyocytes) set in an intricate and extensive branching structure, also commonly described as a discrete myocytal mesh.

The cardiomyocyte is a rather unusual type of cell. It has an especially organized micro-structure consistent of long chains of myofibrils which are in turn constructed

by chains of sarcomeres, the contractile units of the cell. Individually, each of these cells presents a long and thin structure, resembling a cylindrical shape. It ranges from 50 to 100 µm long, and about 10 to 20 µm of diameter.

Myocytes are known to be coupled to an average of 11 neighbours. Almost half of those links are transverse (Fig. 2.2(a)), and the rest could be defined as end-to-end couplings. The first of the structuring elements of this tissue are the *intercalated discs* (Fig. 2.2(b)). The function of these discs is to support the synchronized contraction of the muscular tissue while keeping cell coupling during contraction and dilation of the heart. These structures also allow the spread of action potential (electric signal) between cells.

But the general structure of myocardial tissue is a little bit more complex. Historically, many heart anatomists have defined the heart as a syncytial mesh [43]. However, this mass of cells is more commonly seen as a functional (not true biological) syncytium [65]. The most accepted description of the micro-structure of this unique functional unit has different levels of organization (Figs. 2.2(c-d)) that commence at the *endomysium*. The endomysium is a collagenal[1] mesh that wraps muscular cells and supports intercalated discs. This interlacing mass is sometimes straightforwardly referred as a *weave* where we can find another level of structural arrangement. A clustering of endomysial weave forms the *perimysium* (Figs. 2.2(c-d)), which aggregates collections of myocytes and serves as a channel for blood vessels and nerves. These collections of myocytes have been demonstrated to present extensive local branchings as pictured in Figure 2.2(e). The branching and insertion angle between bundles is known to be acute, making close adjacent groups of cells run almost parallel to each other. Moreover, these branching groups have been observed to form sparse coupled laminar (*myolaminae*) structures (observed to be about 3 or 4 myocytes thick) that allow sliding or shifting between them during systole and diastole of the heart [68, 21] (Fig. 2.3). Finally, an external layer of collagenal tissue, known as *epimysium*, covers the whole organ. This structure has been defined as a reinforcement supporting the strong mechanical stress that myocardial cells are subjected to [4].

Despite the long established knowledge of this microscopical organization of the myocardium, researchers have disagreed about higher levels of interpretation of its architecture, beginning at the conceptualization of the *myocardial fibers*. The heart presents an heterogeneous formation, unlike the skeletal muscle (which has a highly structured anatomy). However, the previously defined arrangement of myocytes into bundles surrounded by the perimysium has been interpreted in the past as distinguishable anatomical organization and denominated as *myofibers*. These bundles are clearly noticeable on dissection of the myocardium as cleavage planes become visible (see Fig. 2.3) after removing the epimysium [80, 58, 4]. However, this definition has been seen by some experts as a *convenient description rather than an anatomical entity* [44] and has repeatedly been denoted as a potential source of subjectivity for further interpretation of the anatomical formation of the myocardium [70, 42].

Another stressed argument comes from the knowledge and interpretation of myolaminae (Fig. 2.3). Many researchers have extensively reported the existance of

[1] *Collagen:* Strong fibrous protein found in bone, cartilage, skin, and other connective tissues.

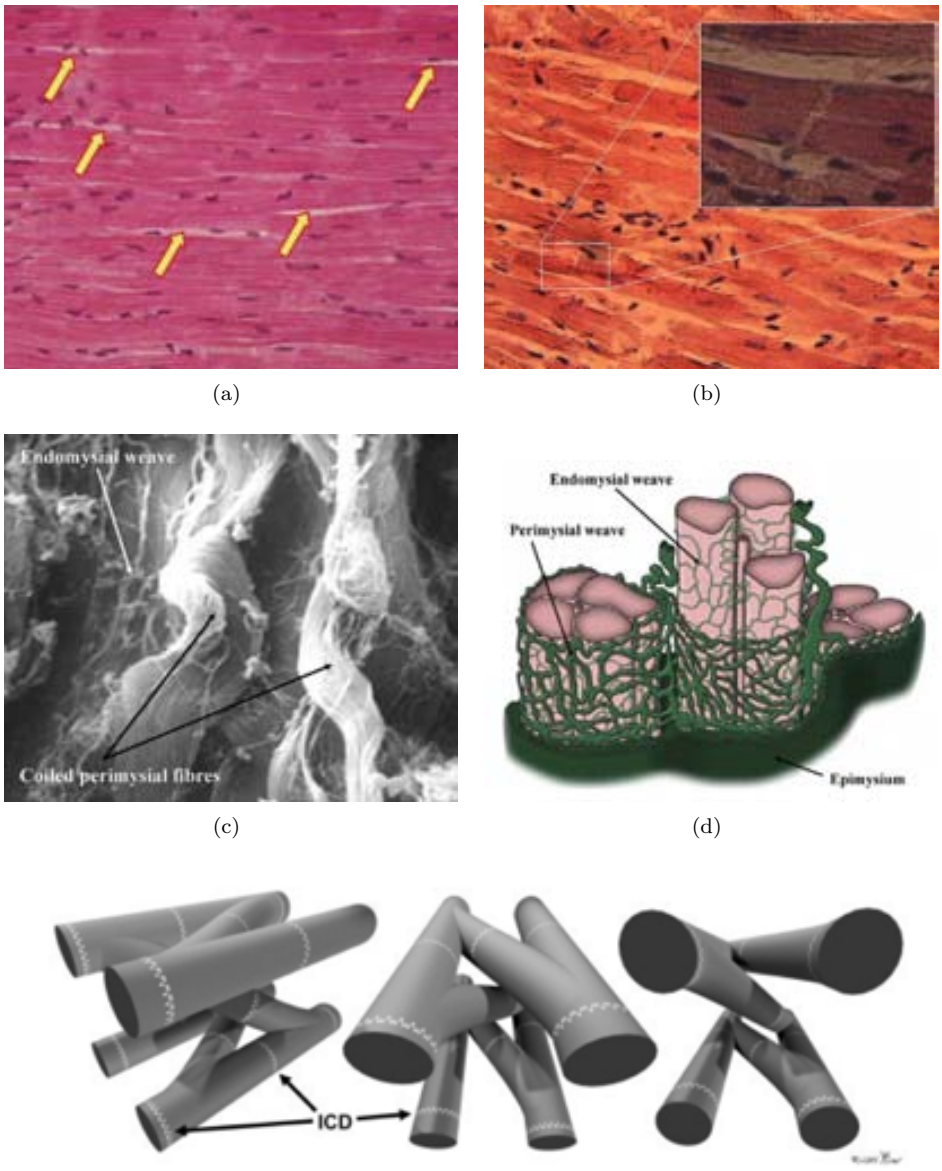

(a) (b) (c) (d) (e)

Figure 2.2: Images adapted or obtained from (a,c,d) from [4], (b) CC BY-SA 3.0, Dr. S. Girod and Anton Becker, and (e) from [6].

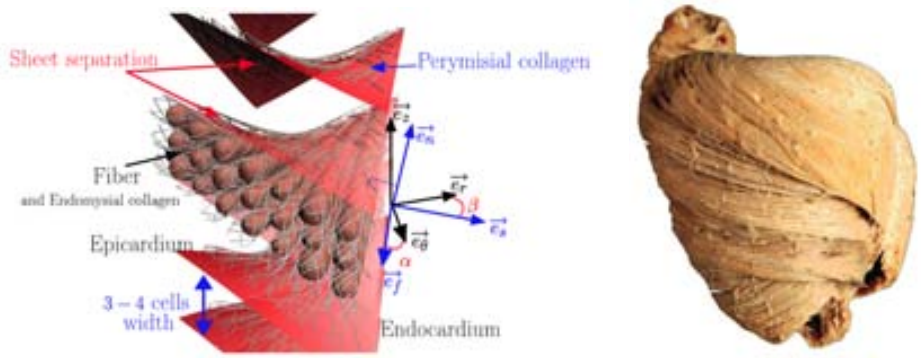

(a) (b)

Figure 2.3: Illustrative figures of the concept of myolaminae. (a) Diagram about the controversial laminar formation of myocardium from [99]. (b) Preparation of a porcine heart removing layers of its musculature in several stages from [5].

laminar formations in the heart muscle [93, 68, 21, 38]. And even more recently, has even been pointed out that a second local fiber layering orientation is also patent [**?**]. However, against previous affirmations, some works noticed that myolaminae seems to have highly discontinuous beginnings and endings throughout the whole myocardium [22]. This observation sets a precedent to argue against the concept of myocardial fibers [4].

An alternative reading of the microscopic ventricular myocardial architecture is based on shoulders of an understanding of the myocardium as more strict biological syncytial mesh [70, 42, 4, 22]. In this description, the myocardial wall is defined as a continuum of fibrous tissue with a unique function that describes a uniform structure within the myocardial wall. As it will be extensively described in Section 2.1.3, the supporters of concept define myocardial structure as a concentric circular organization of myocytes changing angulation at different depths within the myocardial wall.

Some renowned heart anatomists have described such continuity and organization in the past [111, 48], as well as the description of myocardial fibers and myolaminae being interrupted throughout the myocardium [48]. However, this "syncytial" interpretation of the myocardial structure has not generally been endorsed by the entire scientific community. It is broadly accepted that the myocardial micro-structure has well-defined general orientation patterns that could be used to understand myocardial anatomy. It has been widely stated that this stability defines pathways that yield to a reproducible and unique interpretation of the muscular architecture of the heart [111, 29]. At this point, we can soundly state that the scientific community seems to have agreed in the use of the statistical criterion of the predominant direction of myocytes at a given point to define architecture and functional anatomy of the myocardium. Nevertheless, they do not agree in the final structure of this intriguing organ.

2.1.3 Ventricular myocardial architecture

It is not until 1628, when William Harvey in his book "*Exercitatio Anatomica de Motu Cordis et Sanguinis in Animalibus*" described the heart acting as a blood pump on a closed circuit circulatory system. His work was widely recognized and consolidated basic knowledge about the systemic circulation. He also might have been the first anatomist to remark the potential functional significance of heart muscular fibers to its function. After him, in 1664, Nicolas Steno focused even more on the muscular contraction of the heart. He made the first descriptions of the muscle being a helical structure. From this point in history onwards, heart anatomists lived a vivid discussion for almost four hundred years about the architecture of this muscle.

Richard Lower was the first to recognize on a study of 1669 a more complete helicoidal structure [73] guided by its naked eye observation of the principal groups of cardiac muscular cells (Fig. 2.4(a)). In his study he described 2 groups of distinct layers. He defined the first layer as a continuous muscle from endocardium to epicardium, and he was the first to recognize that those musculatures where manifestly continuous creating a hole at the apex extreme. The second layer was defined by a progressive transverse musculature at mid-thickness of ventricular myocardium.

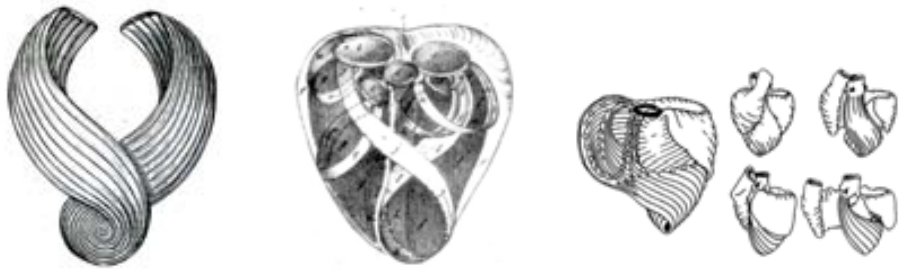

(a) (b) (c)

Figure 2.4: Lower's (a), Senac's (b), and Torrent-Guasp's theoretical models of the musuclar arquitecture of the heart. Images from their respective works [73, 107, 65].

Many following studies stressed and extended the concept of separate layers previously proposed by Lower. These studies include the work of renowned scientists as Jean Babtiste Senac (1749), Caspar Friedrich Wolff (1792), Gerdy (1823), Weber (1831), and Ludwig (1849). Among them, Senac acknowledged the same structure, but he highlighted that inner fibers have a nearly horizontal and circular disposition. For its part, Wolff descriptions extended the interpretation of mid-wall as two distinct layers progressively adapting to respective endo and epicardial layers. Others studied a more abstract definition of the muscular architecture. It is the case of Gerdy who described muscular connectivity as an open "figure of eight". No much later than him, Ludwig noted a similar architecture, claiming, however, the existence of an uninterrupted "figure of eight" of muscular fibers conforming the left ventricle.

Later on, in 1863, James Bell Pettigrew, affirmed to recognize up to seven layers

of musculature. But more importantly, in his findings he emphasized the potential functional significance of the middle layers for ventricular ejection. This observation was also supported by other conceptual models as the *triebwerkzeug* (translatable as propelling tool) originally presented by Ludorf Krehl in 1891 [66]. This model proposes that the myocytes of the left ventricle are organized radially at its core which imposes the necessary structure for cardiac function (Fig. 2.9(a)).

However, not all anatomists agreed with this concept. MacCallum (1900) and Franklin Paine Mall (1911) took back Senac s studies and made the first active comparison between myocardial and skeletal muscle. They described the existence of recognizable fibers in the myocardium. Using this information they also supported the previously seen connection between subendocardial and subepicardial fibers. In their work they define this populations of fibers as an structure forming pronounced V shape that its more opened while going to middle regions of the ventricular wall. Further than that, they tried to obtain more extensive and simple schema to explain the whole ventricular wall. However, their work only found to support the existence of two muscular fascicles conforming this organ. From this definition it is important to remark that they found manifest connectivity between ventricles. This was an opposed statement to Winslow s earlier work (1714) in which he defined the walls of both ventricles as discrete entities simply enclosed by a subepicardial muscular layer.

All the formerly introduced studies of the heart architecture were the foundations upon which the new conceptual and mathematical models were designed. To the best of our knowledge, we can identify 3 major models in dispute. These include the **Helical Ventricular Myocardial Band**, the geodesic description of ventricular architecture of **Streeter s model**, and finally, the syncytial approach or of the **three-dimensional mesh model**:

A The Helical Ventricular Myocardial Band

In 1957, Francisco Torrent-Guasp contributed a new and revolutionary structure (Fig. 2.4(c)) in his studies of ventricular anatomy. After more than 1,000 dissections, he defined the heart as a unique muscular band wrapping the whole myocardium [114].

In this description, the heart is seen as a unique muscular structure starting at the pulmonary artery (PA) and finishing at the Aorta (Ao). As illustrated in Figure 5.11, this muscle wraps the left ventricle and part of the right ventricle (forming what he named Right and Left Segments), connecting to a helical structure starting at the basal ring going inside the left ventricle towards the apex, and returning to connect with the Aorta (Descendent and Ascendent Segments), wrapping with this turn the entire anatomy of the heart.

Three keypoints of this theory are in the structures around the two extremes of the organ, at the apex, the basal ring, as well as in and the union between ventricles. In the first structure, the apex, his description of muscle organization at this point (which he named *apical loop*) goes no further than previous explorations of heart architecture.

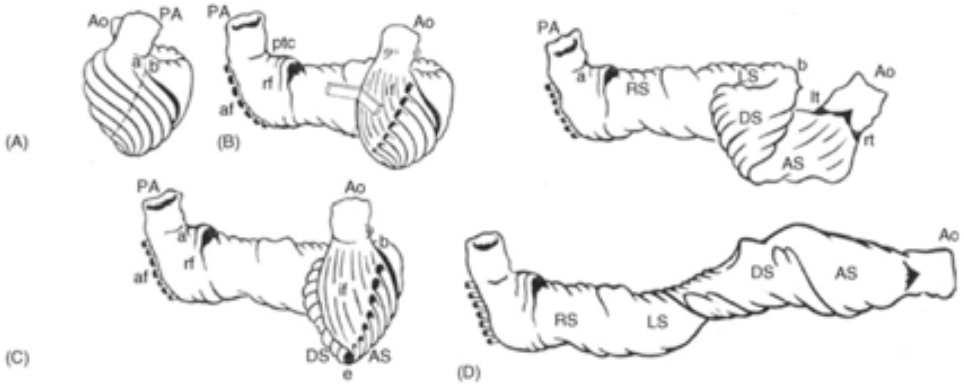

Figure 2.5: Steps of the unwrapping proposed on the theory of the HVMB by Torrent-Guasp. Diagram from [47].

It recognizes the helicallity of fibers as well as the continuous connectivity between endocardium and epicardium. We can see this formation in the connection between the Descendent and the Ascendent Segments of the HVMB. In the second structure, the basal ring, he defines an special formation that was only similarly recognized by Ludwig and his closed form of eight . This means fiber continuity at basal level. Torrent-Guasp named this structure as the *basal loop* for the characteristic curl formed by muscular fibers in this part of the heart. This structure is an important one to define the connectivity between Left and Descending Segments of his theoretical band. It remarks that endo and epicardial are connected at the basal level as they are in the apex. Finally, the connection of ventricles also deserves special attention. According to his dissection observations, the anterior union between both ventricles presents a weak coupling (mostly a collagenal clustering) rather than a few epicardial fibers. In fact, he used that weak spot to initiate his unravelling as shown in Figure 5.11(A-B). Alternatively, the posterior union of ventricles is defined as a strong muscular structure and defines part of the continuity between his definition of Right and Left Segments.

For an easier conception, Torrent-Guasp himself, presented a more intuitive simile of his theory. This particular tangling of muscular fibers could be represented as a torsion of a rope as pictured in Figure 2.6.

The concept of the Helical Ventricular Myocardial Band (HVMB) evolved in his hands to the point of being able to define a logical correlation with its function [29]. As discussed earlier in this text, cardiomyocites are known to propagate electrical impulses in the same direction of their contraction. Based on this fact, Torrent-Guasp proposed that electromechanical propagation through the HVMB imposes an elaborate activation pattern that meets with the physiology of the heart (Fig. 2.7).

Electromecanical activation travelling across RS and LS would cause contraction at basal level (favouring pressure increase as well as a bottleneck). After that, the two

Figure 2.6: Intuitive simulation the Helical Ventricular Myocardial Band introduced by Dr. Francisco Torrent-Guasp in his own articles. Figure from Torrent-Guasp s website (http://www.torrent-guasp.com/PAGES/VMB Form.htm).

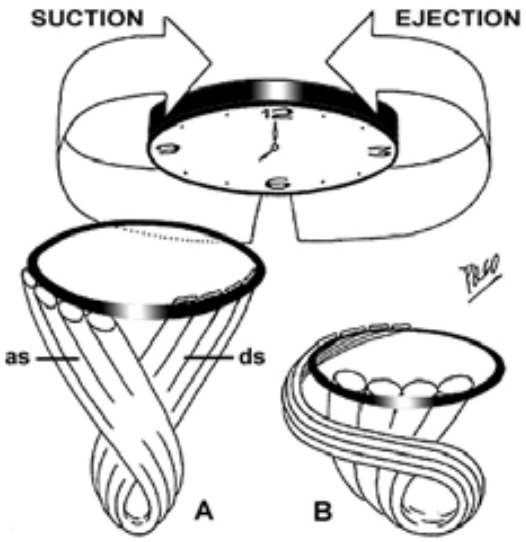

Figure 2.7: Description of the the contraction of DS fibers explains blood ejection by twisting and shortening of ventricles (B) and subsequent contraction of AS fibers forces the inverse action for blood suction (A) according to Torrent-Guasp. Figure from Torrent-Guasp s website (http://www.torrent-guasp.com/PAGES/VMB Function.htm).

remaining segments will be in charge one after the other of propelling and sucking blood. According to his description, the first of these contractions explains long axis shortening that effectively reduces ventricle as well as ventricular twist during systole. In this way, blood could be efficiently ejected to the great arteries. After that, the contraction of the AS would explain an active diastolic function. Resulting from the previous DS contraction, AS would be at this point sustained to elongation and increase of it obliquity. The contraction of the AS would explain simultaneous shortening and rectifying of its fibers and thus ventricles would rapidly increase their volumes. A powerful suction force for the atrial blood is thereby generated.

Several clinical reviews approve this theory [65, 13, 15, 86, 35, 34] and its implications have been also considered for its clinical application [116], electromecanical simulation [121] even including the definition of a simplified matematical model of the conceptual structure [81]. However, because of its "simple" structural formation, and the fact of being a dissection based methodology, it has gained many detractors as well.

B Streeter model

Another upmost heart anatomist, Daniel Deninson Streeter Jr., brought important insight of the myocardium micro-structure by means of thorough histological studies between late sixties and late seventies. Streeter was one of the most prominent anatomists to discard the concept of muscular bundles on the heart, and his histological studies [111] verified the well-defined general orientation patterns in the muscular tissue.

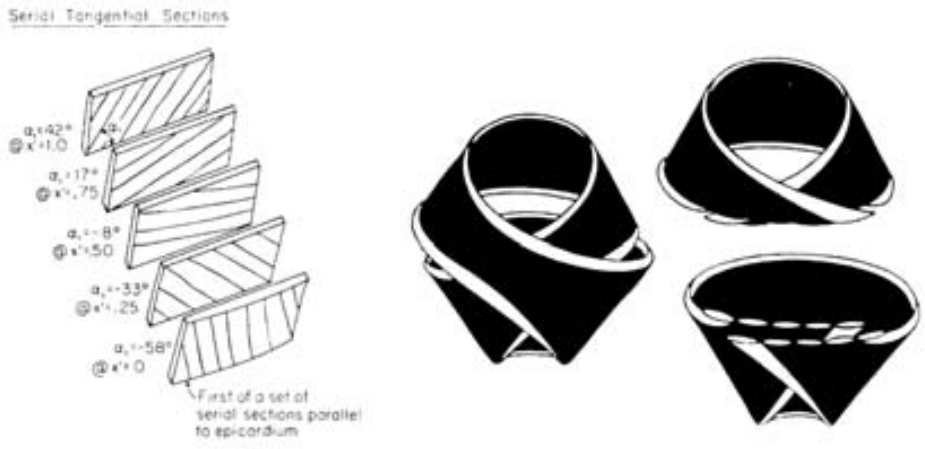

(a) (b)

Figure 2.8: Illustrative figures adapted from Streeter's work [109]. (a) Illustration of a representative set of fiber angulations across myocardial wall. (b) Schematic diagram of the concept of the continual toroidal formation of the myocardium against the concept of myolaminae.

He described that the great majority of myocytes are organized in tangential fashion to the ventricular walls. After that, he stated that the structured formation of the myocardium allows the description of myocardial fibers as arranged chains of cardiomyocytes. These fibers were noticed to exhibit a pattern of smooth change of direction across the wall of the ventricle (Fig. 2.8(a)). This progressive transverse pattern was partially noticed in the past by notable heart anatomists as Lower, Wolff, Pettigrew, Krehl, and even MacCallum/Mall, and it has been supported in subsequent studies [113, 46, 87].

In his studies he also introduced a proposal for major mathematical description of fiber orientation. Based on tangential organization and transmural variation of the fiber inclination, he proposed a summarized description of fiber pathways conforming LV as nested geodesic functions. It is important to notice that this architectural conceptualization also recognizes the continuous connectivity between the endocardium and the epicardium. This connectivity is defined by a transverse angle of myocites in the base and the apex. Upon these principles, macroscopical architectural formation of the left ventricle was defined by Streeter as the isogeodesic toroid pictured in Figure 2.8(b).

An important fact of this conceptualization of myocardial architecture is that it has been seen by many authors as an alternative to the HVMB of Torrent-Guasp. However, as stated by Torrent-Guasp himself *very few of those who are quoting* ... [Streeter s work]... *know that it was, actually based on my anatomical dissections and studies* [2]. Nevertheless we should remark that this theory has been in fact known to be inconsistent with any laminar descriptions of the myocardium [68, 38, 21].

This description of the ventricular myocardium has also become an important referent in electromechanical simulation of the heart by the most recent studies. However, it can make a difference [56] and according to Anderson [74] the *mathematical models of ventricular function have accepted these measurements of helical angles, but have ignored the fact that a significant population of cardiomyocytes are joined together to intrude transmurally in epicardial to endocardial direction, or vice versa* .

C The three-dimensional mesh

Finally, another contemporary conceptualization of the myocardium comes from the hand of the prominent anatomists Robert H. Anderson and Paul P. Lunckenheimer.

These scientists undermine the concept of the HVMB [103, 4, 5, 75, 74] and describe the muscular formation of the myocardium close to a biological syncytium or *three-dimensional mesh*. This approach states that the ventricular walls present a complex morphologic aggregation of cardiomyocites. Initially this conceptualization seems to be concurrent with Streeter s definitions of tangential and smooth angular variation of myocites throughout ventricular wall. However, this interpretation avoids the incorporation of the concept of geodesic pathways. Moreover, it has a distinct description of the link between muscular morphology and physiology. Firstly,

[2] http://www.torrent-guasp.com/PAGES/VMB Form.htm

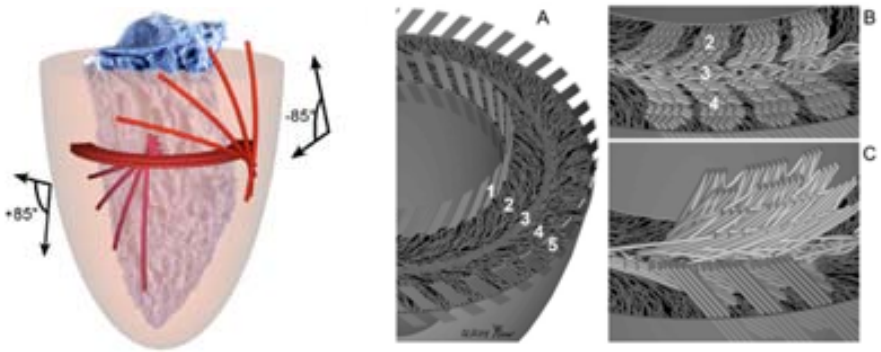

(a) (b)

Figure 2.9: Illustration of the concept of the Khrel s Triebwerkzeug (a), and a more detailed description of how the structural alignment of fibers should be in this model at the equatorial short axis. Both diagrams obtained from [74].

this theory conveys with the structural definition of Khrel s triebwerkzeug conceptual model(Fig. 2.9). It has special focus in the central ventricular mass that defines a circular mass that, acording to their description, would be in charge of major ventricular constriction (short axis). Meanwhile, the oblique disposition of cardiomyocites is understood to produce the second component of ventricular contraction (long axis) able to complete efficient blood ejection. In this theoretical interpretation, cardiomyocite is an individual functional unit suspended on a collagenal connective tissue that supports the complete syncytial physiology. Arquitecturally speaking this translates in the interpretation of independent models that complete the function of continuum mechanics (Fig. 2.9).

Very recently [77], part of this conceptualization has also been linked into a mathematical model. However, it only presents a modelization of the equatorial short axis sections of the left ventricle.

2.2 Computational reconstruction of heart s muscular anatomy

As discussed in the previous chapter, observation and measurement of myocardial architecture and formation has been historically driven by directional and histological studies. These techniques have obviously brought important breakthroughs to understand myocardial formation. However, they also brought strong disagreements among the scientific community. On one hand, many aspects of any dissectional procedure have discarded these techniques as **globally acceptable foundation for an objective interpretation**. On the other hand, histological procedures present major difficulties to assess higher levels of architectural formation of biological structures

further than at the strict microscopical level.

Nevertheless, new techniques have arisen more recently from the use of magnetic resonance imaging. These techniques are at this point the perfect fit for automated computation of biological structures. In this section we present a brief review of this imaging modalities, its computational processing, and its current applications to the study of heart anatomy, which is the focus of our work.

2.2.1 Diffusion Weighted Imaging

The nuclei of hydrogen atoms immersed on a magnetic field and exposed to a certain electromagnetic radiation are known to absorb and re-emit this radiation. This briefly explained concept is the physical principle known as Nuclear Magnetic Resonance (NMR). It is a measurable phenomenon as different hydrogen proton densities of different materials characterize contrasting signal strengths of hydrogen resonance. This constitutes the base of Magnetic Resonance Imaging (MRI). This technique enables the obtention of highly detailed volumetric sections of the human body. It allows from simple anatomical exploration of organs to the distinction of pathologic tissues. Unlike X-ray and Computed Tomography[3] (CT), MRI is a non-ionizing radiation, meaning no harm to patients.

Diffusion Weighted MRI (DW-MRI) is an specific modality of magnetic resonance conceived to capture water diffusion patterns into biological tissues. The principle of this imaging technique is based on the fact that molecules suspended on a fluid present *brownian motion*. This is no more than a presumably random drift of particles in isotropic environments as shown in Figure 2.10(a). This motion is known to be originated by kinetic and thermal energies of the environment. This imaging technique sensitizes magnetic resonance image capture to motional processes such as water flow or diffusion. This is only possible for an specific direction in each capture, but the repetition of this process in a set of distinct directions provides complete spectrum of spatial diffusion.

DW-MRI is a rather young technique. The specific methodologies for the retrieval of useful data for medical imaging come from the 1990 s observation of Michael Moesley, in his study of white matter [85]. He discovered through diffusion weighted magnetic resonances (Fig. 2.10(b)) clear anisotropic diffusion of water in neuronal tissues. The observed anisotropic diffusion was direct consequence of the obstruction of cell membranes, thus revealing details of tissue architecture. This technique could be applied for the study of either normal or pathologic tissue (as long as it is not dehydrated).

2.2.2 Caracterization of diffusion

Measured diffusion throughout diffusion weighted imaging of biological tissues needs an spatial characterization for its mathematical or computational interpretation and

[3] *Computed Tomography*: Computer assisted tomography based on X-ray radiation.

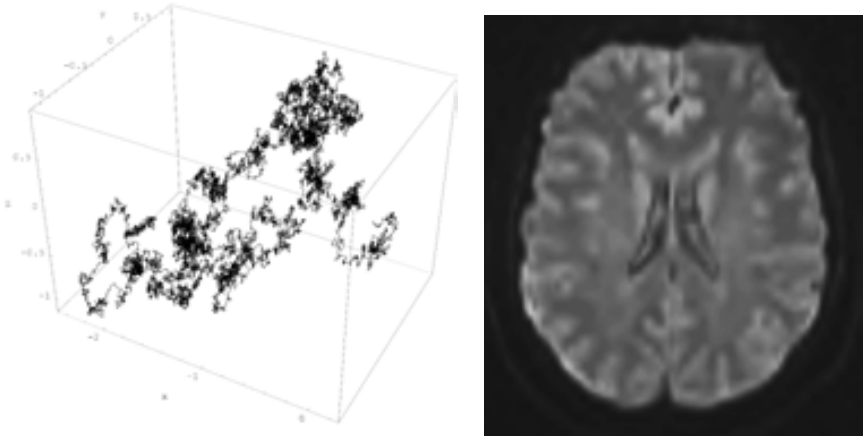

(a) (b)

Figure 2.10: Brownian motion (a), and a sample DW-MRI of a brain (b). Left image under CC BY-SA 3.0, T.J. Sullivan, right image from http://www.mridoc.com/neuro.html.

use. Following we are going to introduce from the most basic **diffusion tensor** model to modern **high resolution** alternatives. This overview closes discussing the **applicability of these techniques to the study of myocardial architecture**.

A Diffusion Tensor model

As a result of his observation, Moesley proposed to characterize this directional information with a generalized conceptualization of scalars, vectors, and matrixes known as *tensors*. This is what Filler et al. completed in 1992 [31] and it is what we know as **Diffusion Tensor Magnetic Resonance Imaging (DT-MRI)**. This modality is also often referred as diffusion tensor imaging (DTI).

Thinking on the anisotropic diffusion of water in biological tissue as brain s white matter, the use of second order diffusion tensor model was proposed [31, 95]. Mathematically, this tensor can be expressed as a 3x3 symmetric and positive defined matrix D (see Eq. 2.1).

$$D = \begin{matrix} D_{xx} & D_{xy} & D_{xz} \\ D_{yx} & D_{yy} & D_{yz} \\ D_{zx} & D_{zy} & D_{zz} \end{matrix} \tag{2.1}$$

This matrix is the covariance matrix of displacements of water particles modelled as a Gaussian probability distribution function for each voxel in a set of DW-MRI captures.

By means of matrix diagonalization we can obtain a description of main directions

of diffusivity of water within each voxel. In this decomposition of D (Eq. 2.2):

$$D = VPV^{-1} \tag{2.2}$$

V (Eq. 2.3) is an invertible matrix formed by 3 linearly independent eigenvectors $(v_1\ v_2\ v_3)$:

$$V = [v_1\ v_2\ v_3] \tag{2.3}$$

and P (Eq. 2.4) is a diagonal matrix which its diagonal entries are the corresponding eigenvalues $(\lambda_1\ \lambda_2\ \lambda_3)$:

$$P = \begin{matrix} \lambda_1 & 0 & 0 \\ 0 & \lambda_2 & 0 \\ 0 & 0 & \lambda_3 \end{matrix} \quad \text{where } \lambda_1 \geq \lambda_2 \geq \lambda_3 \geq 0 \tag{2.4}$$

The geometrical interpretation of a diffusion tensor could be even more clarifying. A second order tensor can be understood as an ellipsoid defined by the former eigenvectors and eigenvalues as the directions and lengths of its axes respectively (Fig. 2.11). In a fully isotropic environment this eigenvalues will tend to be equally valued. In consequence, this ellipsoid will become spherical. However, in an anisotropic environment this inequality will tend to be exaggerated, and principal directions of diffusion will be valued with the largest values. Accordingly, this ellipsoid will shape from flattened spheres (planar diffusion) to sharp ellipsoids (linear diffusion) representing the diverse configurations of diffusion (Fig. 2.11).

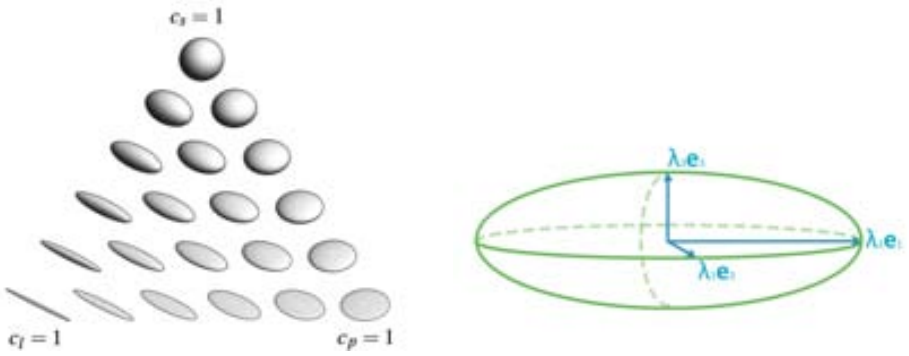

(a) (b)

Figure 2.11: Diffusion tensor characterization. (a) Possible shapes of an ellipsoid characterizing diffusion (image from [64]). (b) Components of a sample tensor (image from [98]).

The use of diffusion tensor has also brought interesting biomarkers based on the distribution of water diffusion [95, 122]. For example, Fractional Anisotropy (FA)

[95] expressed in Equation 2.5 describes directional dependence of eigenvectors. In other words, FA measures the degree of anisotropy. Measures like this have invariance to rotation and scale, and represent scalar properties that can be used clinically to identify pathologic conditions without having to recur to complex spatial distributions of tissue.

$$FA(D) = \frac{\sqrt{(\lambda_1 - \lambda_2)^2 + (\lambda_2 - \lambda_3)^2 + (\lambda_1 - \lambda_3)^2}}{\sqrt{2(\lambda_1^2 + \lambda_2^2 + \lambda_2^2)}} \tag{2.5}$$

B High Angular Resolution models

In good conditions, the size of each voxel on a normal DW-MRI capture corresponds to a physical measure of about 1mm^3. This implies some consequences. Myocyte size could vary, because its muscular nature, but it is around 50 to 100 µm long, and 10 to 20 µm thick. Capture resolution is far to exhaustively represent this spatial distribution. In consequence, each voxel of this data is representing predominant (or simply, the mean) directions of groups of fibers.

In this environment, the formerly introduced tensor analysis may be seen as a simplistic characterization of diffusion. Taking into account the resolution capabilities of diffusion weighted MRI, it is easy to see that the characterization of a general fluid flow with a single ellipsoid could not be able to represent all detail of anisotropic water diffusion with low level singularities (Fig. 2.12) as crossing, concentration (flow sinks, kissings, convergence), and dispersion (flow sources, divergence).

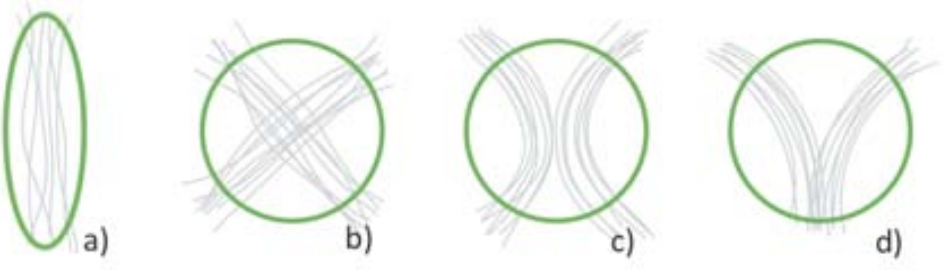

Figure 2.12: Figures of singularities in a flow for the need of higher dimension models. Diagram from [98].

In some areas of exploitation of diffusion weighted imaging for computational reconstruction of biologic tissue as in the study of the brain, limitations imposed by a tensor model have proven to be an important issue. Given the state of art resolution capabilities, it has been observed that most regions of the brain (almost exceeding two thirds of it) have a more complex configuration than what a second order tensor can encode [120]. Each voxel could present intra-voxel organizations including crossings, kissings and divergences of neuronal pathways. New models to capture complex diffusion patterns have been conceived to overcome these shortcomings. Given the strong

spatial resolution constraints of DW-MRI, these new approaches propose higher angular resolution characterization of diffusion.

(a) (b)

Figure 2.13: Illustrative examples of HARDI processing of diffusion weighted imaging from [120]. (a) Shows the shape of an individual voxel characterized with high angular resolution, and (b) shows the differences between fitting single and double tensors to HARDI data in a region of a DW-MRI sample.

In order to solve this problem, Tuch sought to use dense uniform geodesic sampling in diffusion to define High Angular Resolution Diffusion Imaging (HARDI) [120]. This measure brought a way to resolve multiple fiber orientations within a single voxel in regions of fiber crossing (Fig. 2.13). Several proposals have tackled with the modelling of this spatial diffusion signal. The most straightforward methodology is the extension of tensor model aggregating multiple independent second order tensors. However, the most popular approaches define more complex orientation distribution functions (ODF) to recover the fiber orientations and corresponding volume fractions that best explain the measured diffusion. Among them, popular choices of characterizations include the use of mixture of Gaussians [**?**], Q-ball imaging [**?**], spherical deconvolution [**?**], DOT [**?**], etc. Alternatively Diffusion Spectrum Imaging (DSI) [**?**] could be considered another high angular resolution methodology. This technique exploits diffusion characterization in the domain of resonance signal rather than image as the former methods.

C Diffusion characterization for the study of myocardial architecture

In the concrete context of cardiology, DT-MRI has proven to provide extremely useful information about the shape and distribution of cardiomyocytes. As introduced in Section 2.1.2, even if the myocardial muscle has been defined as a complex myocytal mesh, this mesh tends to have spatial coherence in areas of close adjacency (see Figure **??**). As a result, water diffusion will be produced mainly in one direction which defines the principal orientation of muscular tissue and corresponds with the direction of the first eigenvector λ_1. This behaviour has been histologically proven [105] and concur on the validity of DT-MRI as a measuring of cardiac microstructure. The two remaining eigenvectors (λ_2 λ_3) have been considered by other researchers for its reconstruction

[51, 99, 5, 72] and also cross-validated with histology [68], but their meaning remains still controversial.

It is also known that HARDI models can bring more detail than DT-MRI. On its application to the study of the heart, it is evident that at some point of the myocardium we will find multiple fibers on a single voxel, which HARDI would represent with more accuracy. However, in the study of the myocardial architecture, this microscopical detail may not be as crucial as it is on the brain, specially when approaching the issue from a macroscopic perspective. Diffusion tensor simplicity may invalidate exhaustive representation of the microstructure of the muscular tissue, but instead could help represent gross details of this micro-architecture. In fact, as we have already remarked in this text, DT-MRI has been repeatedly validated for its use on the characterization of myocardial tissue.

Finally, spatial resolution obtained with this methodology can be of higher detail than naked-eye dissection procedures, and it is more coupled and repeatable than series of destructive histological tests all over the anatomy. Consequently, DT-MRI has been established as the reference imaging modality for measurement of the whole cardiac architecture.

2.2.3 Reconstruction of myocardial architecture

Diffusion weighted data and its derived methodologies offer the possibility to explore volumetric sections of biological tissue. But this data requires practical representation for its inspection. The most straightforward representation is to offer 2D slices (Fig. 2.14)(a). However, this representation of this multidimensional data in a bidimensional environment is clearly limited. An extension of this methodology is to use glyphs[4] to make this data more readable (Fig. 2.14)(b). One of the first applications of cardiac modelling by means of diffusion tensor MRI presented results with 3D glyph based representations of the diffusion tensors [119]. This could in fact be considered a 2,5D representation. It shows discrete diffusion data in a 3D space but represented in slices of the volumetric data (Fig. 2.14)(c).

However, more contextual detail is needed for anatomical interpretation of muscular tissue in the myocardium, and many works have faced that challenge. The most common method to retrieve anatomical structure from DT-MRI studies is by tracking principal directions of tensors. This technique is known as *Fiber tracking*, which is no more than the name that *streamlining* receives in the area of reconstruction of fibrilar structures as the heart and brain. In this application streamlining is a concept straightly inherited from the study of fluid mechanics [41]. By definition, an streamline is a curve that is tangential to a flow at any point of that curve. In essence, the use of streamlines is focused to trace local streams (through fitting curves) on a fluid from discrete measurements of its cinematic. This applies to the myocardium, brain, and general diffusion studies. Discrete measurements of anisotropic water diffusion in the cells and similar biological structures describe the local shape of the tissues. Hence,

[4] *Glyph*: In the context of computer graphic representations, a glyph is a graphic symbol that offers visual cue of higher dimensional data.

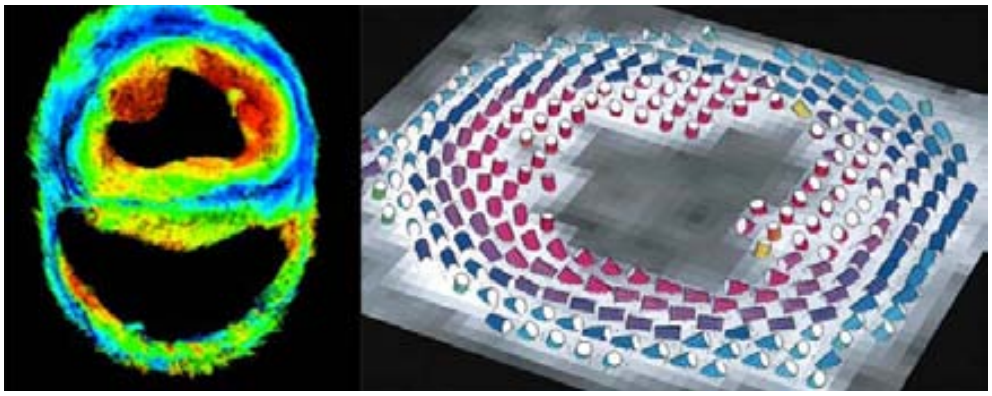

Figure 2.14: 2D (left) and 2'5D (right) representations of principal eigenvector directions in DT-MRI data in its application to cardiac description. Figures adapted from [125, 119].

the trace of these directions can give information of its architectural disposition. We usually refer these representations as *tractographies*.

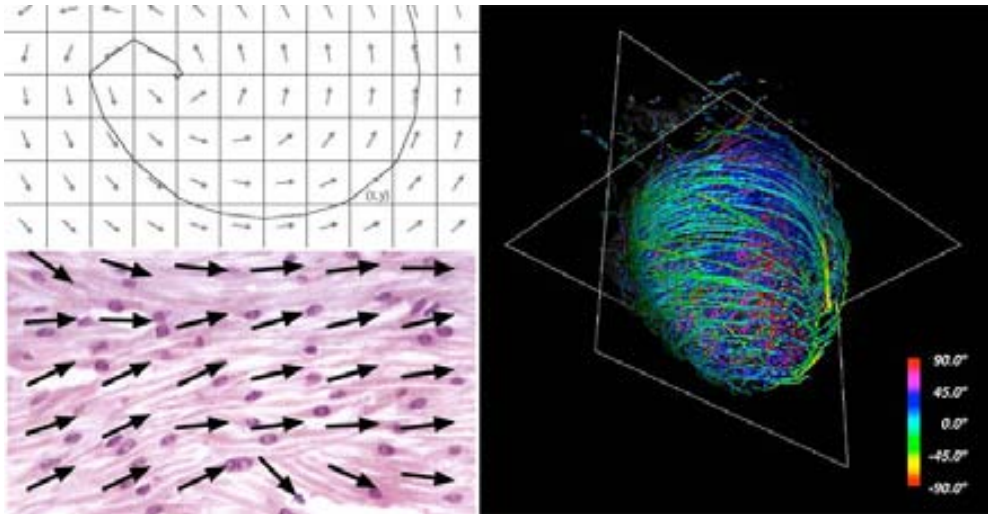

Figure 2.15: Illustrations from the definition of the discrete myocardial architecture (lower left), streamline reconstruction on a vector field (upper left) and a final tractographic reconstruction (right).

In other words, this technique could be seen as a connectivity mapping in the discrete measurements of diffusion weighted MRI modalities as DT-MRI or even in any HARDI alternative. This brings the opportunity to automatically reconstruct and visualize complex biological patterns of myocardium for its interpretation. Generally speaking, tractographic representations are performed following the track that particles in a fluid would trace (Fig 2.15). This fluid characterization is usually based

on discrete samplings of fluid dynamics as in tensor or vector fields. Using DT-MRI as an example, we can understand such vector fields as the fields defined by primary eigenvectors. Therefore, a tractography over this field will represent architectural bonding between cardiomyocytes and thus would help us represent the myocardial architecture (Fig 2.15).

Topmost classification of tractographic methodologies could be made into two main categories, *deterministic* and *probabilistic* tractography. On one hand, deterministic tractography enables to determine fluid characterization by computing a curve restricted to the vector field. This is often a step guided integration to obtain adequate direction at each stage. This integration can be achieved by numerical integration with techniques such as Euler or more complex Runge-Kutta methods [33, 99]. On the other hand, probabilistic methodologies could be seen as an extension of previous methods to offer stochastic tracking of fibers. This is achieved by introducing random variations in the methodology and evaluating its probabilistic outcome. In general, we will find parametric methods as well as non parametric ones. Probabilistic characterization of multiple deterministic tractographic reconstructions over bootstraped diffusion data has been a popular way to define non parametric probabilistic tractographies. It has offered a satisfactory way to deal with the uncertainty introduced by the noise in the image capture to deterministic tractography [62, 67]. Otherwise, from a parametric point of view, probabilistic models are being used to introduce a prior knowledge of fiber distribution and guide fiber tracking processes [9, 32].

2.3 Current challenges

Even though we are focused in myocardial study, in a broader study of biological anatomies throughout the tractographic reconstruction of data recovered from diffusion MRI, one cannot overlook the importance of its application to brain research. The formerly introduced imaging techniques were pioneered in this area [125] and have been extensively applied to recover spatial distribution of neurones in white and grey matter. Representation derived from tractography is being used as well to visualize and study the anatomy of the brain in health and disease.

However, to the best of our knowledge, brain research is currently focused on a different problem in the use of these techniques to diffusion weighted imaging. Briefly, the brain is mainly formed by neurones which are well insulated structures (by *myelin*[5] sheaths) organized in apparent fascicles. Thanks to this highly structured formation, the study of major neuronal structures was achieved in the first histological studies of the brain in the 19th century performed by scientists as Joseph Jules Dejerine [23], Camilo Golgi [39], and Santiago Ramón y Cajal [124]. Their findings preceded the development of modern imaging techniques such as DW-MRI. This modern techniques have opened new possibilities to achieve in-vivo and non-invasive measurement of

[5] *Myelin:* Dielectric fatty material usually recovering the axons of neurones to improve their electrical propagation by insulation.

brain neuronal wiring [60]. Hence, their challenges are currently focused on the clinical diagnose branch by studying white matter integrity, fiber connectivity, or surgical planning, and even for patient prognosis. This are obviously demanding areas where the application of any computational procedure there is no margin for error due to the high significance of microscopical architecture to physiologic functions of the brain.

Meanwhile (at least within the scope of this thesis: the study of muscular architecture of the myocardium) in heart applications of tractographic reconstruction of DW imaging, research is currently focused on bringing an automated reconstruction of the gross anatomy of ventricular muscle. The main idea is to bring better tools for an easier study and interpretation of this organ. These tools have to liberate the process from surgical or medical subjectivity proven to bring undesirable instrumentation and controversy in the past. Nevertheless, it is important to highlight that grosser architecture of muscles does not mitigate the need for robust evaluation of the precision of any computational procedure. Even though it is not meant for clinical practice it is of paramount significance as well as in brain research applications.

The confluence arises in the (2.3.1) **pursue of better visualization techniques to ensure more meaningful anatomical representations**, and the common (2.3.2) **need to provide validation techniques for any computational processing and outcome**.

2.3.1 Visualitzation of architectural structures

As proposed by one of the first tractographic reconstruction of white matter DT-MRI [7], this technique was rapidly applied to the reconstruction of the myocardium [125], and has been extensively applied since [52, 125, 33, 99, 5, 108, 83] (see Fig. 2.16). From the thorough study of these applications, we can identify specificific challenges that should be examined carefully in our development. Those challenges include (A) **general issues in the visualization** of tractographies, (B) the i**mportance of anatomical completness of these reconstructions**, and (C) **how to translate complex and detailed structures into more comprehensive models that depict principal biological structures for an easier interpretation**.

A Visualizing tractographies

Any visual representation of data should maximize the illustrative potential of graphics to help understand the data being described. Usually, an effective representation of data requires to be composed with complementary information that can offer an enriched depiction. In the context of tractography, color coding of streamlines has been known to be able to provide meaningful information of myocardial anatomy. In fact, customized color schemes provided the first evidences of the fiber structure (Fig. 2.16(a)) and have been extensively applied since.

Most of these methodologies have offered interesting advances, but did not provide generalized and automatized solutions [52, 125, 33, 99, 5] for color coding. First, these

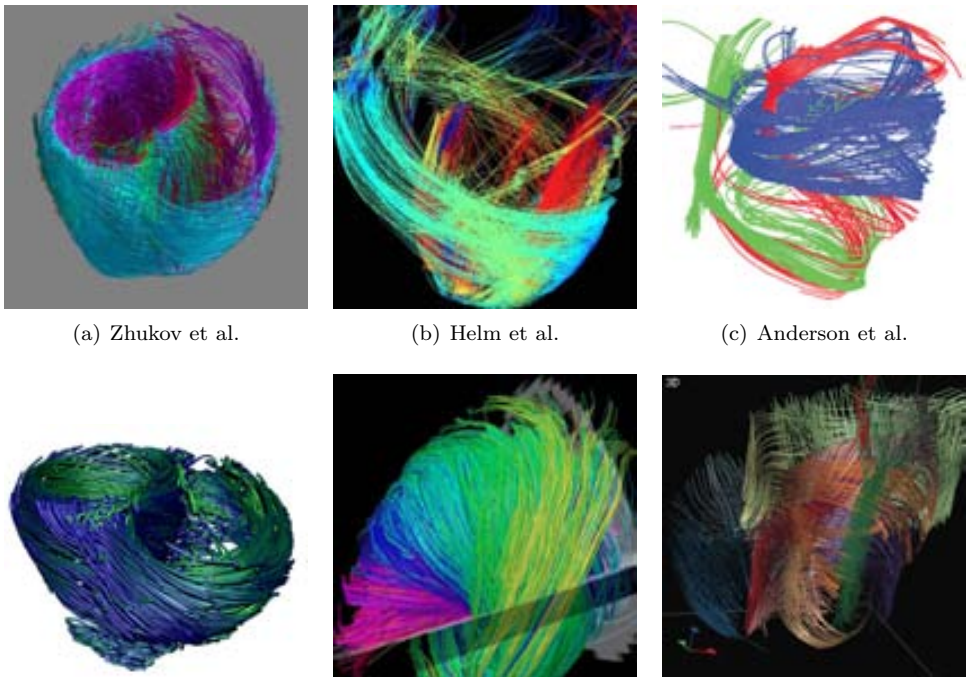

(a) Zhukov et al. (b) Helm et al. (c) Anderson et al.

(d) Rohmer et al (e) Sosnovik et al. (f) Chen et al.

Figure 2.16: Illustrative examples of tractographic reconstructions in the literature. Images gathered from (a) [125], (b) [51], (c) [5], (d) [99], (e) [108], and (f) [18].

approaches usually assume global reference coordinate system to be correctly aligned to cardiac anatomy. This offers limited flexibility to the variations of anatomy and input data, or even requires manual manipulation in order to achieve a meaningful relation to the anatomical formation. Second, manual color coding has also been used to offer visual segmentation of manually selected fiber aggregations [5]. These kind of representations could be susceptible of incorporating subjectivity to the interpretation of architectural substructures like surgical procedures did in the past. Finally, an interesting alternative to this problem has been to consider the definition of parametric models of the heart. However, by their complexity, they are usually restricted to the left ventricle [52, 37]. Taking all these facts into consideration, it is clear that any comprehensive visualization of fiber tracts should **involve an automatic assignment of colors providing information about the orientation of the myocardial fibers coherent to ventricular anatomy**.

B Anatomical completeness

Tractographic reconstruction of heart muscle should offer us the possibility to attain objective representations of myocardial architecture. However the application of this

methodology is not entailed to objectivity per se. Some past studies of reference (introduced in Chapter 2) have lead to completely opposed interpretations that support rivalling conceptualizations of the myocardial formation [16, 5, 86]. This can come as a result of building interpretations over partial reconstructions of the anatomy of the heart [52, 125, 33].

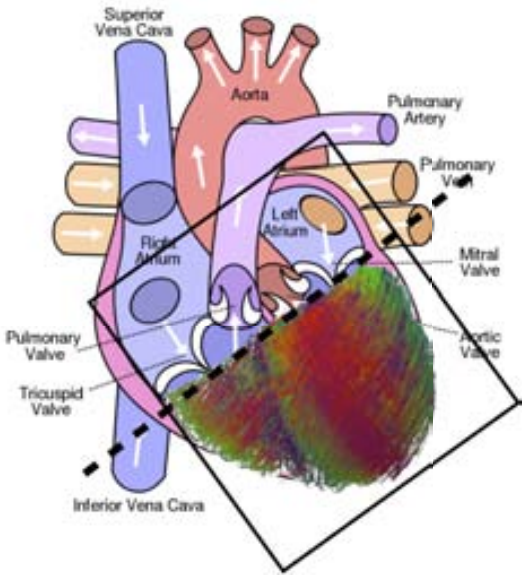

Figure 2.17: Rough superimposition of a tractographic reconstruction (from [125]) over an anatomic heart diagram. The dotted line represents the section performed to remove auricles from the reconstruction. This section may neglect important muscular structures. Heart diagram under CC BY-SA 3.0, Yaddah Wapcaplet.

There may be several reasons why a tractographic representation is fractioned or incomplete. The most important seems to relate with intentional segmentation of data. In order to limit the domain of tractographic reconstruction, studies generally use volumetric thresholding masks to conceal parts of the anatomy. Reportedly, this has helped to avoid noise of input data, or simply to remove unwanted parts of the anatomy as the thin muscular tissue conforming the heart auricles. However, it is clear that sub-optimal segmentations performed by such masks could leave important parts of myocardial architecture out. For example, neglecting the myocardial base (see Fig. 2.17) is an important matter since its formation is a heated argument about ventricular anatomy. Similarly to the former limitation of reconstruction, some recent studies have presented results based on the reconstruction of specific parts of the ventricles [5, 35, 34, 83]. Such studies may be justified for diagnostic matters as in detecting or quantifying specific muscular remodelling after myocardial infarction. However, this focus disables these representations as a base for architectural interpretation since they may not be exhaustive, or may subject to subjectivity. Henceforth, if we want to **attain objectively interpretable architectural reconstructions of muscular architecture, we will have to be able to represent the complete**

anatomy.

C Abstract architectural structures

One of the most important problems to tackle in the study of biological anatomies from a tractographic point of view includes setting generalized methods to pursue more meaningful anatomical representations than individual streamlines. The most common approaches include the use of fiber clusterings and segmentations (see Figure 2.18). These methods have already helped to attain more abstract, concise and manageable representations for visual inspection of the brain [84, 104]. However, input parameters of these procedures as the number of clusters have proved to be critical and usually lacking of general automatization. Which, in turn, could be crucial in the study of the muscular heart anatomy to avoid introducing subjectivity (even utilizing expert opinion) on the process. Another interesting approach considers the depiction of local fiber coherency for visual assessment [102]. Techniques like these aim to obtain representative information about architectural patterns and present a viable alternative.

Figure 2.18: Examples of fiber clustering in the application to brain study. Left (from [89]) shows clustering of the *corpus callosum* and right (from [91]) shows the main seven fiber bundles of the brain.

The study of streamlines from this non-individual point of view has been limited in heart studies. As far as we can tell from literature review, this is a result of the distinctive entanglement of its architecture. Direct application of brain procedures resulted on mere depictions of specific and well known structures as the papillary muscles[18] (Fig. 2.16(f)) rather than on a comprehensive description of its entire anatomy. It is then, an important challenge for tractographic representation of the cardiac muscle architecture to **pursue methodologies for the representation of its more predominant structures**.

2.3.2 Confidence on recontructive computation

The evaluation of current analysis methods of diffusion image modalities as tractography remains challenging. Reconstructed fibers are the mathematical solution to satisfy a set of rules in an specific environment. However, factors as noise in data acquisition, alterations in data processing, or simply structural complexity may difficult the correct reconstruction of individual streamlines representing underlying biological tissue architectures. In the case of DT-MRI, this includes the well known limitations to represent low level fiber singularities as crossing, concentration (flow sinks), and dispersion (flow sources). As a result, streamlines reconstruction may create a false impression of precision. Some authors have approached this problem with probabilistic fiber tracking. These methods usually use deterministic streamlining originating on the same point over bootstrapped diffusion data [62, 67]. Hence, they are capable of estimating confidence measures and improving final reconstructions (including complex structures as fiber branching). Other authors have suggested to tackle this problem representing safety margins for specific fiber bundles. These margins have been described by confidence intervals based on the study of variations across different fiber tracking configurations [53, 11] (see Fig. 2.19). Other related works pay attention to specific fiber bundles [59, 40] either by measuring quality by overlap, or by computing inner similarity measures based on diverse distance estimates. Alternatively, other authors with akin goals have proposed the characterization of significant local geometry features of streamline reconstructions [102, 40]. Although these features could be really interesting for an architectural study, they do not seem to be sufficient for the study of the streamline form and shape global behavior.

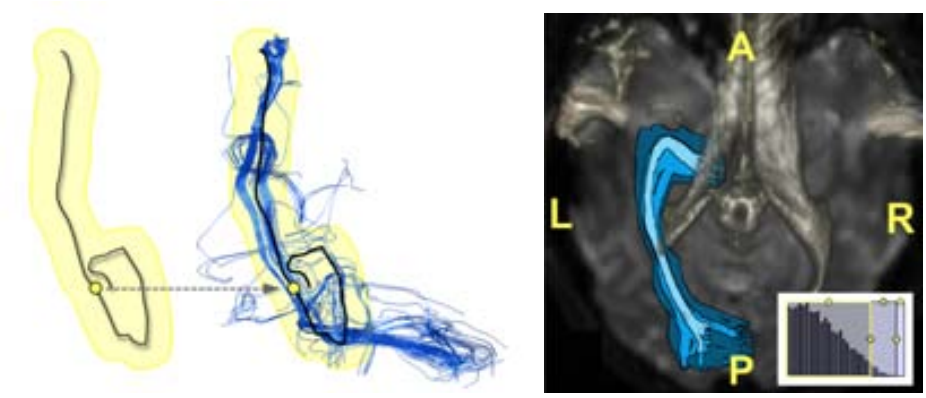

(a) (b)

Figure 2.19: Uncertainty on fiber tractography. (a) Fiber tract represented with a safety margin, and the result of all bootstraped reconstruction in the same location demonstrating safety margin does not represent real uncertainty. (b) Optic radiation visualization of 3 levels of uncertainty around a particular neuronal structure. Illustrations from Brecheisen s work [11].

2.4 Main contributions of this Thesis

In this PhD thesis, we focus on the development of computer graphics and vision techniques to help cardiologists to obtain an objective interpretation of the myocardial architecture from Diffusion Tensor MRI. In particular this work has focused in three main points:

- **Multi-resolution representation of heart s architecture for a better interpretation of muscular structures:**

  Even using objective measures from modern imaging techniques as Diffusion Tensor Magnetic Resonance Imaging (DT-MRI) no consensus about myocardial architecture has been achieved so far. In previous scientific efforts, reconstruction of this data by means of a variety of streamlining techniques has been established as a reference technique for representing cardiac architecture. It provides automatic and objective reconstructions at low level of detail, but falls short to give abstract global interpretations.

  In this thesis we introduce a **novel multi-resolution technique applied to achieve simplified streamline reconstruction of DT-MRI data**. We present different **reduction approaches** to provide multi-resolution data **that better preserve relevant anatomical details of the cardiac architecture**. Further, in this development, we solve reconstruction and representation issues to correctly adapt tractography to its use for heart reconstruction as well as to fit it in the multi-resolution domain.

- **Definition of objective measures of the confidence on our reconstructions of the heart architecture:**

  It is a well known fact that several factors, including integration methodologies and data itself, can introduce systematic inaccuracies obtaining real structures in a tractographic representation. Thus, an important step a tractographic reconstruction and representation is to offer an exhaustive evaluation of certainty on the reconstructions. This is even more important when a new methodology arises.

  In order to comply with this requirement, we have developed a complete **evaluation framework that allows measuring confidence in fiber tracts**. This methodology goes from the analysis of **local effects on anatomical data** in pre-processing methods applied to DT-MRI data, to the **global analysis of geometric properties of tractographic reconstructions** in the multi-resolution framework. This evaluation is both based on the **quantification of anatomical coherence of myocardial tissues** and **reconstruction confidence based on the same principle**.

- **Tools providing evidence of the existing models of the myocardial structure:**

The scientific transversality of this work is evident at this point. The evaluation of the tools and techniques presented in this thesis for the study of anatomical properties of the myocardium is another important part of this thesis. This work has been done under supervision of the medical doctors that collaborate with our research group.

Our approach produces reduced set of tracts that are representative of the main geometric features of the myocardial anatomical structure. This methodology and evaluation allowed obtaining validated representations of the main geometric features of the muscular formation, making easier to decipher the main properties of the architectural organization of the heart. Fiber geometry is preserved along the process of detail reduction, which **validates the simplified model for interpretation of cardiac architecture as well as its utility for anatomical interpretation**.

Chapter 3

Multi-resolution tractography

Simple can be harder than complex: You have to work hard to get your thinking clean to make it simple. But its worth it in the end because once you get there, you can move mountains.

Steve Jobs

As stated in Chapter 2, tractographic reconstruction of Diffusion Tensor MRI data has become a standard way to reconstruct muscular anatomy of the heart. However, obtaining a widely interpretable modelling of its architectural formation is still a big challenge. In this chapter we are going to introduce our contribution to this area of research. First, we will introduce our novel multi-resolution approach focused in offering more abstract representations of heart s muscular architecture (Section 3.1). Second, we will present our base methodology for an anatomically coherent reconstruction of the myocardium and all the considerations taken into account to achieve proper reconstruction of its architecture (Section 3.2). Finally, this chapter will conclude with all details needed for the embedding of tractographic reconstruction in the former multi-resolution methodology. We will focus on all details from reconstruction to visualization to attain simpler and easily interpretable representations of the myocardial anatomy (Section 3.3).

3.1 Multi-resolution DT-MRI

In any context, it is difficult, or even impossible, to understand the gross geometric features of an object in front of us just by examining its details from a close distance. However, if we step away from this object we can probably get a more contextual view of it, providing us the opportunity to understand higher-level architectures. We can easily extrapolate this idea to the tractographic reconstruction of the myocardial architecture. The state-of-art methodologies have brought very detailed information

about heart anatomy. These fully detailed tractographic reconstructions have proved their validity for low-level descriptions. However, they might fail to help on a higher level of analysis because of their inherent complexity. Any tractographic reconstruction that offers a more contextual view and avoids unnecessary detail should offer easier interpretation of the muscular architecture of the heart. In this PhD thesis we want to attain simpler reconstructions of muscular architecture of the heart. We are, in fact, choosing an opposite direction to the approaches chosen in the study of other biological tissues, as in the reconstruction of neuronal connectivity of the brain. The motivation of this approach is well defined in Chapter 2 where we describe the current controversy about gross ventricular myocardial architecture.

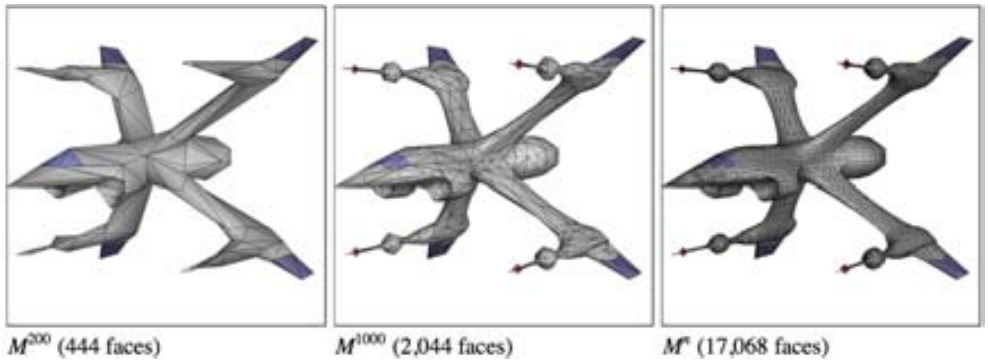

(a)

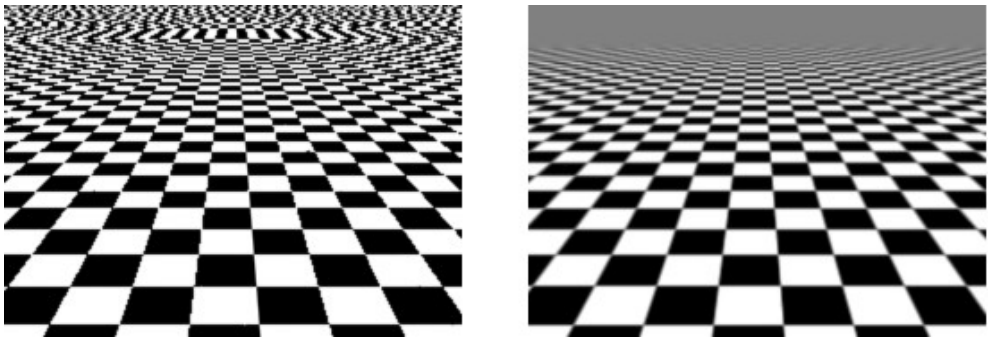

(b)

Figure 3.1: Multiscale applications on CG. (a) Progressive meshes from [55], and (b) a generic visualization comparing the improvement introduced by texture mipmapping.

Computationally, this concept can be seen as multi-resolution approach. The clearest way to understand a multi-resolution model lays on its application to computer graphics. In this environment, it is common to replicate the latest situation in which an object can be viewed from close or far distance. For the closer objects, the topological (Fig. 3.1(a)) and texture detail (Fig. 3.1(b)) are primordial to show the best possible quality. The same objects represented in distant situations require,

instead, less detail in both properties. The reason is both computational (to reduce computing complexity) and for the ambiguity related to contextualization of the detail in a lower resolution. Naive contextualizations generate visual artifacts known as *aliasing*[1]. One convenient solution to this problem is known in the application of textures to three-dimensional objects and it is known as *mipmapping* [123]. Briefly, this technique is based on the generation of lower resolution samples of the textures for their representation in the most distant objects; a technique broadly known as *pyramid decomposition* [14]. This technique is also used in several other areas including image processing and varied computer vision techniques, and also in specific applications to medical imaging [71]. In many cases, techniques exploiting pyramidal representations have also been known as computations in the scale-space. However, this naming is resulting from a more specific processing of pyramid decomposition. In this applications, the methodology replicates the same computation to the different resolution levels in order to evaluate or refine its objectives from small to large scale.

Multi-resolution strategies have been widely applied to process gross detail of data, but their potential for getting abstract representations has rarely been used. **We propose to exploit this potentiality to build a multi-resolution tractography based on the reconstruction of multi-resolution data**. The preprocessing strategies explored in this thesis conceived to obtain an adequate DT-MRI multi-resolution model will be the focus of this section.

The generation of a pyramidal representation can be concisely summarized as an iterative application of low-pass filtering and subsequent density reduction (Fig. 3.2). The concept of "pyramid" comes from the output of repeated application of this procedure. For example, from an image with dimensions $(2^D + 1)$ x $(2^D + 1)$ we can obtain N images $F_0 \dots F_{N-1}$ with respective sizes of $(2^{D-l} + 1)$ x $(2^{D-l} + 1)$ for each level l (Fig 3.2).

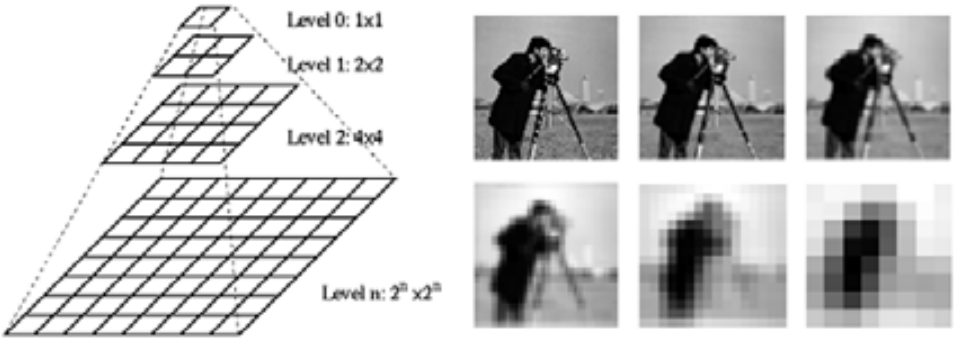

Figure 3.2: Pyramidal representation. (a) Schematic representation of a pyramid of n resolutions. And, (b) a visual depiction of the effect of a Gaussian pyramid.

[1] *Aliasing*: Distortion of signal arising in discrete representation of continuous signals due to limited sampling. For instance, aliasing in images is commonly manifest in the incorrect representation of geometric shapes with jagged distortions.

We have evaluated the possibilities for the application of a multi-resolution methodology to the tractographic reconstruction of DT-MRI captures of the myocardium. Following, we introduce the application of the isotropic approach of Gaussian pyramids, and an anatomic filtering alternative that explodes anisotropic filtering for the construction of pyramid representations from DT-MRI. Further, we will explore the use of Wavelets in order to produce pyramidal representations of data.

3.1.1 Gaussian pyramids

The first and the still standard multi-scale generation approach is the linear Gaussian pyramidal representation [14, 123]. This technique applies a Gaussian filtering and later linear reduction via a regular sub-sampling of the full-scale input data. The low-pass Gaussian filtering step offers attenuation of noise, thus extracting high frequency signals. In other words, it can extract features of interest reducing minor details making it possible to apply posterior spatial reduction. We can understand reduced representations as summaries of the original information that represent it at different levels of detail. The reductions are statistically complete in such a way that the Gaussian smoothing keeps local information before applying sub-sampling.

We can apply this filtering to any signal including images and volumes by the convolution (filtering in Fourier domain) of a Gaussian G to the input I:

$$F = G * I \tag{3.1}$$

$$\text{where } G_d(x\ \sigma) = \frac{1}{(\ \overline{2\delta}\,\sigma)^d} e^{-\frac{\|\vec{x}\|^d}{2\sigma}} \tag{3.2}$$

being d its dimension, and σ its standard deviation.

In the discrete domain this convolution can be seen as a weighted sum of neighbouring pixels in the input image by a Gaussian kernel. Combined with a linear sub-sampling strategy we can obtain the different levels (GP_0 GP_n) of the Gaussian pyramid as follows:

$$GP_l(x\ y\ z) = \begin{array}{cc} I(x\ y\ z) & \text{for l=0} \\ \sum\limits_{i,j,k} h(i\ j\ k) GP_{l-1}(2x-i\ 2y-j\ 2z-k) & \text{otherwise} \end{array} \tag{3.3}$$

in this expression, l stands for the pyramid level of detail. For its part, h denotes the Gaussian weighting function, usually referred as the Gaussian kernel. This gaussian kernel is no more than discrete coefficients of the filtering function described in Equation 3.2.

For computational purposes, and exploiting separability of Gaussian kernel, we could apply one-dimesional Gaussian kernels independently for each of the volume

dimensions. Further, and alternatively to the formulation in the Equation 3.3, we can also reduce computation on the obtention of specific levels of the pyramid level since they could be obtained independently of the preceding ones by increasing the Gaussian kernel accordingly to the desired level of detail.

This technique can be applied to the DT-MRI datasets in order to simplify its complexity in such a way that we expect that reconstructed tractographies from lower resolution levels of the pyramid offer simplified reconstructions of the anatomy. Dimension of volumetric data of the first eigenvectors in DT-MRI data is treated as three independent volumes representing the three components of such eigenvectors.

Gaussian kernel offers interesting properties as shift, scale, and rotation invariance as well as linearity and non enhancement of local extrema. All of them are derived from the isotropic nature of the filter. These properties have provided a useful scheme for the extraction of local properties in heterogenous environments in the past. However, after a deeper examination, it is clear that in the context of DT-MRI imaging we have not made use of key anatomical information at our disposal. We have to look for a new robust filtering in DT-MRI.

3.1.2 Anatomical filtering

We want to use the anatomical information available in DT-MRI datasets. For this reason, we will study the application of *anisotropic filtering* to the generation of more robust pyramidal representations of diffusion data. An adequate approach thinking about anisotropic filtering could be thought as a specialization of previous filtering but with a slightly modified kernel. The Gaussian kernel could be modified to fit diffusion features acquired in DT-MRI. However, it will not make rigorous sense. As it has already been discussed, we use the first eigenvector (the one with the most significant magnitude) to reconstruct muscular structures. This eigenvector is known to code the direction of myocytes. The remaining two eigenvectors have been extensively discussed on the literature but no agreement has been achieved. So, if we apply the modified Gaussian kernel using the complete tensor information we will mix different sources of data and we will not succeed to build a robust filtering. Consequently, we have bet for a more strict definition of anisotropic filtering, the one we define as **anatomical filtering**. This filtering will take into account the only reliable information available, the myocyte direction. Hence the anatomical nomenclature chosen.

We propose to use a Structure Preserving Diffusion (SPD) operator [36] oriented along DT-MRI primary eigenvector, ξ_1. Given the original volume to be filtered, $Vol(x\ y\ z)$, the diffusion process is given by the following heat diffusion equation in divergence form:

$$SPD_t = \mathrm{div}(J \quad SPD) \qquad \text{with} \qquad SPD(x\ y\ z\ 0) = Vol(x\ y\ z) \tag{3.4}$$

for denoting the gradient direction of the divergence operator, and J a symmetric

tensor driving the diffusion process. In order to restrict diffusion to ξ_1, J is defined as:

$$J = Q\Lambda Q^t = \begin{pmatrix} \xi_1^1 & \xi_1^2 & \xi_1^3 \\ \xi_2^1 & \xi_2^2 & \xi_2^3 \\ \xi_3^1 & \xi_3^2 & \xi_3^3 \end{pmatrix} \begin{pmatrix} 1 & 0 & 0 \\ 0 & 0 & 0 \\ 0 & 0 & 0 \end{pmatrix} \begin{pmatrix} \xi_1^1 & \xi_2^1 & \xi_3^1 \\ \xi_1^2 & \xi_2^2 & \xi_3^2 \\ \xi_1^3 & \xi_2^3 & \xi_3^3 \end{pmatrix} \tag{3.5}$$

for ξ_i DT-MRI eigenvectors. In our case, Equation 3.4 is applied to each of ξ_1 components. In [36] it is shown that (3.4) has a unique solution that corresponds to solving the heat equation along the integral curves of ξ_1.

Decimation is obtained as in the Gaussian approach, by the posterior linear reduction via regular sub-sampling of the full-scale input.

We expect that this methodology will be more adequate for an anisotropic dataset even though it will certainly not preserve properties as the ones owned by the gaussian filtering. Yet, some criteria and indicators will be presented in Chapter 4 to thoroughly evaluate this behavior.

A Implementation details

The formerly introduced filtering results conceptually straightforward. With this processing we want to compute at each voxel the value of the Gaussian interpolation of mentioned voxel and a directional selection of neighbours in a given stride. The volume diffusion defined by Equation 3.4 is implemented using one-dimensional Gaussian kernels for weighting the values of the volume Vol along the direction given by ξ_1. We observe that this would imply integrating the field ξ_1 for large times (scales). In order to avoid such integration, we will iterate the basic diffusion operator given by the volume diffused a minimal time unit t_0 (scale) as seen in Fig. 3.3.

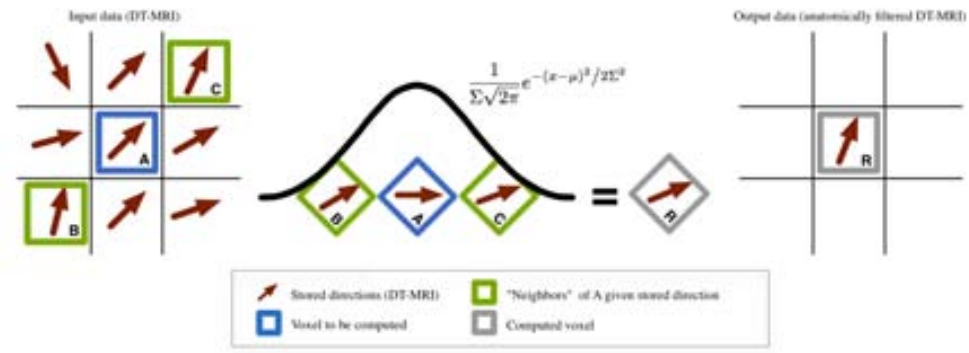

Figure 3.3: Toy example of anatomical filtering procedure. Each voxel is processed to contain a gaussian interpolation of his direct neighbourhood taking into account the stored anatomical direction.

By uniqueness of solutions to parabolic PDE [27], the kth iteration corresponds to the solution to Equation 3.4 at time kt_0. For each voxel, $(x\ y\ z)$, the volume diffused at the minimal scale, $SPD(x\ y\ z\ t_0)$, is given by:

$$\begin{aligned} SPD(x\ y\ z\ t_0) = & g_{-1} SPD(x - \xi_1^x\ y - \xi_1^y\ z - \xi_1^z\ 0) \\ & + g_0 SPD(x\ y\ z\ 0) \\ & + g_1 SPD(x + \xi_1^x\ y + \xi_1^y\ z + \xi_1^z\ 0) \end{aligned} \tag{3.6}$$

for $(g_j)_{j=-1}^{1}$ the coefficients of a 1-dimensional gaussian kernel of size 3. By iterating Equation 3.6 k times:

$$\begin{aligned} SPD(x\ y\ z\ kt_0) = & g_{-1} SPD(x - \xi_1^x\ y - \xi_1^y\ z - \xi_1^z\ (k-1)t_0) \\ & + g_0 SPD(x\ y\ z\ (k-1)t_0) \\ & + g_1 SPD(x + \xi_1^x\ y + \xi_1^y\ z + \xi_1^z\ (k-1)t_0) \end{aligned} \tag{3.7}$$

we compute the solution to (Eq. 3.4) at time kt_0. In the case of DTI primary eigenvector, the iteration (Eq. 3.7) is applied to each of its components.

B Boundaries

As in any diffusion process, boundary values deserve special treatment. In our case, due to DTI acquisition, the most undesired artifacts could appear at myocardial boundaries as a consequence of blending anatomical information with arbitrary adjacent data. A common way of coping with boundary artifacts is by propagating the values of the diffused function outside their domain of definition, that is, the myocardium. This propagation has to be performed across the domain boundaries in order to produce consistent extensions.

We propose a boundary propagation based on the gradient of the distance map to a mask of the myocardial volume. Each non-anatomic voxel value is replaced by the closest boundary voxel value in the direction of the gradient.

In general, a *distance map* [100] consists of a gray-scale image (or volume) in which the value of each pixel (or voxel) represents the minimum distance of those to a given subset of the data. This is, in most cases, the minimum distance from the background to an object pixel by a predefined distance function. In the first step towards boundary propagation, we define this map computing from the binary image (see Fig. 3.4(a)) an euclidean distance map (see Fig. 3.4(b)) where we measure distance from each background voxel to the myocardium mask. This means that each voxel p of the distance map (EDM) follows the expression:

$$EDM(p) = \begin{cases} \min\limits_{k\ M} d(p\ q_k) & \text{if } M(q_k) = 1 \\ 0 & \text{otherwise} \end{cases} \tag{3.8}$$

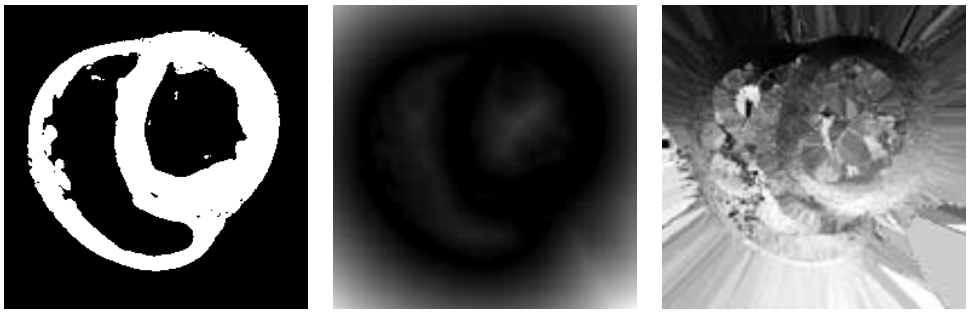

(a) (b) (c)

Figure 3.4: Stages of boundary propagation. From an anatomical mask (a), we define an euclidean distance map (b) to achieve boundary propagation (c).

where M represents the mask volume, and $d(p, q)$ denotes the euclidean metric:

$$d(p,q) = \sqrt{(x_q - x_p)^2 + (y_q - y_p)^2 + (z_q - z_p)^2} \tag{3.9}$$

for points $p = (x_p, y_p, z_p)$ and $q = (x_q, y_q, z_q)$.

After that, we compute the volume gradients ∇f for each voxel of EDM convoluting this volume with a Sobel operator.

$$\nabla f = \frac{\partial f}{\partial x}\hat{x} + \frac{\partial f}{\partial y}\hat{y} + \frac{\partial f}{\partial z}\hat{z} \tag{3.10}$$

Once we have this directions we use them to find the right propagation values PV.

$$PV(p) = p + \frac{\nabla f}{\|\nabla f\|} * EDM(p) * (1 + \epsilon) \tag{3.11}$$

where ϵ defines an margin to avoid precision errors and procure the correct voxel for propagation.

Finally, F, the resulting image with propagated boundaries (Fig. 3.5):

$$F(p) = PV(p) * M(p) + P(p) * \bar{M}(p) \mid p \in P \tag{3.12}$$

3.1.3 Wavelet decomposition

Thinking of multi-resolution models we cannot leave aside the application of discrete Wavelet transforms (DWT). In this work we will do a prospective evaluation of the most simplistic yet powerful approach known as Haar Wavelets.

(a) (b)

Figure 3.5: Input (a) and output (b) of a discrete Haar Wavelet decomposition.

As sines and cosines are used to codify signals in Fourier analysis, Wavelets are basis to codify other functions. The main advantage of the later ones is that besides being localized in frequency they are also localized in time. This second localization can be very convenient for many image processing techniques.

A DWT can be understood as a discrete hierarchical sub-band coding technique. If we take the discrete Wavelet transform of an image as an example we can see that this signal decomposition can be understood as the application of different filters. A first level transform of an N $\times$ N image (Fig. 3.5(a)) will provide 4 images (Fig. 3.5(b)) corresponding to the Wavelet coefficients:

- **LL**: Low frequency components of the input image
- **HL**: Horizontal high and vertical low components
- **LH**: Horizontal low and vertical high components
- **HH**: High frequency components of the input image

In one hand HL, LH and HH codify all detail in the input image. On the other hand, similarly to what we say earlier in Gaussian pyramids, LL is the representation of general features of the input image. This representation considered a first scale, further scales are obtained hierarchically applying DWT to low frequency components of the previous levels of decomposition.

Many advantages of wavelets come in the exploitation of their high frequency components as in image compression or de-noising. However, in the scope of this thesis we will only explore the effects of the low-pass filter proposed by Haar Wavelets. This

filter is no more than a local averaging operator. However, this presents a different alternative than the previous filters and should be analysed.

3.2 Tractographic reconstruction of the myocardium

A tractography is no more than an aggregation of curves (streamlines) that describe behaviour of fluid flows, offering a three-dimensional representation of such flow. The general applicability of this technique to the reconstruction of myocardial anatomy has been described on the previous chapter. Now we are going to deepen on the methodology specifics that we have applied to offer adequate reconstructions of myocardium from diffusion tensor images.

In order to define a streamline we will have to focus on three main issues. Those involve the mathematical description of curves that accomplish the representation of a flow (defined in our case by a discrete vector field resulting from the measurement of water diffusion in muscular tissue), and the criteria to start and finish the individual curves that will represent such flows.

3.2.1 Adapting DT-MRI to fiber tracking

By definition, a streamline is a curve tangential to the vector field at any point of such curve:

$$\frac{d\overline{x}_s}{ds} \times \overline{u}\left(\overline{x}_s\right) = 0 \tag{3.13}$$

where $\overline{x}_s(s)$ is the instantaneous parametric representation of the curve, and $\overline{u}\left(\overline{x}_s\right)$ is the correspondent local direction in the vectorial field being reconstructed. Briefly, the curve must be tangent to each point of the data being reconstructed.

Therefore, if we parametrize the initial 3D streamline trajectory in time t as:

$$\gamma(t) = (x(t)\ \ y(t)\ \ z(t)) \tag{3.14}$$

and we define the the primary DTI eigenvector as:

$$\overline{\mathbf{V}} = (u(x\ \ y\ \ z)\ \ v(x\ \ y\ \ z)\ \ w(x\ \ y\ \ z)) \tag{3.15}$$

then, the streamline is given by the cross product of the curve s (equation 3.14) first derivative and the primary eigenvector (equation 3.15):

$$\frac{d\overline{\gamma}\left(t\right)}{dt} \times \overline{\mathbf{V}}(\gamma(t)) = 0 \tag{3.16}$$

However, it is not feasible to solve equation 3.16 analytically. For this reason, we have chosen instead a fifth order Runge-Kutta-Fehlbert [30] integration method with adaptive integration steps based on an estimation of the integration error. This method solves the following differential equation:

$$\frac{d\gamma(t)}{dt} = \overline{\mathbf{V}}(\gamma(t)) \tag{3.17}$$

where the initial point (*seed*) of the streamline is defined by:

$$\gamma(0) = (x_0 \;\; y_0 \;\; z_0) \tag{3.18}$$

Nonetheless, this methodology cannot be applied without further preprocessing of input data or adaptation of the algorithm to the specifics of DT-MRI. As described in detail in Chapter 2, DT-MRI characterizes diffusion in tensors. Given the anisotropic property of the water diffusion in muscular tissue, the principal information about the architectural distribution the muscle lays mainly on the primary eigenvector of that tensor. This fact can be concisely summarized by recognizing that the direction of these vectors is aligned with the direction of the long axis section of muscular cells. However, in this scenario we have to bear in mind that water diffusion will likely occur symmetrically since there is no prevalent tendency on the random drift of particles that define diffusion. Hence, it is important to highlight that the sign of primary eigenvectors does not correspond to any physiological property.

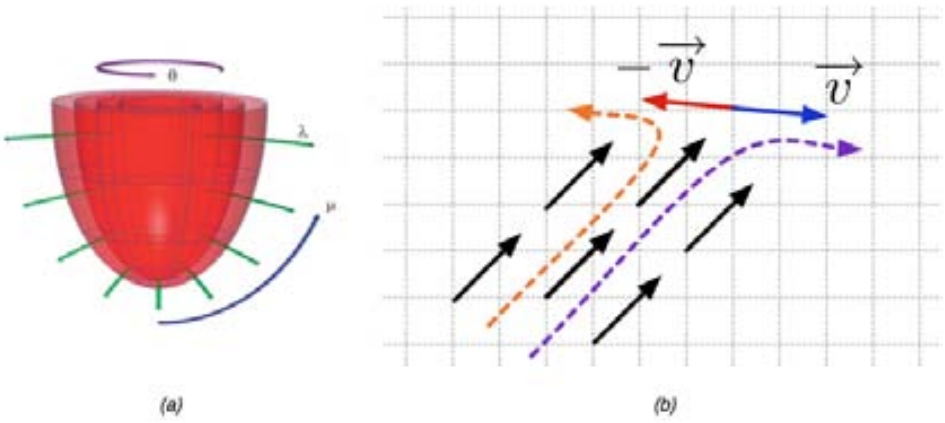

Figure 3.6: Mathematical model to describe left ventricular anatomy (a). This description may help to define local coordinate systems that ease the confrontation of ambiguities in the direction of water diffusion captured by DT-MRI (image from [52]). And a toy-schema highlighting the ambiguity presented by an opposed eigenvector (b).

The previous definition of streamline is inherited from the study of fluids. In that field, orientation of vectors stand for fluid stream directions. Thus its reconstructions

present no ambiguity. However, if we apply the former deterministic reconstruction using principal eigenvectors as the description of muscle, we will encounter obvious ambiguities (Fig. 3.7(a)) in the form of opposing fibers. The few extensively described approaches to solve this problem in the tractographic reconstruction of the myocardium are based on either local properties of the flux or parametric models of the heart. On one hand, local approaches as the one proposed by Rohmer [99] reverse the vectors encountered in the integration process if the angle between previous and current eigenvectors are great enough to consider them fliped (Fig. 3.6). On the other hand, the alternative is to use parametric models of the ventricles [51, 37] (Fig. 3.6) that allow to define local coordinate systems that will, in turn, help to arrange the eigenvector sign coherently.

From our point of view, the local approach enforcing local flow regularity might introduce suboptimal fibers not consistent with the global structure (see Figure 3.6). Furthermore, although parametric models provide a good solution to arrange orientation, they are usually restricted to the left ventricle by their complexity. Alternatively, in this work, **we propose a geometrical reorganization of the eigenvector field coherent to the ventricular anatomy**. In order to tho so, we apply a geometrical reorganization of the vector field using local coordinate systems coherent to ventricular anatomy and fluid mechanics.

Ventricular anatomy can be roughly described by means of a longitudinal axis and angular coordinates with respect to this axis on axial cuts (Fig. 3.2.1). Therefore, we propose an automatic definition of a reorientation axis just using geometrical analysis of such rough segmentation of the left ventricle. Given that the shape of the left ventricle could be succinctly described as a hemiellipsis, a definition of its long axis could be straightforwardly defined. We propose to mirror this structure into a resulting ellipsoid. Therefore, we can directly study this geometry observing it as a Gaussian process. We can characterize this shape by the geometrical analysis of the covariance Σ of spatial locations of all voxels v in the ellipsoid E:

$$\Sigma = \begin{matrix} \sigma_{xx} & \sigma_{xy} & \sigma_{xz} \\ \sigma_{yx} & \sigma_{yy} & \sigma_{yz} \\ \sigma_{zx} & \sigma_{zy} & \sigma_{zz} \end{matrix} \quad \text{where} \tag{3.19}$$

$$\sigma_{ab} = \frac{1}{N-1} \sum_{i=1}^{N} (a_i - \mu_a)(b_i - \mu_b) \tag{3.20}$$

$$\text{being} \quad \mu_d = \frac{1}{N} \sum_{i=1}^{N} d_i \tag{3.21}$$

where the expressions a_i, b_i, and d_i will represent specific references to x, y, or z Cartesian components of the ith voxel $v_i \quad E$. For its part, N stands for the cardinality of the set of voxels representing the ventricular cavity.

With this description, as in the study of tensors in DT-MRI presented in Chapter 2, we can obtain the eigenvectors of Σ that define the ellipsoid axes and magnitudes.

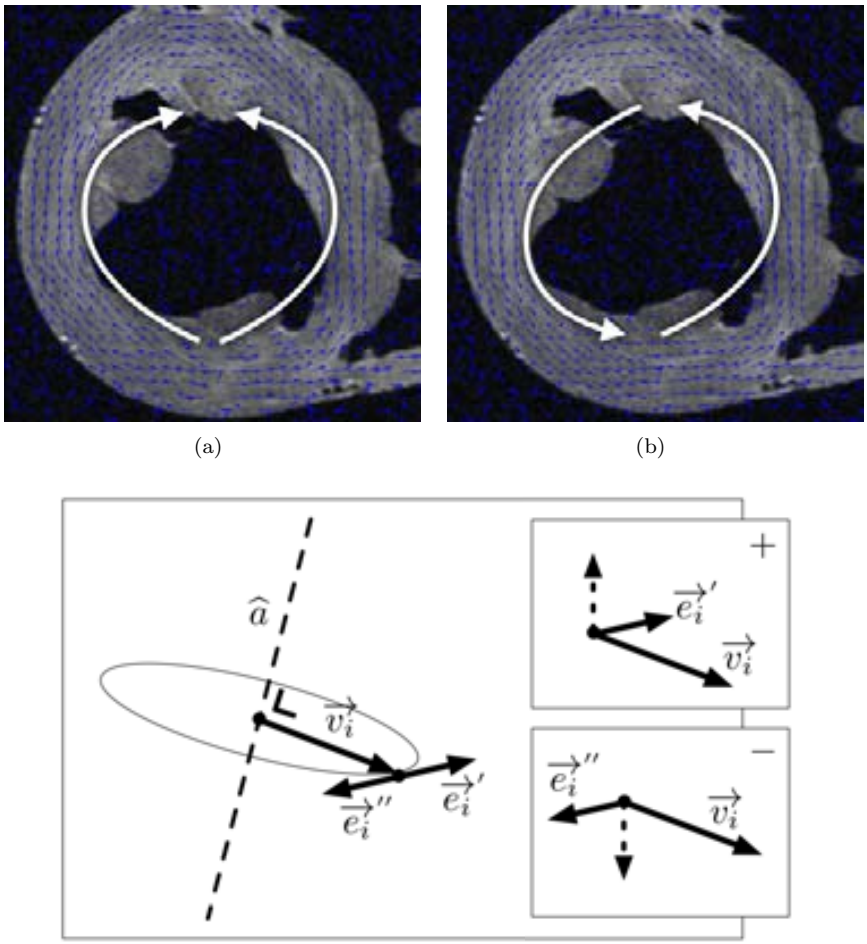

Figure 3.7: Solving DT-MRI orientation ambiguities for deterministic tractography. (a) Orientation of the vectorial field, (b) and reorganization on a radial basis. (c) Schema of our anatomical axis based reorientation.

The direction of the eigenvector with the larger eigenvalue will define the greater axis crossing this ellipsoid, and getting through the apex. If we recall that the apex is known to be devoid of muscular tissue, we can define this point being a safe crossing point for our reorientation approach. Hence, the previous definition can theoretically apply as our reorientation axis. However, from a practical point of view, this axis is not immediately adequate. The physical formation of ventricle cavities does not define a perfect ellipsoidal structure, thus the automatically computed axis may not cross the myocardium at that point. For that reason, we do an automated search of the apical extreme on the volumetric mask that defines left ventricle cavity segmentation

used previously. As defined in Algorithm 1, this search is performed starting from the inferior extreme of the mask (closest to the apex) by iteratively recovering horizontal (short axis) slices of the volumetric mask. In the resulting images we can look for the intersections with the region tagged as ventricular cavity and perform a centroid computation. The first existing centroid will define a plausible crossing point for our anatomical axis of reorientation. However, it is important to remark that in order to obtain more robust selection of this point, it has been empirically proven to be preferable to avoid choosing first intersections. To improve this search, we establish a threshold restricting the minimum area of an acceptable intersection.

Data: M, 3D mask of the left ventricular cavity
Result: p, optimal crossing point for anatomical axis

foreach *slice* s *in* M **do**
  $region \leftarrow Intersection(M\ s)$;
  $area \leftarrow Area(region)$;
  if $area > threshold$ **then**
    $p \leftarrow Centroid(region)$;
    break;
  end
end

Algorithm 1: Computation of the apex point to define an anatomical reorientation axis based on rough segmentation of the left ventricular cavity.

Now, with neither requiring a complex parametrization of the myocardial anatomy nor local regularity assumptions, we can use our anatomically defined axis to perform automatic reorientation of the principal eigenvectors to meet with the general requirements of the tractographic methodology. To perform this reorientation we will force the sign of the cross product between each vector v_i defined perpendicularly to the anatomical axis a and crossing the ith voxel in the anatomy, and the eigenvector e_i at such voxel (see Fig. 3.7(c)). Thereby, if we choose a positive sign to regularize, we will reverse all eigenvectors which cross product have negative result. We can intuitively describe this operation as making sure that all vectors are coherent to global axis of rotation. This procedure is automatic and applied to the whole anatomy ensuring valid organization of the resulting vector field to the fiber tracking methodology as pictured in Figure 3.7(b).

3.2.2 Seeding strategies

As we have seen in the general definition of our fiber tracking algorithm, a seed is the starting point of this tracking process. The disposition of seeds (usually referred as seeding) has an important part in tractographic reconstruction. Somehow, seeds will determine the fibers that will be reconstructed, and therefore, may be a crucial parameter to control in order to have satisfactory visualizations. Furthermore, as we identified in Section 2.3, one of our objectives is to define complete and valid

representations of myocardial anatomy. Is for that reason, that we will have to take into account an adequate seeding methodology to lean towards that objective.

The most naive seeding strategy would be assuming that each voxel of the anatomy should be a seed initiating a fiber tract. However, this may imply extremely intensive computations without offering special advantages, and including the disadvantage of an obviously cluttered representation. Thereby, most strategies will try to do a more sparse distribution. The most straightforward sparse alternatives include *structured seeding* and *random seeding*. In the case of structured seeding, we should use a regular grid to distribute seeds in the anatomy to reconstruct. Imagining this distribution in an environment where anatomy may present thin structures (as it is the case of right ventricular wall), it is easy to see that this strategy may not ensure a complete representation of the anatomy when choosing a sub-optimal spacing between seeds. As an alternative, random seeding imposes arbitrary distribution of seeds. This ensures that all parts of the anatomy are being treated equally no matter the density chosen before reconstruction, and thus, avoiding the former drawback. *Manual seeding* has also been considered in the research dedicated to the reconstruction of myocardial architecture [35, 34, 5]. This non-automatic approach has been chosen to set controlled areas of reconstruction, and therefore, to validate specific architectural formations. This is a choice that is common in tractographic reconstruction of the white matter where prior anatomical knowledge could be safely employed. However, it should be avoided whenever it is possible to ensure objectivity of the procedure in heart anatomy. This is why random seeding has become to be the most practical choice, even though many works fail to mention their approach to solve this problem. This oversight may come as a result of the favourable adaptability of integration methods. Even if seeds are incorrectly chosen, rest of the integration will fit correctly to the data. Enough density of the seeding could palliate its importance in tractographic visualizations. However, it is clear that choices like this cannot be neglected in an environment like medical research.

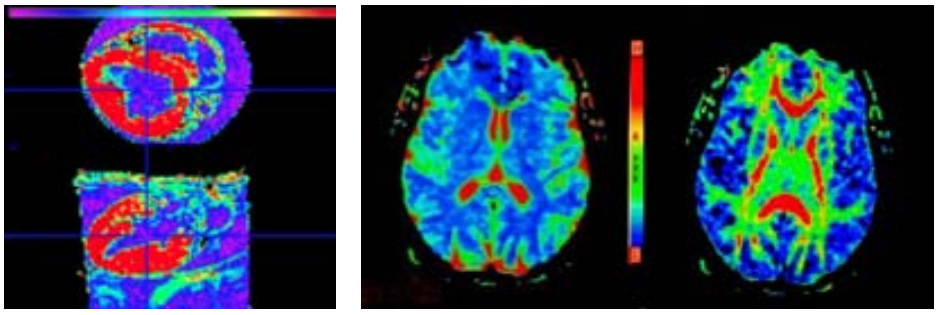

(a) (b)

Figure 3.8: Images picturing the stability of Fraction Anisotropy (FA) in the heart (a) and the brain (b). In contrast to the detail that FA offers to detect different structures in the brain, it is clear that the response of this biomarker in the heart is an stable parameter along the whole muscle.

Our first proposal to offer a refinement of randomized seed distribution was to combine this strategy with *fractional anisotropy* (see Chapter 2) inspired in its use for brain studies. Given the underlying properties of the biological tissue, this parameter could be seen as a characterization of consistency of the structural disposition of myocytes on a measured voxel. Thus, it could be employed to define the goodness of a seeding point. However, this measure in cardiac evaluation (at least for non-diseased tissues) is a quite more stable measure than in the brain (Fig. 3.8). In order to propose an actual improvement, we tried to find a similar indicator of spatial coherence of myocytes. With this measure rather than an intra-voxel indicator, we propose a new way to characterize coherence among neighbouring tissues. We have computed this measure as a local variance of muscular tissue directions in a neighbourhood of each voxel. For each voxel we have computed it as:

$$I_{coherence} = max(\sigma_{eig11}, \sigma_{eig12}, \sigma_{eig13}) \tag{3.22}$$

for $\sigma_{eig1i}, i = 1...3$ as the variance of the three components of the first eigenvector of the DT-MRI data in a $NxNxN$ cube centered at each voxel.

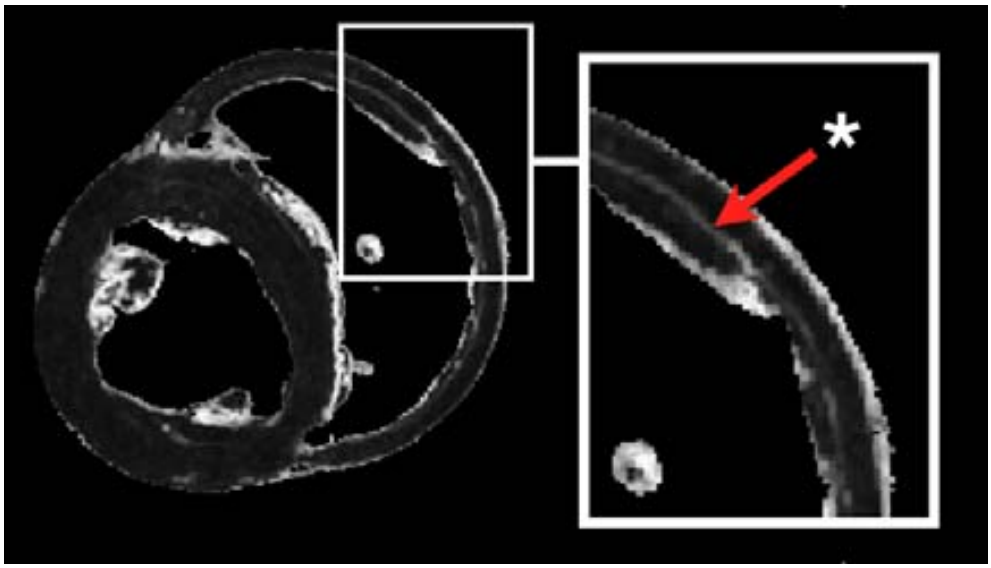

Figure 3.9: Representative slice of the volumetric output of the proposed measure of spatial myocyte coherence. It reveals clear differences of organization over the whole myocardium. Annotation (*) shows the separation of muscular populations in the right ventricle wall manifest in our coherency measure.

From a single slice of the volumetric data resulting of this process (Fig. 3.9), we can identify evident differences in the myocardial tissues. At a first glance, we can see that high coherence indexes are common to many areas of the heart (as it was in the case of fractional anisotropy). But more surprisingly, there are many specific localizations with poor coherence indexes. Some of these low-coherence regions do

not discover new heart architectural properties. For example, the wall of the right ventricle shows a thin low-coherent region in the middle. This is the consequence of the well-known existence of two layers with opposing fibers that form this myocardial wall (Fig. 3.9(*)).

The contributed seed selection methodology based on muscular tissue coherence is our response to achieve robust tractographies. It is not a game-changing strategy, but it offers the certainty of a more robust selection of data at the starting point of streamlines. It is not statistically relevant for streamline fitting, but it is important for any low level visual analysis of the reconstructions. Our final selection is based on a random picking of seeds in the most coherent areas consequently. In this way, we are avoiding the possible errors originated by purely random selection, as well as providing a complete reconstruction of the myocardium.

3.2.3 Finalization criterion

Finally, each fiber tracking reconstruction needs a finalization criterion. Well known choices include truncation by estimated fitting error in the integration methodology, plausible fiber length or curvatures, as well as the use of previously mentioned biomarkers such as fractional anisotropy.

In our development we considered many of those alternatives. On one hand, as we discussed earlier in seeding procedures, an indicator as FA offers a very stable value along the myocardial wall. Thus, we discarded its use as a finalization criterion, given that this measure presents no crucial information of the anatomic formation of the muscle. On the other hand, bearing in mind that we do not want to introduce any kind of artefactation to the reconstruction procedure, we decided to discard options that cut fibers by their length or abrupt angulation. As far as we know, these factors have not been documented in the surgical and histological study of the myocardium and we cannot impose this kind of restriction or assumption. However, it is important to remark that in order to limit computational consumption, length of fibers is actually being restricted in our tractographic reconstruction. However, the maximum length is big enough to avoid imposing structural restrictions.

The only strict termination criterion established in our methodology is the standard Runge Kutta criterion, the use of numeric fitting error in the integration methodology. This measure evaluates the goodness of curve approximation to the vector field. Imposing a more strict termination criteria helps in terms of confidence of the reconstruction, since only the best fittings will be presented with such restriction. Besides, this strategy helps to diminish noisy reconstructions originated on thin parts of the muscular anatomy of the heart, as it is the case of the auricles. Thus, this criterion helps to achieve less cluttered visualization of ventricular anatomy. Moreover, later we will stablish a measure of fiber confidence that will help us to significantly improve this results.

3.3 Embedding tractography in a multi-resolution framework: reconstruction and visualization details

In the previous section we introduced our specific tracking methodology (Section 3.2.1) as well as our approach to set parameters as the seeding strategies (Section 3.2.2) and finalization criteria (Section 3.2.3) to obtain reconstructions of DT-MRI data of the myocardium. Now, we are going to analyze the main details of this application to the visualization of this reconstructions, doing a special remark on its application to the multi-resolution framework presented in Chapter 3.1.

Full-scale tractography: Originally in this chapter we introduced myocardial tractography as an aggregation of fiber tracks reconstructing the discrete captures of biological architecture by means of diffusion tensor imaging. However, from a visualization point of view, its representation could be performed further than a representation of these curves in the space. The common methodology involves presenting fiber tracts by means of warped tubes. These structures (usually known as *streamtubes*) offer richer and more versatile visual representation of this kind of anatomical structure.

General scale of reconstruction: In order to procure comparable reconstructions at several scales of the pyramidal decompositions we should choose a re-scaling strategy. The first choice is to consider the re-escalation of lower pyramidal scales to the original proportions in order to reconstruct. However, this strategy implies offering a plausible super-sampling of reduced scales, which in turn almost certainly implies the introduction of an extra interpolation step that we want to avoid. A post processing of reconstruction can offer this reconstruction on a safer environment. We can process reconstruction at the native size of lower scale where any processing is better defined. Further, an escalation of resulting fiber tracks does not impose any assumption about the interpolation of the eigenvector field; it is a simple augmentation of a solid structure. Therefore, in our methodology we will scale reconstructions in order to provide comparable outputs on the scale space.

Representativity of a single tract in the scale space: At this point, it should be definite that each level of detail should be able to represent different ammounts of information. This should be clear on its reconstruction and we made it possible by representing fiber tracts on an inverse scale. This meaning that lower scales will be represented by thicker tubes. Otherwise, higher scale reconstructions will be represented by thinner tubes.

Seeding in the scale space: As a result of the previous representation, a simple consideration should be made about seeding too. As we go to lower scales, a single stream is a representative of more streams in their neighbourhood. Therefore, if we used the same number of streams at each level, the lower scales will become obviously cluttered. Our selection is to offer a number of seeds relative to the size of data. As we will see in Chapter 5, using around one hundred seeds per million of voxels applied as a good and general rule of thumb in our work.

Parameters of integration: As we choose different scales in the pyramidal decomposition we should be aware that parameters of integration like the integration step. All them could be proportionally scaled safely to meet with scalar reductions of DT-MRI data.

Color coding of streamlines: As highlighted in this chapter, another important issue about tractographic visualization its related to coloring. Color coding of streamlines could offer more effective visualizations of the anatomy. Earlier works managed to define useful color coding relative to the transverse (longitudinal) fiber angle. This provides visual cue to separate ascending from descending fiber populations, easing the interpretation of major formations in cardiac anatomy. However, as stated earlier, these methodologies often rely on a global reference frame, that meaning that anatomical alignment with Cartesian axes is assumed in order to compute color coding as a function of these axes. Alternatively, having in mind to provide a general and automated solution for this problem, we sought to use our anatomical axis presented in Section 3.2.1. This axis crossing heart's anatomy through the left ventricle, in accordance to rough anatomical segmentations, can provide a anatomically coherent (global to the whole myocardium) reference frame to define architectural fiber properties.

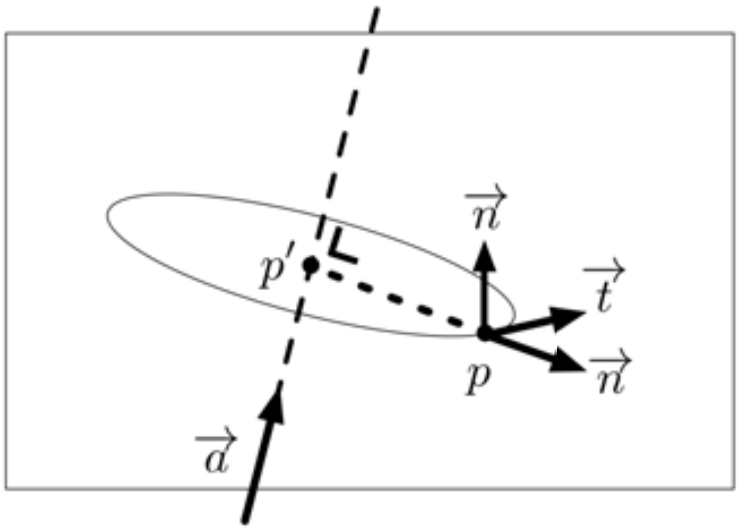

Figure 3.10: Schema of the definition of local coordinate systems for the computation of transverse fiber angles. This measure serves for posterior color mapping.

This can be achieved with local coordinate systems at any point of the heart anatomy using such anatomical axis. The basis of this coordinate system (see Figure 3.10) at a given point p of the anatomy is built with:

1. The vector $\vec{n}$, unit vector that represents direction from p to its orthogonal projection p' into the anatomical axis $\vec{a}$,

2. t, unit vector defined as the positive tangent of the circle perpendicular to a that passes through p with center in p ,
3. and b, the result of the cross product between t and n , coincident with the anatomical axis direction.

Using the relation between the fiber and such local coordinate references we can provide fully automated characterization of axial and longitudinal angulations of fibers at any point of the ventricular anatomy. Besides, this can be part of a fully automated framework, independent of the capture specificities that may vary between captures, anatomies, etc.

Ease of exploration: With the former strategy we can obtain valuable information for visual combination with tractographic reconstruction. In this thesis, further than that, we propose the introduction of powerful tools for the navigation of this features providing different color mappings that can add valuable information to the identification of muscular formations. For instance, that includes fine tuning of these color maps to describe longitudinal (transverse) orientation of fibers in order to convey different views of the anatomical structure. The first proposal is to use binary color schemes, this should be capable to highlight principal ascending of descending populations as stated in earlier works [125, 99]. We also offer the personalization of color mappings over a distribution of color based in linear and non-linear hue variations. These schemes allow easier evaluation of the different angulation degrees over neighbouring fibers. An finally, we have also introduced the suppression of certain fibers by fiber angle filtering using transparency coding, that may help to explore the inherently cluttered representations of full-scale tractographies.

Chapter 4

Validation framework

Nature is simple, scientists are complicated.

Dr. Francisco (Paco) Torrent-Guasp

One of the current biggest challenges of tractographic reconstruction and visualization of biological tissues both in the heart and the brain lays in its validation. A stable and regular reconstruction may create a false impression of precision due to diverse sources of error. Undoubtedly, this problem also applies to the tractographic methodology presented in this thesis, especially when applying novel pre-processing strategies to achieve multi-resolution tractographies. Hence, it is of paramount importance to provide robust information about this reconstruction. In this chapter, we will present our theoretical approach to **validate the use of a multi-resolution strategy** and our resulting statistical framework to provide **new measures of confidence for tractographic reconstruction**.

First, we will analyse our methodology s potential sources of error in order to propose an evaluation strategy to attain our objective (Section 4.1). Second, we will focus on local and semi-local evaluation from an image (volume) analysis point of view (Section 4.2). Third, we will provide a global analysis of the multi-resolution tractographic reconstruction by means of the geometric study of streamlines (Section 4.3). Fourth, we will present a novel approach to compute tractographic confidence measures based on our previous geometrical study (Section 4.4). Finally, we will deepen into the combined visualization of confidence measures and multi-resolution tractography (Section 4.5).

4.1 Keypoints for multi-resolution tractograpy validation

In Chapter 3, we introduced a methodology for multi-resolution tractographic representations. Our focus focus was to provide better interpretable representations of the muscular architecture of the heart. To the best of our knowledge, this is an unprecedented methodology to represent DT-MRI data and perform tractographic reconstructions. Hence, no evaluation framework has been still established to date.

Briefly, our methodology proposes a pre-processing of diffusion data to obtain a multi-resolution model. This model is achieved by means of an iterative process of filtering and subsampling of data as we pictured in Figure 4.1. Subsequent to this pre-processing stage we use the resulting different levels of detail to reconstruct fiber tractographies. Reconstructions performed over lower resolution data should offer several levels of abstraction of the heart muscle.

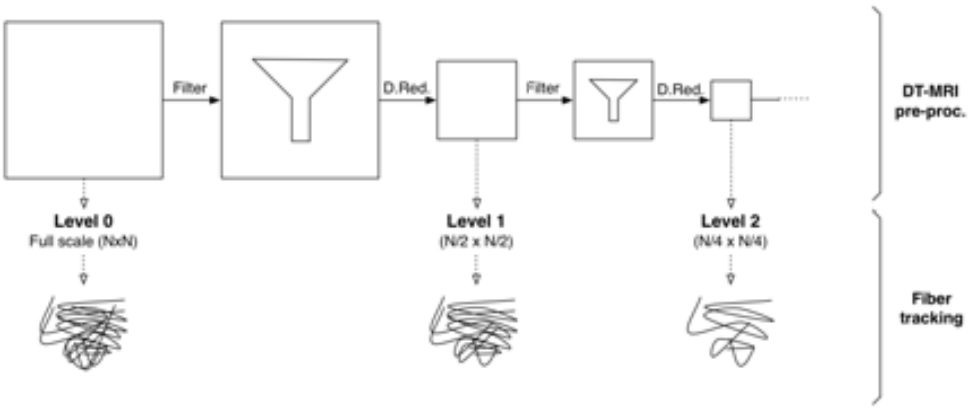

Figure 4.1: Diagram of the stages of multi-resolution pre-processing of data and fiber tracking reconstruction for a multi-resolution tractograph model.

We are conscious that in this process we may introduce several errors or alterations of the anatomy. For this reason we need tools for its evaluation and validation. During the process of this thesis we have explored different evaluation indicators for this evaluation, and we have come to establish a detailed framework for this kind of application.

In a general overview of the multi-resolution methodology we can find two critical points that will be important from now onwards. On one hand, we have to take care of the possible **alterations of anatomical information in the filtering step for each of our specific filtering methodologies**. On the other hand, we have to take into account the possible **error and data loss introduced in the decimation of resolution**.

4.2 Local image analysis

The methodologies of this work are based on partial information of the DT-MRI. To do the representation of cardiac anatomy we only need the volumetric vector fields defined by the principal eigenvector of the diffusion tensor obtained from diffusion MRI. In this section we are going to evaluate our methodologies from an image analysis point of view over this data. On one hand, we will provide a discrete indicator of the effects of our processing based on the study of variations of the vector field. On the othe hand, in order to go further from the limited scope of the former evaluation method, we will introduce a methodology based on the evaluation of preservation of anatomical features we can be detected in the input data. This is an image analysis approach that aims for further detail on the effects of multi-resolution pyramids applied to diffusion data.

4.2.1 Angular precision

Our first approach for an evaluation of the effects of our processing methodologies requires an evaluation of variance between structures presented in this data after its application. The need for similarity/variance evaluation methods among structures captured in DT-MRI data is widely known in the literature [3, 98]. Even though, these techniques do not apply directly to our specific environment. Usually, these measures require comparison over the complete shape of the tensor, or biomarkers extracted from it such as fractional anisotropy or mean difusivity. The reduced set that the primary eigenvectors define leaves a narrower spectrum of possibilities. However, our application is not the first to rely solely on this data alone. In these applications the use of pair-wise angular differences among volumetric datasets has somehow become an de facto standard for this kind of evaluation. For example, it is typically applied to measure variance in volumetric registration or comparison of models of cardiac captures [94, 88, 72, 69].

A measure like this can offer interesting information on the spatial affectation (Fig. 4.2(A)) of a given procedure, as well as the possibility to obtain statistical insight of how it affects data (Fig. 4.2(B)). We propose to evaluate each methodology by observing statistical distribution of angular differences. Nevertheless, it is important to remark that the pair-wise nature of this technique is not well defined for the evaluation of data at different scales as our multi-resolution methodology provides. In this process, filtering can be seamlessly evaluated. Alternatively, each reduction stage will require an adequate strategy to pair data in order to realize the evaluation. If we revisit the tractographic integration methodology we can find a suitable strategy to do such adaptation. The tractographic integration considers the discrete input vector spaces as continuous throughout linear interpolation. Therefore it is possible to apply this strategy to allow evaluations across scales in multi-resolution models. We will apply linearly interpolated upscaling of lower detail levels of the pyramid in order to enable the pair-wise comparison. It is important to remark that this strategy will merge the effects of scale reduction and interpolation in the final indicator.

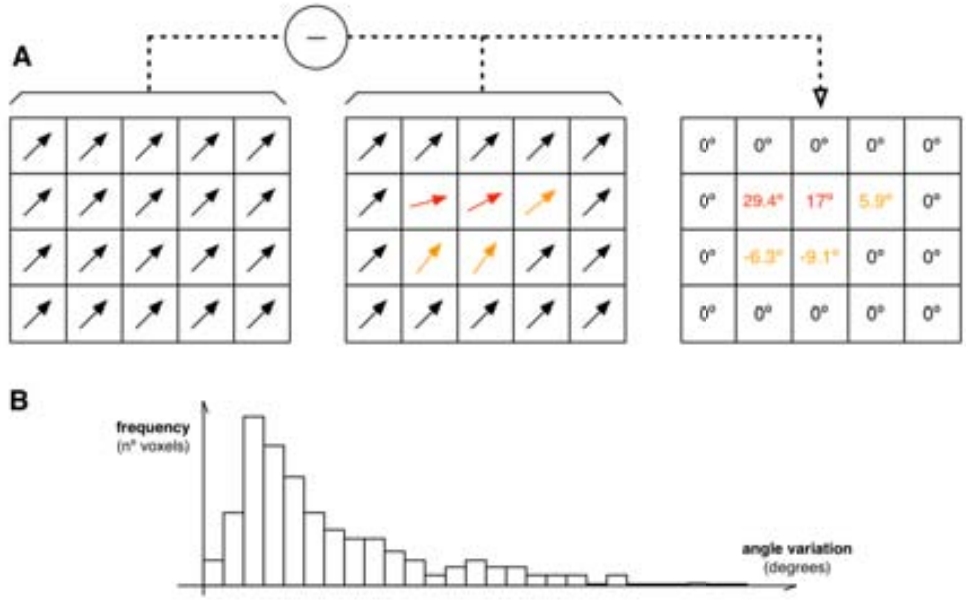

Figure 4.2: Study and statistics based on angle difference between vector fields. (A) Shows a toy example illustrating how this measure can bring local information about variation. (B) Hypothetic histogram of angular variation between two vector fields. This graph can show frequencies of angle variation between two volumes denoting its general tendencies.

4.2.2 Preservation of local features

The previous approach can be a usefull evaluator of local effects over multi-resolution data. However, this local detail may be limiting to obtain proper indicators of the general effects and validity of this processing to heart anatomy. In order to incorporate anatomical detail, we considered a feature based approach of evaluation. This method aims to provide a semi-local indicator based on detectable anatomical features in the input data. The new alternative appears from the novel measure of myocyte spatial coherence presented in the previous Chapter of this thesis. This measure has exhibited important features of heart anatomy that we consider of great significance. Our new evaluation approach will lay on measuring how satisfactorily this features can be preserved along multi-resolution processing.

In order to develop a well fitted evaluation methodology to this problem, we first have to **automate accurate identification of the detectable populations** from our coherence study. A superficial analysis of our coherence study exhibits two main populations of local fiber distributions along the myocardial mass. We can find distinct highly structured and unstructured groups. A methodology like bimodal Otsu thresholding can automatically isolate the populations on many samples (Fig. 4.3(a)). However, it is not reliable for all of them. Otsu offers accurate clustering for

all specimens in the highest level of detail of the pyramidal representation (Figure 4.3(b)). However, differentiated myocyte populations can become mixed in lower levels depending on the applied filtering technique. Even though, Otsu binarization provides obtain two virtual populations (Fig. 4.3(c)). Hence, a better strategy should be developed.

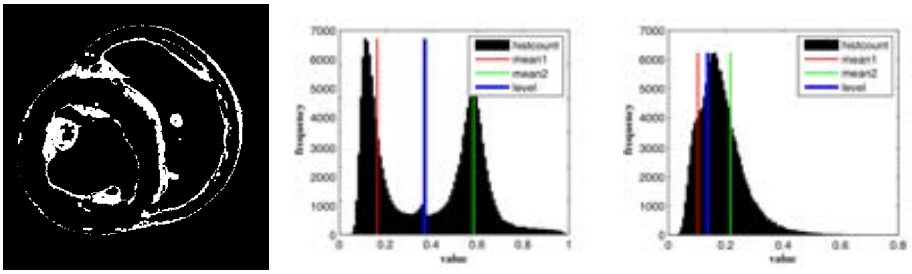

(a) (b) (c)

Figure 4.3: Otsu's processing of input data (a), and its behaviour as a measure of separability in a advantageous (b) or disadvantageous (c) distribution of information.

Without leaving histogram analysis, our proposal is to use a more complex statistical measure. **(A) Normal distribution fitting through a *gaussian mixture model*** (GMM). This technique allows us to represent sub-populations on the density distribution formed by the histogram computed on each of our samples. From this computation, we can manage to obtain enough information to **(B) differentiate if populations can be properly isolated**. Or, in the opposite way, differentiate if populations have been mixed and feature preservation is not correctly accomplished.

A Adjust of the Gaussian Mixture Model

Gaussian mixture adjustment has been implemented through *expectation maximization* (EM). In a nutshell, EM is a generic iterative technique for the estimation of parameters in statistical models to achieve its maximum likelihood in arbitrary distributions. In the present case, we will unmistakably use normal distributions to build the statistical model. And the objective is to fit them to the input data which is the density distribution of our images.

The operation is based on an iterative two-phase algorithm:

1. **E-step:** In this step, the current model (means and covariances of the candidate gaussian distributions, also known as components) is known. But, the assignment of individual input data to a given component is not. So, this data will receive a probabilistic assignment (hence the "expectation" naming) to the assumed model (p_{nk} in equation 4.1).

$$p_{nk} \equiv P(k \quad n) = \frac{\mathcal{N}(x_n \quad \mu_k \ \Sigma_k)P(k)}{P(x_n)} \tag{4.1}$$

given

$$\mathcal{N}(x_n \quad \mu_k \ \Sigma_k) = \frac{1}{\Sigma_k \quad \overline{2\delta}} e^{-(x_n-\mu_k)^2/2\Sigma^2}$$

$k = 1 \quad K$ gaussians $n = 1 \quad N$ data points

$P(k)$ population fraction in k

$P(x_n)$ model probability at x_n

μ_k the K means $\Sigma_k$the K covariances

2. **M-step**: After that, this step supposes that previous assignment of input data is correct. But, now, the model is unknown. Consequently, new parameters (μ_k, Σ_k, and $P(k)$ in the equations 4.2, 4.3, and 4.4) of the model will be computed to maximize (hence the maximization naming) the overall likelihood given the current assignment.

$$\mu_k = \quad p_{nk}x_n \quad p_{nk} \tag{4.2}$$

$$\Sigma_k = \quad p_{nk}(x_n - \mu_k) \otimes (x_n - \mu_k) \quad p_{nk} \tag{4.3}$$

$$P(k) = \frac{1}{N} \quad p_{nk} \tag{4.4}$$

The initial parameters for this process must be ascertained. In our experiments, two main strategies have been chosen with almost identical quantitative results:

1. Chosing a random classification of input data and compute an initial estimation of μ_k, Σ_k to fit this distributions.

2. Clustering input data with k-means [78] and estimating μ_k and Σ_k fitting this distributions.

Additionally, a valid finalization criteria must be given. Our choice has been to monitor sample assignment waiting for stable labeling. However, even when convergence is guaranteed in EM methods, we cannot know how many epochs it may spend to achieve this objective. In this manner, the implementation includes an empirically chosen cutoff at 500 cycles.

B Class separability

We can benefit from the use of GMM to get a precise class identification through the fitting of a set of normal distributions. Regardless of that, the ability to distinguish different classes with the mixture model does not guarantee an unambiguous separability among them. Figure R shows two distinct scenarios of real fittings to distributions extracted from our sample. Although both achieve an accurate fitting, in the first example the two most prominent classes can be more easily split than on the second.

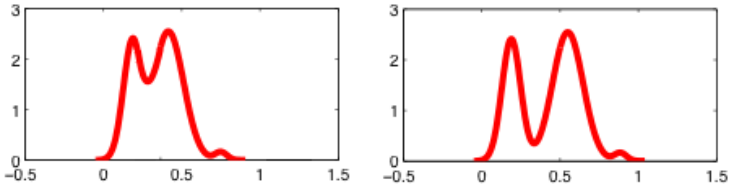

Figure 4.4: This gaussian mixture fittings of real distributions show how the separability between classes can be different. This separability should be quantified in order to know when classes are really separable or not.

We want to measure this separability. Already available parameters as distribution means and variances are difficult to relate on their own. For that reason, we have chosen Fisher's linear discriminant (eq. 4.5) to compute this measure.

$$J(w) = \frac{\mid \mu_1 - \mu_2 \mid^2}{\Sigma_1^2 + \Sigma_2^2} \tag{4.5}$$

where μ represents the mean, Σ the variance of each adjusted gaussian, and subscripts denote the classes being compared. This index is commonly used in linear discriminant analysis to characterize or separate classes. In this context, it is intended to be used as a criterion to maximize the intra-class scatter while minimizing the inter-class scatter. It can be seen as a signal-to-noise ratio for the class labeling. We can take advantage of this index ($J(w)$) as an indicator for our application.

4.3 Global geometric analysis

In the previous section we have presented evaluation proposals from an image analysis of our multi-resolution schema applied to diffusion MRI data. These proposals can achieve a local or semi-local point of view of the effects of the reduction of resolution. However, the objective of this PhD thesis goes further than that. Our primal objective is to provide a validated multi-resolution tractographic methodology for the study of the architectutal structures in the myocardium. The previous validation methodologies can be seen as a first approach to evaluate the pre-processing stage. But now we

want to offer a methodology to evaluate the performance of our methodology in the global geometric domain of tractographic reconstructions.

Any fiber tract that is part of a tractographic reconstruction can be understood as an independent curve. A curve can be geometrically descrived by several parameters than can help us to perform comparisons and determine similarities. Ideally, from any given streamline we can provide comparisons to its neighbouring fibers, to homologous reconstructions in alternative specimens, or even comparisons between the several streamlines resulting from diferent methodologies (or tunings) of data and integration techniques. These are no infrequent applications, in fact, similarity evaluation among streamlines is common in the literature. Mostly these evaluation methods have been focused in fiber tract clustering and comparison method [18, 89, 84, 82]. Solutions to this problem include from the use of euclidean metrics to different geometric heuristics that include, for example, comparisons driven by end-point distance between fibers originating nearby.

Taking into account our particular objective to provide a methodology to evaluate the tractographic multi-resolution model outcome we should consider the problem from a rather different point of view than direct fiber comparison. We face different scales to compare and this will imply important differences in order to provide evaluation metrics. It is straightforward to see that the purpose of the multi-resolution model is to *condensate* neighbourhoods of fibers obtaining a more contextual and meaningfull representation. When a tractography is *summarized* we can say that each fiber tract in this summary must be a representative of several streamlines in the more detailed levels of detail. Our main problem is then more of an evaluation of *representativity* than a straightforward similarity measurement.

Bearing in mind our earlier *coherence* evaluation, we can think of this evaluation as a *coherence* study extended to the whole geometry of the streamlines rather than local information. We want to obtain indicators of geometrical coherence in the neighbourhood of streamlines. This should help us evaluate the quality of representativity of the fiber tracts versus the original reconstructions in full-scale and unprocessed data, which is assumed to be our reconstruction of reference.

We want to pursue this evaluator to analise how our pre-processings of data affect integration methodology. In this way we want to be able to find the best fitted methodology to provide validated multi-resolution tractographies. We propose a global shape evaluation metric of neighboring groups of streamlines. This method has been thought to be independent from diffusion data and specific tractographic reconstruction methodologies. Now we are going to present the different parts of this methodology. First we will define streamline neighbourhoods, second we will solve fiber correspondence, and finally we will define a descriptor to evaluate geometrical coherence of fibers.

4.3.1 Definition of context

Homologously to a random seeding procedure, we choose random locations over the whole myocardium anatomy to build a set of contexts C. Each context C_i represents the center of the neighboring area that constitutes this context (see Fig.4.5). Each neighboring area will be composed by a set Z_i of streams. Those streams will in turn be defined as the fiber tracts δ_j reconstructed taking each S_j location in the set Z_i as their seeding point. We define S_j locations of a given C_i context as

$$S_{j=1:8} = \begin{pmatrix} C_i^x \pm E/2 \\ C_i^y \pm E/2 \\ C_i^z \pm E/2 \end{pmatrix} \tag{4.6}$$

where x, y, and z stand for Cartesian locations in anatomical units, and E is defined by minimum voxel size in diffusion data. We specify this configuration as a rule of thumb in order to conform context size to the resolution of data. However, the definition of contexts is not limited to this concrete definition. Selection of contexts should be flexible enough to fit to any other seeding procedure and disposition of stream seeds inside the neighboring area. For example, tractography methods independent of track origins may need to find these contexts sorting streamlines as proposed in similar scenarios in the past [19].

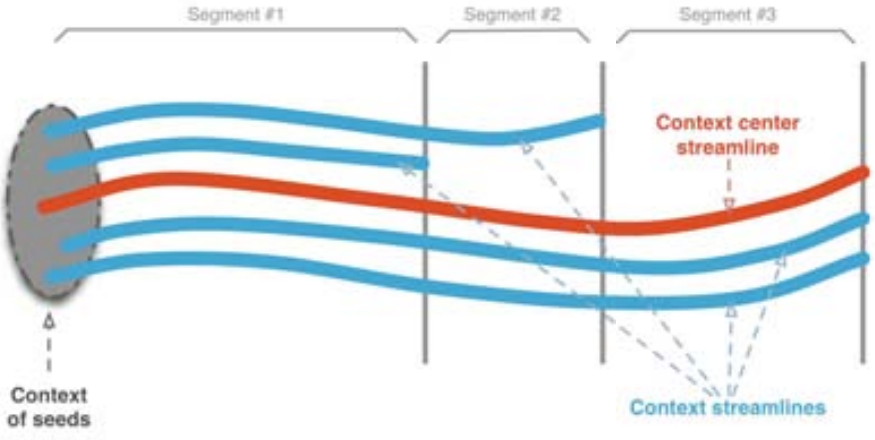

Figure 4.5: Diagram of context formation. This example shows how from a context of seeds (undefined shape for illustration purpose) generates a context of streamlines. This context is not be represented by all streamlines in all its length. Thus each "segment" represents maximal groups of streamlines at different lengths.

The center of each context will be the seed of what we call the "context representative". This is the stream that will be evaluated to assess its capacity as a representative of the complete context.

Another destacable issue about the formation of context is related to its leght.

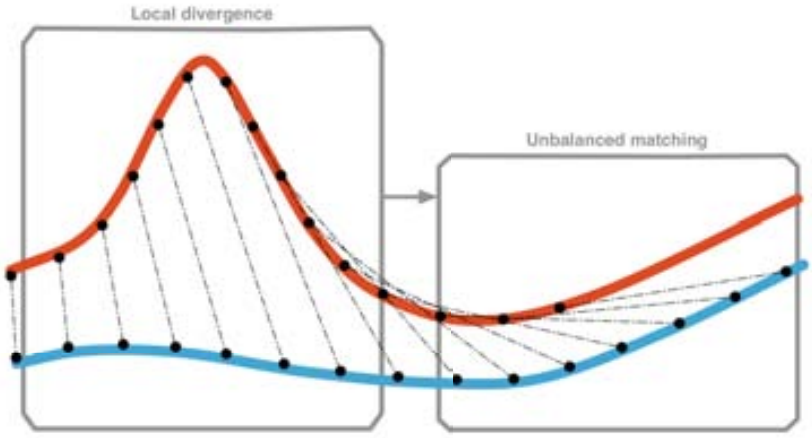

Figure 4.6: Artefact from determining correspondences between fibers based on arc-lenght locations: A local divergence of fiber tracts in a context vicinity can lead to unbalanced matchings in posterior evolution of their paths. However, we take advantage of that bias in our confidence measure.

Due to termination criteria, not all fibers reconstructed on a same context will be reconstructed with same lenght. We considered the creation of virtual "segments" to define maximal leghts covered by maximal number of streams as shown in Figure 4.5. The first segment will have full representation of the context. The rest of those segments will present inferior representations and may cause less robust estimations.

4.3.2 Definition of correspondence

In most cases, streamlines are computed using adaptive integration methods and present unevenly distributed points. This difficults to stablish a seamless correspondence among fiber tractes. Therby, we first obtain a more flexible definition of these curves by arc-length parametrization (eq. 4.7) of streamlines fitting (in the least squares sense [10]) data with b-spline curves. This parametrization allows us to compute infinitesimal descriptions of curves.

$$t \mapsto \mathbf{R}(t) \tag{4.7}$$

After that, the first step towards a descriptor of fiber similarity is to introduce how to define spatial correspondences over streamlines. This has been a recurrent topic on related research [20, 104, 59, 90, 11, 40, 102, 19]. In this work, we will define the correspondence based on arc-length matching of streams in each context. We benefit from our parametrization to resample contexts based on a custom defined arc-lenght parameter, and this will be used as a the correspondence between curves.

This matching heuristic could present unbalanced matches (Fig. 4.6). Some of

the previous works in the literature pointed this limitation and already proposed alternatives. However, we take advantage of this problematic. Contexts that present such offset could be almost certainly considered as poor contexts. This offset will tend to cause increased error ratios and help to discard those contexts. This heuristic applied in our framework is likely to help reducing false negatives even though that might increase false the positive ratio. Nevertheless, this is a reasonable strategy looking for a confidence metric.

4.3.3 Context descriptor

A $\mathbb{R}^3$ curve could be defined with its curvature, torsion and a Cartesian location. We use this parameters as a basis to generate context descriptors.

Firstly, in order to obtain these variables, we define Frenet-Serret frames (Eq. 4.8) along every t $R_j(t)$ parametrized streamline starting at the formerly defined S_{ij} seeds of each context C_i. Secondly, with that information, we compute curvature and torsion as differential variations of Tangent and Binormal vectors (Eqs. 4.9-4.10).

$$T(t) = R\,(t) \qquad B(t) = R\;(t) \qquad N(t) = T(t) \times B(t) \tag{4.8}$$

$$\kappa_R(t) = \;T\;(t)\; = T\;(t) \cdot T(t) \tag{4.9}$$

$$\epsilon_R(t) = -B\;(t) \cdot N(t) \tag{4.10}$$

Frenet-Serret frames could be unstable in front of inflection points, and thus the curvature and torsion functions. In order to overcome this hurdle, we propagate a custom Normal vector at $t = 0$.

After these computations, we have formulated three independent indicators to compute curve similarity on the contexts. Looking for an evaluator of general stability, we introduce a three-dimensional descriptor $\bar{D}_i$ (Eq. 4.11) for each context C_i based on this indicators. This descriptor has been built with the standard deviation of curvature (Eq. 4.12) and torsion (Eq. 4.13) errors, as well as the mean Euclidian distance (Eq. 4.14) versus the context-representative curve γ_i (Eq. 4.17).

$$\bar{D}_i = \begin{matrix} std(d\kappa_i) \\ std(d\epsilon_i) \\ mean(dPos_i) \end{matrix} = \begin{matrix} \sqrt{\frac{1}{d\kappa_i}\sum_{j=1}^{d\kappa_i}(d\kappa_i(j) - \mu_{d\kappa_i})} \\ \sqrt{\frac{1}{d\tau_i}\sum_{j=1}^{d\tau_i}(d\epsilon_i(j) - \mu_{d\tau_i})} \\ \frac{1}{dPos_i}\sum_{j=1}^{dPos_i} dPos_i(j) \end{matrix} \tag{4.11}$$

$$d\kappa_i(t) = \sum_{j=1}^{Z_i} \kappa_{\gamma_i}(t) - \kappa_{S_j}(t) \tag{4.12}$$

$$d\epsilon_i(t) = \sum_{j=1}^{Z_i} \epsilon_{\gamma_i}(t) - \epsilon_{S_j}(t) \tag{4.13}$$

$$dPos_i(t) = \sum_{j=1}^{Z_i} d(\gamma_i(t)\ S_j(t)) \tag{4.14}$$

$$where \quad d(p\ q) = \sqrt{\sum_{d=\ x,y,z} (q_d - p_d)^2} \tag{4.15}$$

For each descriptor computation, t is defined in the whole arc-length of the streamlines in each context. This length has been limited to the smallest streamline (first segment) in each context to ensure complete context comparability and robustness.

Several statistical measures have been considered to build the descriptor. The choice suggested in Equation 4.11 has been conceived to offer enough flexibility to classify consistent contexts presenting mild divergence or convergence. It is a general estimator of context coherence. Alternatively, the use of the maximum for each of the distances (Eqs. 4.12-4.14) is a replacement that can help to define a more strict and sensitive descriptor.

4.3.4 Evaluation metric

Based on the former context descriptor we want to build a metric to designate reconstruction confidence as well as the statistical relevance in the distribution. For that purpose, we propose the use of a Mahalanobis distance based metric. We define a M_i metric for each C_i context as

$$M_i = \sqrt{(\bar{D}_i - \mu_D)^T \Sigma_D^{-1} (\bar{D}_i - \mu_D)} \tag{4.16}$$

where $\bar{D}_i$ are our 3D context descriptors, and μ_D and Σ_D stand for the mean and covariance of the complete distribution of context descriptors D.

Mahalanobis distance accounts for axis scaling automatically as well as covariance between variables. On a general $\mathbb{R}^3$ space, samples with equal Mahalanobis distance lie on an ellipsoid representing equal similarity to the mean of the distribution. It could be seen as an univariate metric which makes it adequate to define an easy user customizable input parameter.

4.4 Confidence of tractographic reconstructions

As stated in Chapter 2, many fiber tracking techniques (as the deteministic approach used in this thesis) may be negatively affected by many factors. These factors include noise in th input signal and errors or limitations of the integration method

itself (Fig. 4.7(a)). These issues may produce systematic uncertainty on the quality of reconstruction to represent biological structures that should be unequivocally represented.

Many researchers have introduced alternatives or improvements to provide confidence measures to their specific application. In general, a good confidence indicator has been understood as how an streamline represents an underlying architecture. Most approaches focus this measure to evaluate that a fiber is not under uncontrolled variations introduced by the previously mentioned altering factors. However, in the study of architectural formation of the muscular anatomy of the heart, we think that this measure should be understood differently. As far as we know, in this environment we deal with more rough architectures than in the study of brain. Muscular aggregations are relevant when well coupled. Therefore, we understand confidence also as a measure of robustness for the fibers being reconstructed. In other words, confidence should measure if a fiber represents the underlying structure robustly, but also should represent how relevant is such anatomic structure (Fig. 4.7(b)). Both measures can be achieved at the same time by studying the coherence between neighbouring fibers. A measure that studies spatial coherence will be able to capture any kind of occasional and unpredictable behaviour produced by noise or other integration factors.

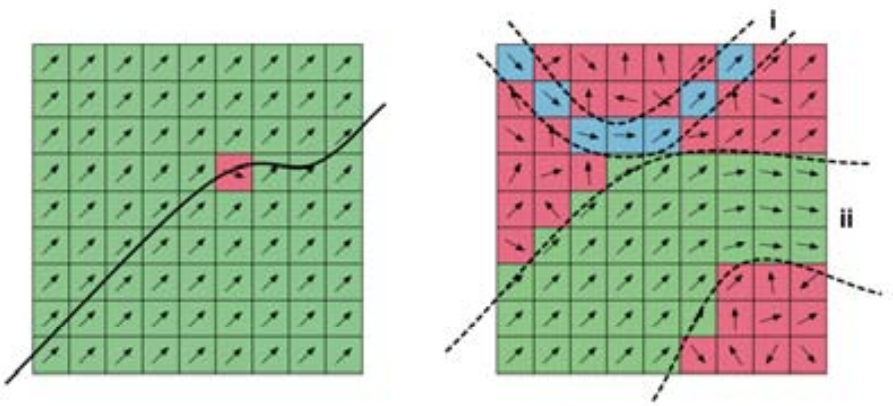

(a) (b)

Figure 4.7: Illustrative toy-diagrams of the effect of noise to fiber tracking (a), and relevance of anatomical structures (b). In the later diagram, we exemplify that two streamlines can have different anatomical relevance. An streamline reconstructing region (i) will be less relevant and more prone to uncertainty than a central streamline in region (ii).

In the previous section we have introduced an evaluation strategy to study neighbourhoods of fibers in order to provide general indicators of the contextualization power and validity of our multi-resolution tractographic reconstructions. However, we will now show that this kind of measure will not serve for this sole objective. We have seen to use this methodology to obtain generalized description of streamline

confidence needed in general applications of tractographic reconstruction. The conceptualization we presented is no more than a geometric study of neighbouring fibers. However it does not measure the context itself. Rather, this study has been focused on the comparison of those neighbouring fibers with an alternative representation. The outcome of this indicator helps to correlate if the alternative representation is good enough to represent the geometric shape of the neighbourhood.

Now we want to propose an adaptation of this measure to determine context stability measure. Our proposal is to efectively do a comparative study, but with a representative obtained from a geometrical caracterization of context data itself. We are talking about comparing contexts to their own geometrical means.

A context representative will be in this case a curve γ_i defined as

$$\gamma_i(t) = \frac{1}{Z_i} \sum_{j=1}^{Z_i} \delta_j(t) \tag{4.17}$$

where Z_i is the number of streams in the ith context, t is defined for the whole arc-lenght of the context, and δ_j represents the arc-parametrization of the jth curve in the context reconstructed from each seed S_j as defined in Equation 4.6.

In this configuration, whenever the context presents a robust and geometrically coherent structure, the descriptor D presented in the previous section (Eq. 4.11) will present lower error rates in its three dimensions ($d\kappa$,$d\epsilon$, and $dPos$). Otherwise, if contexts present heterogeneous formations, this internal measure should present more extreme values based on higher error ratios.

This measure can also help us to determine where in the anatomical structures a contextualization of a neighbourhood is plausible. This information will be of great importance for our multi-resolution reconstructions.

4.4.1 Local geometric metrics

It is important to notice that the approaches presented in the previous sections are conceived to characterize the whole lenght of contexts. These are measures to evaluate global geometric quality of our streamlines. However, we decided to go further and look for more detailed descriptors that can be more useful in visualization and medical analysis of heart architecture. A local descriptor will be able to present infinitesimal description of coherence or adequation of our filtering methods.

Initially, in order to obtain such local measure we defined descriptors at each point of the streamlines only taking local information into the formulation. However, that that brings an unestable measure. Our solution to this problem has been to compute sliding windows of geometrical quality. Each point will be defined by a similarity function in the vicinity of that point in a neighbouring segment.

Boundaries of the stream contexts become an important issue since there is no clear vicinity to stablish the smoothing window proposed as a general solution. To

solve this problem we treated boundaries with value propagation. In this way values will be more robust and will be set in concordance with the local information.

4.5 Visualizing of confidence

Geometric analysis of neighbouring fiber tracts can offer us important information about our confidence in their reconstruction while also being able to represent the robustness of the underlying structures being reconstructed.

In order to provide this valuable information to the user, we want to combine tractographic reconstructions with it in a meaninfull and clear way. As discussed earlier in this thesis, the visualization of tractographic reconstructions can be highly detailed, and due to the inherent complexity of the biological structures being reconstructed, it will tend to produce a cluttered output. Adding more information could mean even more complexity. We want to incorporate this data in a way that augments the structural representation of fiber tracts. Moreover, we think that the structural nature of the confidence measure may even help us to simplify tractographic visualization.

With this visualization objective, we can relate the representation of confidence measures with that of the clustering methodologies. At some point, both of this dissimilar approaches are to provide more meaninful representation of the most relevant structures rather than offering a collection of individual streamlines. The search of a good visualization is crucial. In order to find a better visualization methodology we explored three ways to integrate this data within tractography as those methods in the past. The methodologies include color coding, fiber filtering and topological aggregation.

4.5.1 Color coding

The most straightforward approach to represent information over tractographic representations has been the use color coded streamlines. In chapter 3 we saw this application to augment streamlines with information of their angulation. This approach has also been explored to present other local properties of neighbouring fibers [102] and it is also a common way to present global information about groups of streamlines that present some relation (clusters) [18, 89, 84, 82].

We can color code streamlines mapping a meaningfull color scale to represent the range of our evaluation indicator. This methodology, in all of its variants, allows to preserve complete detail of the tractographic representations while offering additional information to the user. However, this direct representation may not offer any improvement for tractographic visualization. Thus we considered an alternative that reduced the number of fibers according to this measure.

4.5.2 Fiber filtering

An alternative to the former method is to offer any kind of geometric filtering (e.g. by selective seeding [35, 34, 5]). Either manually or automatically, we can show or conceal specific streamlines according to any criteria. This criteria can be clearly imposed by a threshold in our confidence measure. However, as we highlighted in Chapter 2, we do not want to offer segmented visualizations. For that reason we propose a side by side and syncronized representation of structures over an under the specified threshold.

On one hand, this representation could help avoid to completely conceal structures at users discretion. On the other hand, it can also help to identify which structures are being selected or discarted while keeping them localized in the anatomy.

4.5.3 Topological aggregation

Many clustering methodologies in the literature opt methods as the previous ones in order to preserve full detail of the anatomic structures while offering more meaningful data. However, sometimes detail is not crucial for the comprehension of the anatomical structure. Some researchers have preferred to convert fiber clusters into solid structures that somehow model or summarize their general architecture [25, 24, 79]. The most common applications compute envolving surfaces to cover the entire clusters. However, our methodology has a different scope only trying to determine close aggregations of fibers rather than clusters.

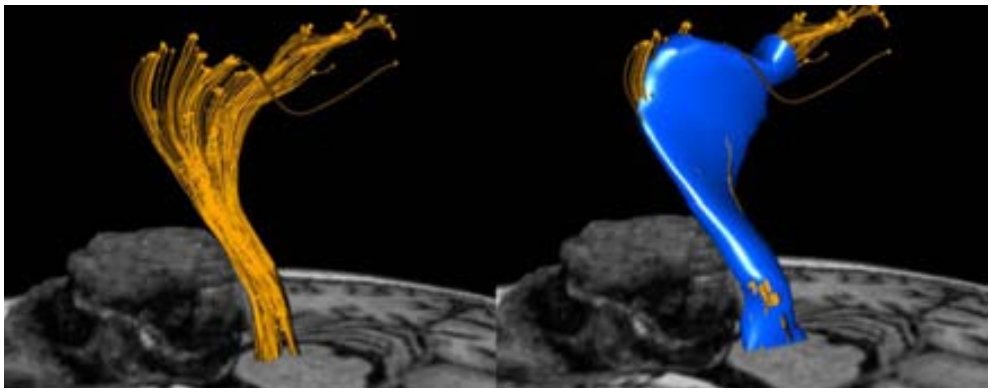

Figure 4.8: Visualization of a brain fiber bundle based on streamlines (left) and a simplified representation with an envolving hull (right). Image adapted from [25].

Our approach is somehow inspired by the trace that a paint brush leaves under different preasures. Whenever preasure is higher, a paint brush leaves wider traces that have special visual relevance in paint. Otherwise, an smaller preasure is used to trace thin lines that can achieve detail but tend to be less noticeable in front of the later ones. If we apply this concept to tractography, understanding preasure as a

function derived from our confidence measure, we can achieve a good representation of this indicator. In other words, this visualization will represent coherence with geometrical cues. Our proposal is to represent fibers controlling streamtube[1] thickness by their coherence (see Figure 4.9). The thickness of this streamtubes should be greater where contexts present low uncertainty. Otherwise, when confidence gets worsened because the contexts do not represent a coherent structure this thickness will be reduced to represent this weakening of the neigbouring stream formation. Thickness will be limited on its higher value by the diameter of contexts where we compute confidence indicators.

We can apply this methodology either globally or locally to our streams. An interesting property of local coding should be that the aggregated representation of fibers will present a tree-like hierarchic structure (see Fig. 4.10). In this representation, coherent areas may be merged into bigger formations representing strong coherence. Otherwise, when fiber geometry is not as coherent (due to micro-structural detail, or to data and integration limitations) it will be represented with reduced thickness streams. Thus, we will have full detail of this structures while minimizing their relevance for the study of major architectures.

This representation should be the most intuitive for visual analysis using either local or global coherence estimates. Moreover, it can be combined with color representation of the same value (or others) to enrich this visualization.

[1] We recall the reader that an streamtube is our structuring element to present streamlines forming final tractographies. See Chapter 3 for further reference.

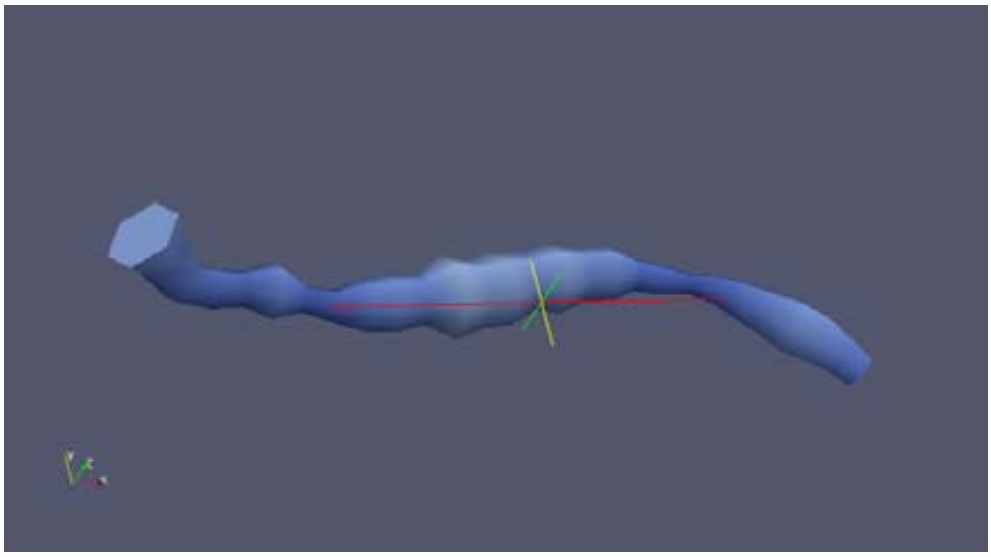

Figure 4.9: Toy-example of representation of an streamtube with variable thickness and color to represent an scalar value along its path.

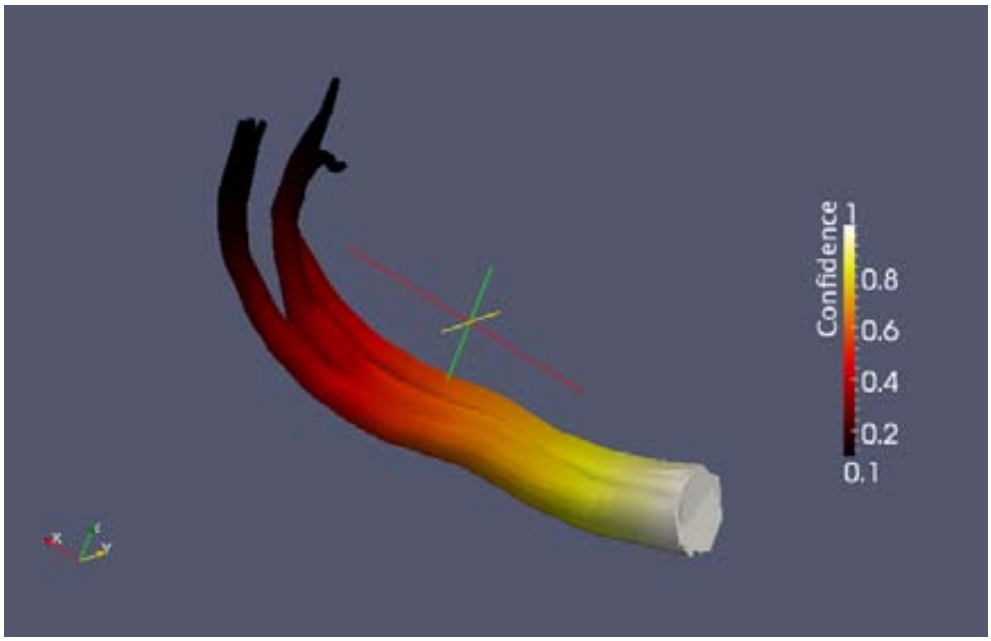

Figure 4.10: Toy-example of the theoretical hierarchical structure that we can achieve with streamtubes with variable thickness. In this situation, the confidence measures of a context of eight fibers are linearly mapped to show progressive thickening/thinning of all fibers. Color represents the same confidence values along their paths.

Chapter 5

Results

Everything should be made as simple as possible, but no simpler.

Albert Einstein

In this chapter we have gathered all results of the methodologies introduced in the development of this thesis. We begin presenting the data used for all experimentation in this work (Section 5.1). Following, we introduce the results on the evaluation of our multi-resolution tractographic reconstruction schemas from local and semi-local image analysis (Sections 5.2-5.3). After that, we focus on global geometric analysis (Section 5.4). For its part, in Section 5.5 introduces the results of visualization in our multi-resolution tractographic methodology. Section 5.6 does the same in the composition of tractographic reconstruction with confidence measures. Finally, Section 5.7 covers a thorough architectural study of the myocardium in concordance to the rivaling state-of-art models of this architecture.

5.1 Johns Hopkins Canine Database

All datasets that will be processed in this work come from the publicly accessible database [61] published by the Institute for Computational Medicine at Johns Hopkins University (JHU). This data was obtained, processed, and studied by Helm et al. [51, 50]. This is, as far as we know, the only publicly available database of *diffusion tensor images* of hearts.

The provided datasets include 9 DT-MRI studies of healthy hearts of dogs of Beagle breed. Each heart was suspended in an acrylic container filled with Fomblin, a perfluoropolyether (Ausimon; Thorofare, New Jersey, United States). Fomblin has a low dielectric effect and minimal MRI signal, thereby increasing contrast and eliminating unwanted susceptibility artifacts near the boundaries of the heart. The long axis of the hearts was aligned with the z-axis of the scanner. These hearts were filled

to maintain the shape of diastolic phase. The fixation of the heart in this shape was proven to preserve fiber angulation as good as a systolic phase would have done [110]. Images were acquired with a 4-element, knee phased-array coil on a 1.5 T GE CV/I MRI scanner (GE Medical System; Wausheka, Wisconsin, United States) using an enhanced gradient system with 40 mT/m maximum gradient amplitude and a 150 T/m/s slew rate. Hearts were placed in the center of the coil and a 3-dimensional fast-spin echo sequence was used to acquire diffusion images with a minimum of 16 noncollinear gradient directions and a maximum b-value of 1500 s/mm^2. The size of each voxel was about 312.5µm $\times$ 312.5µm $\times$ 800µm. Resolution resulting from zero padding in Fourier space allowed us to adapt original image size of 192 $\times$ 192 to 256 $\times$ 256. The final dataset was arranged in about 256 $\times$ 256 $\times$ 108 arrays (depending on the scanned heart) and contains two kinds of data: geometry/scalar data and diffusion tensor data. For diffusion tensor data, each voxel in the array consisted of 3 eigenvalues and 3 eigenvectors. Primary eigenvectors are the most significant directions of water diffusion (higher eigenvalue) and are denoting the longitudinal orientation of myocytes on the given voxel.

5.2 Local analysis: Angular precision

The first evaluation considered in this thesis is based in the estimation of the effect of multi-resolution models to local anatomical stucture of diffusion MRI derived data. For this purpose, in Chapter 4, we proposed an evaluation of angular variations in the different stages of pre-processing that creates a pyramidal representation of data.

If we recall the theoretical proposition from the same chapter, in this evaluation and further we will put special attention to the two main steps that define this process: the **impact of volume filtering** and the **impact of combined dimensional reduction and interpolation**.

- **Impact of Volume filtering**:

  Each input volume will be filtered with the Gaussian kernel as well as with the structure preserving diffusion operator that defines our anatomical filter (from now on also referred as SPD in the text). Each of the resulting volumes will be compared to the unprocessed input data.

- **Impact of dimensional reduction and interpolation in reduced tractography**:

  Each of the reduced volumes (previously filtered) will be compared using the same strategy. However, dimensional reduction imposes an issue to compare differently sized data. To ensure pair-wise comparability of reduced volumes we have scaled those volumes using linear interpolation (see Chapter 4 for further reference). In this experiment we will also have the opportunity to evaluate our proposal to use Wavelet decomposition We recall the reader that this methodology was considered as one single step of processing rather than a filter and a dimensional reduction.

In order to present results from this evaluation, we will first present the detailed effects of the first stages of filtering (A) and reduction (B). Afterwards, we will present a summarized statistical analysis of the effects all the levels of processing (iterative filtering and downsampling) in an adequate context for a multi-resolution analysis (C).

A Impact of volume filtering

Evaluating the filtering step we search for indicators of the best filtering methodology in order to process anatomical information.

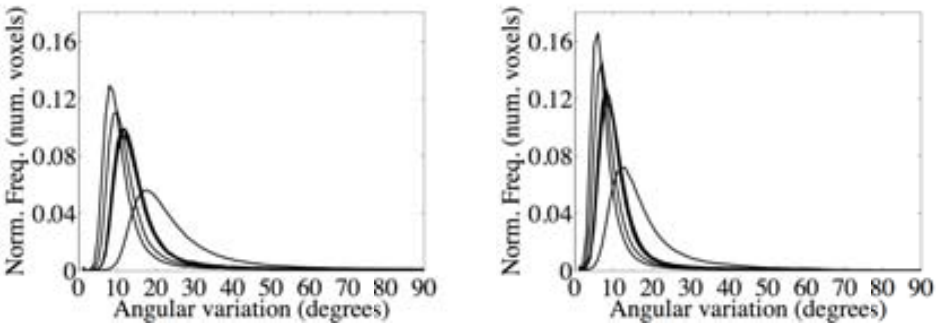

(a) Histogram traces of angular variation in Gaussian filtering

(b) Histogram traces of angular variation in SPD filtering

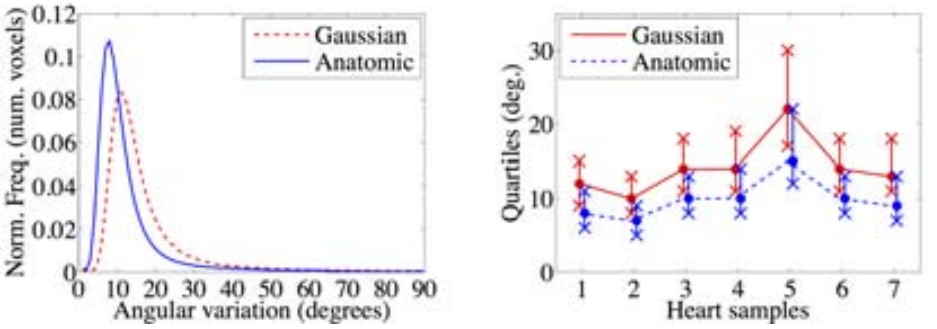

(c) Mean histogram traces for both experiments

(d) Quartiles of angular variation for all samples

Figure 5.1: Voxel-wise statistics between original and filtered volumes

Figures 5.1(a) and 5.1(b) show the histogram traces of angular variation in our samples after applying Gaussian and SPD (Anatomic) filtering. Both methods seem to have similar responses in different orders of magnitude. In order to easily compare both filter responses, we have also included mean histogram traces (Fig. 5.1(c)). The anatomic filter has a better mean response, achieving substancially lower rates of angular variation. In Figure 5.1(d) we can see the specific ranks given by the cen-

tral, second and third quartiles of these distributions for each specimen. This data explicites that SPD approach is better for all samples. Gaussian, alternatively, shows a higher variance. Our anatomical filter performs better than SPD, having its central quartile ranging from 6 to 14 degrees. In contrast, Gaussian has considerably higher values, the second quartile ranges from 10 to 22 degrees. This selects SPD as the best filtering for full-scale representations. We attibute this improvement a consequence of a better contextualization of myocardial anatomy of the anisotropic approach of the SPD filter.

B Impact of dimensional reduction and interpolation in reduced tractography

Re-scaling data for the evaluation of reduction composes the effects of this procedure with the interpolation that will be performed in posterior tractographic reconstruction of this data. In this case, in the evaluation of angular error we can look for insight on the effects of both processes and how each filtering procedure responds to them.

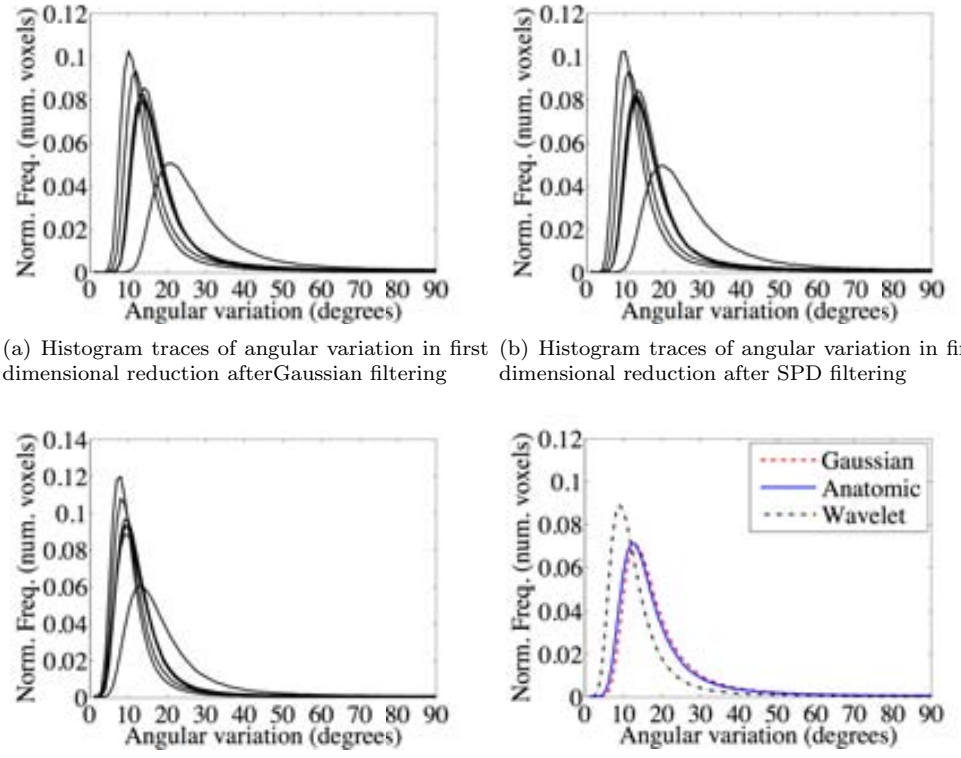

(a) Histogram traces of angular variation in first dimensional reduction afterGaussian filtering

(b) Histogram traces of angular variation in first dimensional reduction after SPD filtering

(c) Histogram traces of angular variation in first level of Wavelet decomposition

(d) Mean histogram traces for thrice experiments

Figure 5.2: Voxel-wise statistics between original and filtered volumes

Figures 5.2(a) and 5.2(b) show the same description as Figures 5.1(a) and 5.1(b) did, but, now they show the results of comparing sub-sampled volumes with original data. In this case we also have Figure 5.2(c) depicting histogram traces for the first level of Wavelet decomposition methodology. If we compare the effects that Gaussian to Anatomic methodologies presented in this step of processing, Gaussian pyramidal representation is still offering an inferior performance than the SPD approach. However, it is difficult to appreciate a significant difference between the two methodologies. In this experiment, SPD have medians in the range of 12 to 24 degrees of angular variation. Meanwhile, Gaussian presents a similar behavior ranging from 12 to 25. It is clear that the linear interpolation applied on the tractography have an stronger impact in the non-isotropic methodology. At this point, we attribute the loss of power of the SPD method to the isotropic nature of the re-interpolation that is used by the integration method to obtain a continuous vector field.

If we focus on the effects of the Wavelet decomposition methodology (Fig. 5.2(c)), we can observe that this approach is achieving better results than the former alternatives. The response of this methodology has clearly better mean response (Fig. 5.2(d)). It is even comparable with the effect of Gaussian filtering previous to the downsampling of the volumes. Outperforming those methodologies, Wavelet filtering seems the best approach to achieve, at least, one level of reduction.

C Effects over multi-resolution

The graph in Figure 5.3 aggregates the response of all hearts in the database to de different steps of processing of the generation of a 4 level pyramid of volumes (fullscale input date + 3 iterative reductions). In this graph, Y-axis represents angular error, and X-axis contains the different processing steps. Each of these steps has been represented by the mean of mean responses of the angular cariation. Each of these means represents the angular variation for each experiment (Gaussian, SPD, and Wavelet). In this steps we can find also represented the standard deviations for each step to clarify the stability of the distribution of angular variation.

As we can see, the angular variation presents an almost steady degradation across the several steps of processing. This graph reinforces how downsampling seems to have an stronger effect on SPD filtering than in the application of Gaussian smoothing. But, in all cases, the outcome of the Gaussian pyramid schema is worse than the anatomical filter based one. Meanwhile, the Wavelet alternative outperforms its alternatives in all the steps of processing.

Relative to the meaning of the degree of angular variation that this procedures introduce to data, we must remark that the acceptable angular differences may vary across applications. We will not use a thresholding measure to interpret this data. In this work we will use it as a measure of confidence in our multi-resolution methodologies in combination with subsequent work presented in this chapter.

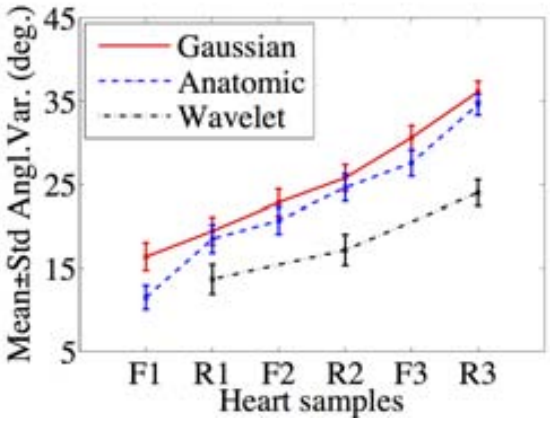

Figure 5.3: Statistical representation of angular variation for all samples and steps of processing in the generation of a 4 level pyramidal representation of data. In this graph F# and R# stand for each iterative application of filtering and reduction.

5.3 Semi-local evaluation: Preservation of anatomical features

One of the contributions of this work has been to find a measure of spatial coherence among neighbouring myocytes (see 3.2.2). This information has been necessary to improve the seeding of the streams constituting our tractographic representations of the heart. However, this information has also been used as the base for the validation of our multi-resolution methodology. Basically, this information unravels the knowledge of different kinds of muscular organization on the myocardium.

We can estimate the preservation of this information across levels of detail, and, therefore, use it as an indicator for the study of different multi-resolution strategies. As stated in Chapter 4, this evaluation starts fitting a mixture of gaussians to characterize the distribution of our coherence measure. Following, we compute separability of internal classes using statistical measures on the gaussians that fitted the distribution. This separability will stand as our evaluation indicator.

Following we will show some settings of the implementation that arose from refining the production of results (5.3.1), as well as all the statistic and visual results of the semi-local evaluation (5.3.2).

5.3.1 Refining distribution fitting and separability measure

In this application we look for two populations in the data. This populations can be straightfordwardly characterized by fitting two gaussians to the distribution. However, in practice, we discovered that results of such fitting can be substantially improved when fitting three gaussians. This additional class usually shows unstable

locations on all the sample. Thus, it does not seem to encode a hidden population. Instead, this third class seems to help to fit parts of the distribution that could not be directly represented with one or two normal distributions such as noise or other dissasociated fenomena. More classes may be used, however, the result of fitting a bigger amount of gaussian distributions returned poorer results. More classes worsen the detection of the principal classes due to an overfitting of the distribution. As a result, in our evaluator we choose to apply this strategy and we choose the principal classes guided by gaussians with the highest priors. This is possible given that the third distribution never shows as relevant as the others because it is coding a residual signal.

For the final study of separability, we have to take more factors into account. Unfortunately, separability in our distributions will not always be computable from means and variances as Fisher discriminant contemplates. It is the case when we obtain successfull fitting of three classes but only one has a significant prior. This situation implies that the two classes that we are looking for in the distributions have been completely merged into a single class. Thereby, we have also computed the ratio between the two most prominent classes to classify them. An empirically determined threshold indicates the separability among classes of all the samples in this scenario. When this clases appear effectiveley merged we consider the Fisher discriminant to be zero in value.

5.3.2 Class separability in filtering and reduction

The empirical application of this evaluation procedure explores the two stages of multi-resolution pyramid generation as we did in the previous section. In this case, though, we do not encounter issues to process dimensional reductions. This procedure is a feature based approach that is methodologically independent from the resolution of the samples. Consequently, both effects can be quantized equally.

Figure 5.4 represents class separability measures in our experiments for the hearts of the JHU database in this setting. The ordinate of this graph represents the range (mean $\pm$ standard deviation computed across all the specimens) of the Fisher s linear discriminant, while the abscissa represents the phases of the reduction algorithms. It is clear that since the very first step (first filtering) we encounter significant separability decay. At this point, the separability rates are lower than in the original volume. However, any value higher than zero is determining two classes as separable. From this fact we can easily appreciate that the SPD based pyramid production overpowers the Gaussian approach at the first stages. In fact, if we based our evaluation solely on this indicator, Anatomic filtering arises as the only viable methodology for at least one level of dimensional reduction. However, this measure is not intended as an exclusive evaluator. We are aware that the resolution and size of these particular anatomical features captured by the coherence measure may be limited to get conclusions on the applicability of each methodology. Still, this evaluation can bring important data about the effects of our methodologies to this low level anatomical features. We will follow the study of this effects in subsequent stages of the multi-resolution

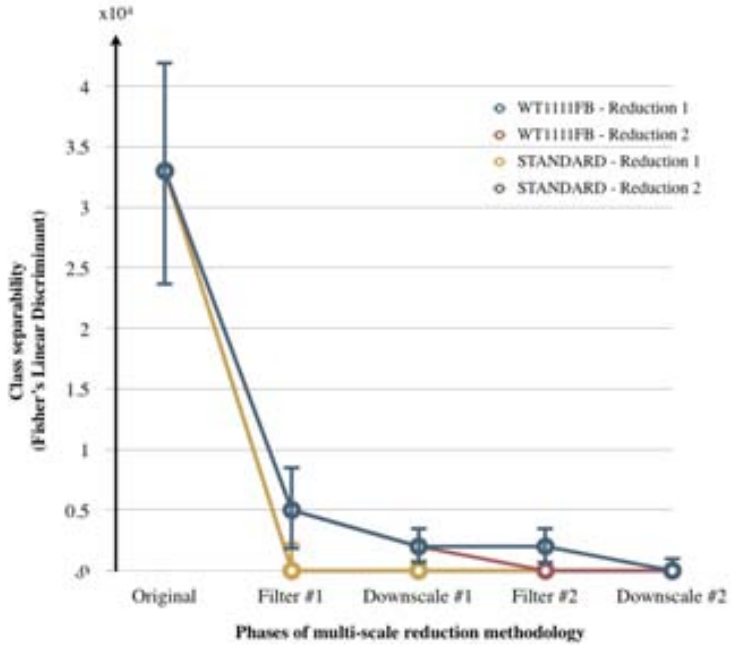

Figure 5.4: Combinated results of class separability

tractographic reconstruction.

5.4 Global streamline geometry analysis

The results of the previous sections helped us to characterize the loss and alteration of information introduced by our methodologies to produce multi-resolution representation of DT-MRI data. With this results we have studied the potentials and limitations of these methodologies. However, our methodology goes further than the local domain that we can study from an image analysis point of view. Our goal is to produce multi-resolution tractographies from this data. We can say that we are not as interested in the evaluation of this local effects in an isolated manner as we are interested in the geometric implications of this whole process to the streamline integration.

In order to elevate evaluation to a more global indicator based on streamline reconstructions, we will use our context evaluation schema presented in Section 4.3 to the data of the JHU public database. This evaluation methodology measures geometrically how an streamline is related to its context of neighbouring fibers.

On its own, this methodology is not conceived to attain comparative evaluation of each of our multi-resolution experiments and its stages rather than providing internal evaluation of neibouring fiber tracts. For that reason, in this section we will first

present an **extension of context evaluation to provide geometric comparison of tractographies**. After that, we will present **results of this evaluation to our multi-resolution strategies**.

5.4.1 Context coherence as a comparative evaluator

The evaluator presented earlier in Section 4.3 was conceived as an indicator to measure how coupled an streamline is to its context. If we consider streamline reconstructions of unprocessed data as our reference geometry (as we did in our study of angular variations in Section 5.2), we can think of a direct alteration of this measure to achieve comparative evaluations of multiple tractographic reconstructions.

We determined that we could consider how reconstructed streamlines in processed volumes relate with their corresponding contexts reconstructed in the unprocessed data. In fact, we decided to compare two different contextualization indexes to achieve the desired comparison. First, we took as a reference the resulting index of comparing streamlines in unprocessed volumes with their own contexts. Second, we built another index which compares streamlines obtained in processed volumes with their corresponding contexts in unprocessed data. And we compare these two indexes to observe the variaton of the second relative to the first (see Figure 5.5). In other words, we can measure how the second index have preserved, improved, or worsened as a representative of contexts depending on each methodology or step of it.

If we move from the individual comparison of contexts to comparing complete tractographies, we can see that each of those comparative indicators can be computed for all streams/contexts in each tractography that we want to evaluate, and also for the original reconstructions. Each one will give us a distribution of contextualization indexes. We will compare this distributions to evaluate the effect of the processing of data. Since this distributions can be paired (contexts/streamlines are reconstructed on the same locations in each volume) we propose to obtain indicators by means of a standard paired Student s t-test [96]. The parameters of this statistical hypothesis test, as well as other statistical indicators, will help us to determine which of those processings are significantly dissimilar to the original reconstructions. Thus, offering us a way to reject unplausible outcomes of our multi-resolution process.

5.4.2 Statistical resuls of geometrical evaluation of multi-resolution methodologies

As we did in previous evaluations, we will separate the results on each filtering and reduction applied to input data. In this way, we want to be able to evaluate the geometric effect of each of these stages to tractographic reconstruction. In this case, the comparison of reconstructions could be done seamlessly along our pyramidal reconstruction and each of their intermediate steps.

	D_i distr.		N	Diff. distr.		95% Conf. Interv.		t	p	h
	Mean	Std		Mean	Std	Upper	Lower			
Orig vs	0.71	0.86	103	0.08	0.70	0.012	0.27	2.17	0.03	1
Gaussian Filter	0.63	0.73								1
Orig vs	0.79	0.13	112	0.11	0.87	0.05	1.47	2.10	0.03	1
Anatomic Filter	0.69	0.97								
Orig vs	1.06	2.21	90	-0.36	2.37	-0.89	-0.01	2.03	0.04	1
Gaussian F + Red	1.42	3.93								
Orig vs	1.06	1.93	110	-0.01	1.19	-0.25	0.20	-0.17	0.86	0
Anatomic F + Red	1.07	1.93								
Orig vs	0.97	2.12	96	0.26	1.73	-0.03	0.58	1.81	0.07	1
Wavelet 1 decomp.	0.71	1.66								

Table 5.1: Statistical Results from paired Student t-test

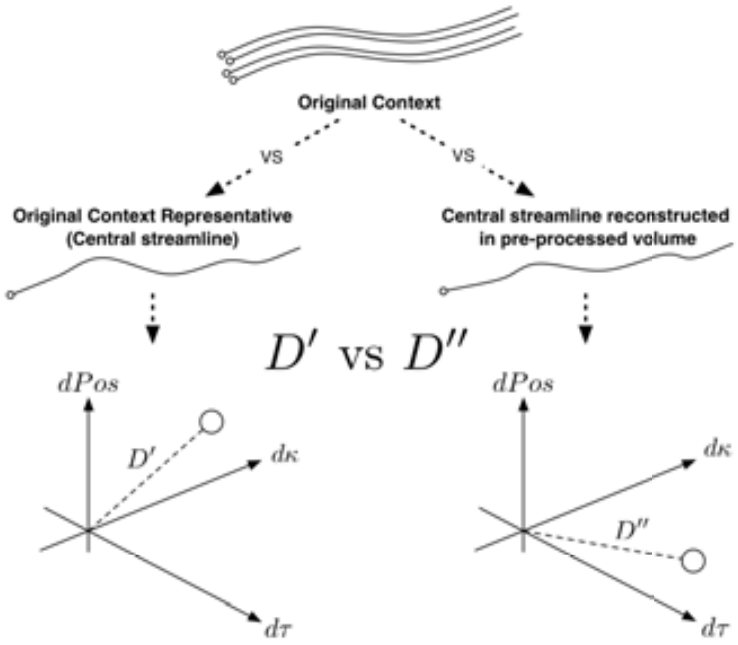

Figure 5.5: Coherence measures as a comparative evaluator. Each streamline computed on a pre-processed volume can be evaluated with our confidence descriptor against its corresponding context in the unprocessed volume. This measure can be compared to with the same descriptor obtained solely from original data.

A Impact of volume filtering

The first two rows available in Table 5.1 present the results from the paired t-tests comparing our filtering procedures with original reconstructions. We can see in this data that the response of both tests (Gaussian/Anatomic) is to reject the null hypothesis -which assumes both distributions are equal-. In both cases, with this response, it is safe to say that a measurable effect is present. At this point, we should remember the reader that a measurable effect, either it would mean that tractographies are not responding equally after this processing to their behavior in the original datasets, do not necessarily mean that they present worsened anatomical representation. A positive difference between those indicators in both scenarios would mean that the tracts reconstructed on processed volumes are better representatives of original contexts than their homologous reconstructions in that data. In order to provide further reference about this behaviour, in this table we have also included the mean and standard deviation of the distribution of paired differences. This distribution represents the paired differences between reconstructions on original data and processed volumes. If we observe at this indicator for the Gaussian approach, we can see that this filter offers an slightly more centered distribution of differences. This would imply a more general similarity towards the original distribution. Rather, Anatomic filter presents

a higher positive difference, implying better contextualization. However, this difference may not be conclusive. Looking at the confidence interval in both cases, we can see that Gaussian offers an slightly less variable response.

Additionally, we looked at the ratio of contexts increasing or decreasing their descriptor. Considering a significant variation over an under a 10% ratio, Gaussian presents an improvement of 46% of streams, worsening of a 32%, and the rest are maintained on a similar degree. Alternatively, in Anatomical filtering, 47% show an improvement, 13% remain stable, and 40% worsened their descriptor. According to this ratios, Anatomic filtering offers moderately better results than its isotropic adversary.

B Impact of dimensional reduction and interpolation in reduced tractography

The remaining three rows in Table 5.1 present the results for dimensional reduction in our three methodologies. If we begin analysing the Gaussian response to reduction, we can also determine a significant effect of this procedure to geometrical reconstruction. However, in this case we can easily appreciate that the mean of the difference distributions is below zero. That would imply an geometrical error increase. Alternatively, the reduction after Anatomical filtering and the first level of Wavelet decomposition offer a more stable outcome. Both methodologies present a very stable outcome compared to original reconstructions. Among these two alternatives, we can see that the Wavelet approach is close to rejection (p-value 0.07). Its confidence interval is wider and shifted, which would present this as a worse alternative than the Anatomical filter approach.

Looking at the ratios as we did in the evaluation of filters, we can see an similar outcome of the later methodologies. Wavelet offers 50%/30%/20% where Anatomical shows 45%/40%/15% (worsening/improving/worsening results). This would reinforce that even the Wavelet approach may performs better in most cases, it should tend to have a bigger effect in worsening.

5.5 Visualizing multi-resolution tractographies

Now we are going to focus on the visualization of the application of our multi-resolution experiments as well as our different proposals to achieve better visual representations of the muscular architecture of the myocardium throughout tractography.

By downscaling two orders of magnitude of the original datasets and applying our streamlining, we get the tractographies shown in Picture 5.6. This side-by-side comparison of the 3 levels of the pyramid gives a clear view of the results of a multi-resolution tractography. We can see that the simplified versions (Figs. 5.6(b)-5.6(c)) of the full-scale tractography (Fig. 5.6(a)) keep the main geometric features of fibers while they clearly allow easier identification of global morphological tendencies.

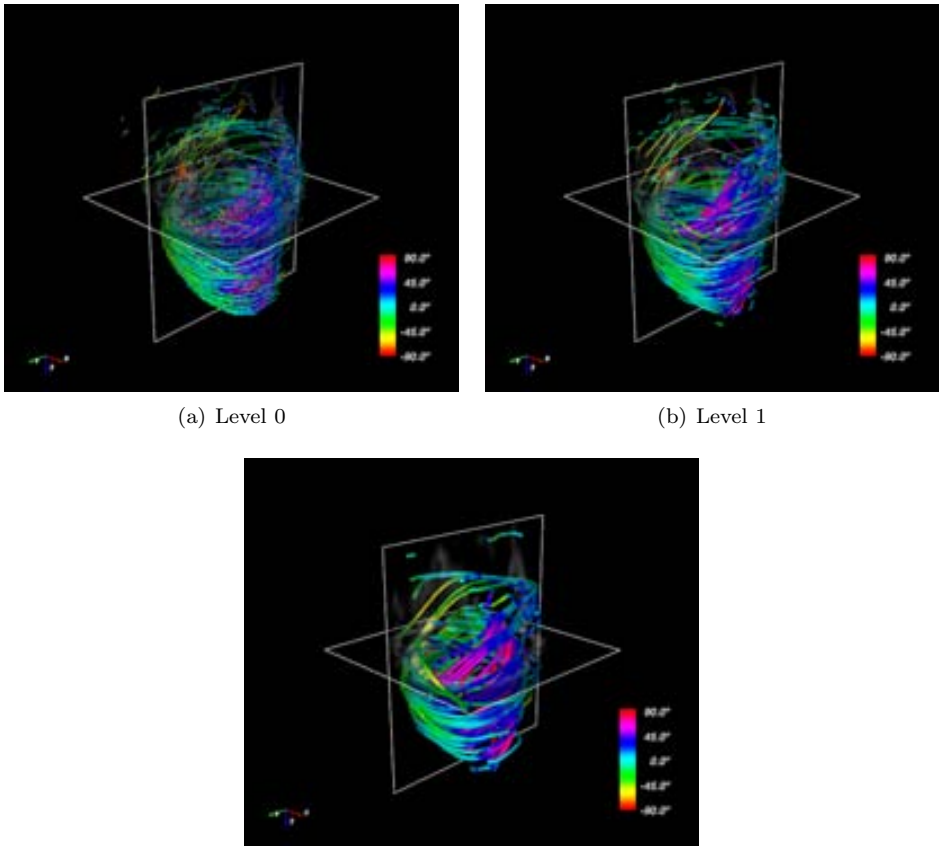

(a) Level 0

(b) Level 1

(c) Level 2

Figure 5.6: Lateral-superior view of the left ventricle. Tractographic reconstruction in 3 levels of detail performed on the same specimen of the database with similar fiber densities.

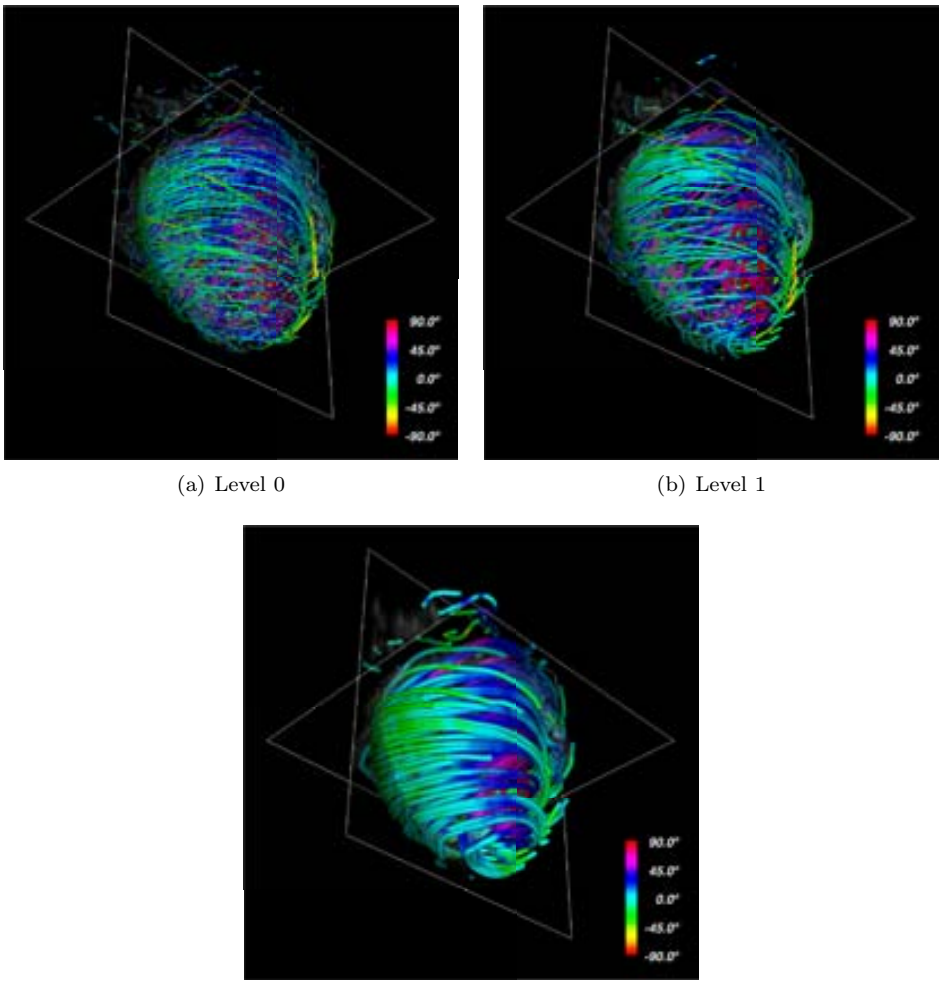

(a) Level 0

(b) Level 1

(c) Level 2

Figure 5.7: Lateral-inferior view of the left ventricle. Tractographic reconstruction in 3 levels of detail performed on the same specimen of the database with similar fiber densities.

Further than that, we can see that the representations in lower levels of detail can somehow summarize important anatomical properties of the muscle. By reducing clutter and representing bigger neighbourhoods of fibers, simplified representations can certainly ease the visualization of complex muscular structures. In Figure 5.7 we can see this effect applied to the reconstruction of the apical region of the myocardium. Lower scales of the pyramid offer a clearer representation of its structure. In Figure 5.7(a) it is almost impossible to understand the anatomical formation of the apex. Instead, as we get to lower detail representations (Figs. 5.7(b)-5.7(c) this structure reveals itself as an helical muscular formation. Fibers in the endocardium (descending fibers colored with colors in the range from blue to purple) cross the apex connecting to the epicardium transforming themselves to ascending fibers. This structure (commonly known as the *apical loop*) is exactly as we introduced in Chapter 2. This helical structures is in fact one of the first, and currently a broadly accepted architectural formation in the study of heart anatomy.

The former tractographies (Figs. 5.6(a)-5.7(c)) employ our first proposed approach of color mapping. In all those figures color of streamlines is set according to the degree transverse angle of their trajectories across the myocardium. The color of these streamlines have been mapped using the complete hue range. In this way, we can offer the most detailed mapping available. However, we have also considered some alternative color mappings to highlight some anatomical properties.

First, Figure 5.8(a), shows a binary color coding of streamlines. In this case, fibers only recieve two colors along their paths. In ascending sections they are colored in red, and green otherwise. This color map allows to visually separate specific formations of the myocardial architecture. In this visualization is easy to appreciate that epicardial fibers present a consistently ascending construction. Alternatively, endocardial fibers present contrary fashion. This supports the observations of many earlier works. However, it is important to remark that this do not state the existence of two isolated populations. Rather, if we look at the tractographies with a more detailed color mapping, we can appreciate an smooth transition across the myocardial wall. This would in fact support one of the most supported descriptions of the myocardial formation [111].

We can also provide user customization of color mapping scales. In Figure 5.8(b) we can see a mapping that only ranges on a subsection of the available hue scale only ranging from red to green. This might help users to highlight particular structures on the myocardial anatomy. For instance, we can see that the color mapping helped to highlight the most extreme ascending fibers in the foremost epicardial layer.

Finally, trying to offer an even more powerful way to explore architectural structures we introduced the use of transparency. Figures 5.8(c) and 5.8(d) show transparency mapping to the descending and ascending fibers respectively. This tool clearly eases the isolation certain parts of the anatomy. However, its bigger potential is in the capacity to reveal underlying structures hidden by other groups of fibers. We can see how external fibers can be diminished to analyse the endocardial architecture (Fig. 5.8(d)).

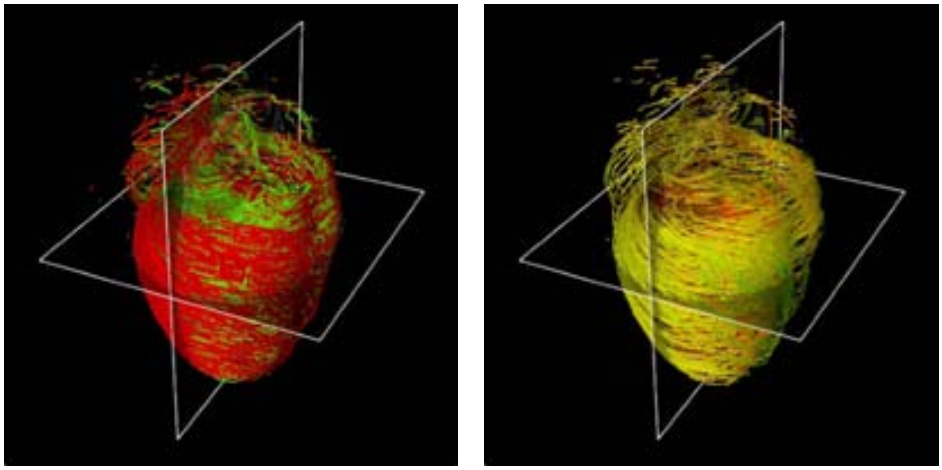

(a) Binary color mapping

(b) Custom range of hue scale

(c) Transparency (descending fibers) + custom range of hue scale

(d) Transparency (ascending fibers) + custom range of hue scale

Figure 5.8: Lateral-superior view of the left ventricle. Tractographic reconstruction of a single specimen of the database represented with 4 different color codings.

5.6 Composing confidence measure and tractography

In Chapter 4 we presented a methodology for the computation of fiber reconstruction confidence. At the same time we sought to integrate this measure into tractographies in order to provide the user with this crucial information of the anatomy being reconstructed by tractography. Following we will present our results in the different visualization scenarios explored in this thesis that include color coding and topological aggregation of streamlines:

5.6.1 Color coding

Our first proposal to compose confidence measures in tractographic reconstruction is by color coding streamlines with this measure. In this way we can offer contextualization of this measure right in the anatomy being represented.

In Figure 5.9 we apply a local mapping that expresses geometric confidence values computed in a geometric vecinity arround each point. This visualization provides detailed insight of the anatomic structure. It preserves full detail on geometry and confidence measure. This is a good alternative for the analysis of details in the architectural formation of the myocardium. It clearly highlights the most strong and weak structures at this low level.

5.6.2 Topological aggregation

Figure 5.10 introduces a visualization sample of our last combined representation of tractography and confidence measure. This methodology, as introduced in Chapter 4, controls streamline thickness in order to provide an meaninful visual cues to the confidence in fiber tracts being represented.

In this visualization is easy to appreciate that the weaker structures (e.g. some streamlines reconstructed in the auricular muscles) are diminished by a reduction of thickness of the corresponding streamlines in that area. This thinning is a result of the limited anatomical coherence of anatomy in DT-MRI, and thus, a limited confidence in the reconstruction. This approach offers clear advantages over the approach uniquely based on color coding.

5.7 Medical evaluation: Anatomical study

In Chapter 2 we introduced several theories relative to different heart structures inferred from works starting in 1663 to date. One of the most complex and discussed theories over the years is the one derived from Francisco Torrent-Guasp s work, the

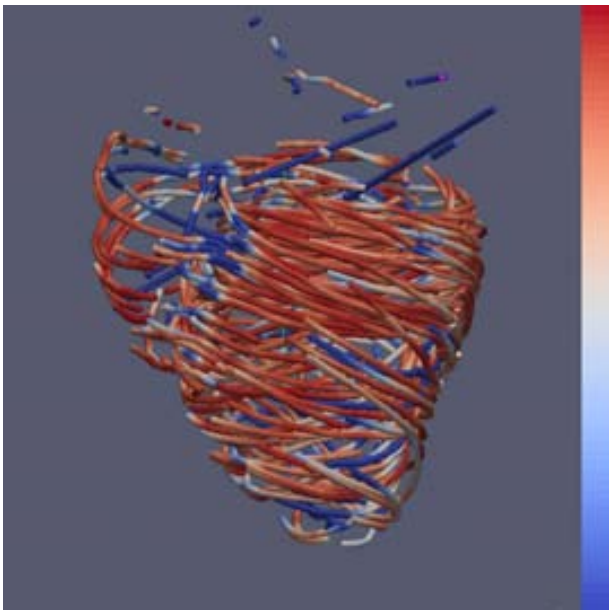

Figure 5.9: Anterior view of the myocardium. Tractographic reconstruction of a single specimen of the database represented with streamline color based on confidence measure. Warmer colors represent higher rate of confidence in the reconstruction.

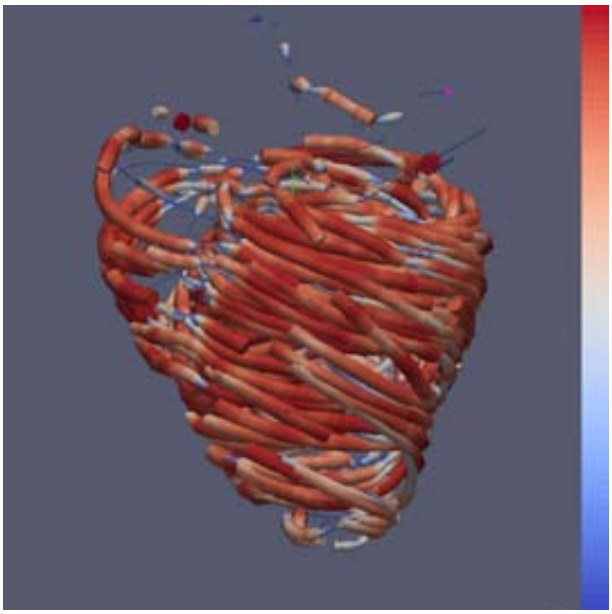

Figure 5.10: Anterior view of the myocardium. Tractographic reconstruction of a single specimen of the database represented with streamline color and thicknes based on confidence measure. Warmer colors represent higher rate of confidence in the reconstruction.

Helical Ventricular Myocardial Band. This has encouraged us to choose this theory as a reference to validate in our work.

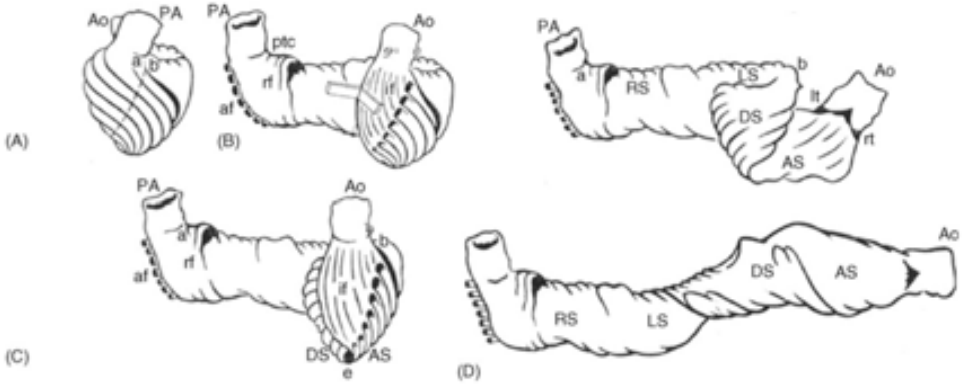

Figure 5.11: Steps of the unwrapping proposed on the theory of the HVMB of Torrent-Guasp.

In this description, the heart is seen as a unique muscular band (illustrated at Fig. 5.11) starting at the pulmonary artery (PA) and finishing at the Aorta (Ao). This muscle wraps the left ventricle and part of the right ventricle (right and left segments) connecting to a helicoidal structure starting at the basal ring going inside the left ventricle towards the apex and returning to connect with the Aorta (descendent and ascendent segments) wrapping with this turn the entire anatomy of the heart.

Next, we will present our results as an analysis from the perspective of **full-scale**, and **multi-resolution** tractography reconstructions.

5.7.1 Heart anatomy analysis from full-scale tractography

On the complete reconstruction it is difficult to recognize so complex structures as the ones described by the HVMB with a naked-eye analysis. There are many critical points to study along the four segments and we have taken a closer look to them all for a deeper analysis. To do this analysis we will compare, step by step, tractographic reconstructions and pictures of Torrent-Guasp s rubber-silicone mould of the HVMB [117]. (Fig. 5.12-5.15)

5.7.1.1 A) Right Segment

Starting the analysis on the right segment we can notice a clear pattern where the reconstructed tracts on the epicardium are orientated towards the basal ring. These tracts loop at the basal ring towards the endocardium describing which looks like as a simple folding (Fig. 5.12). As we track through lower streamlines, this lines are

organized more horizontally but preserving a slight slope. We can see that these lines describe trajectories that wrap around the left ventricle connecting to further folds at the basal ring (Fig. 5.13).

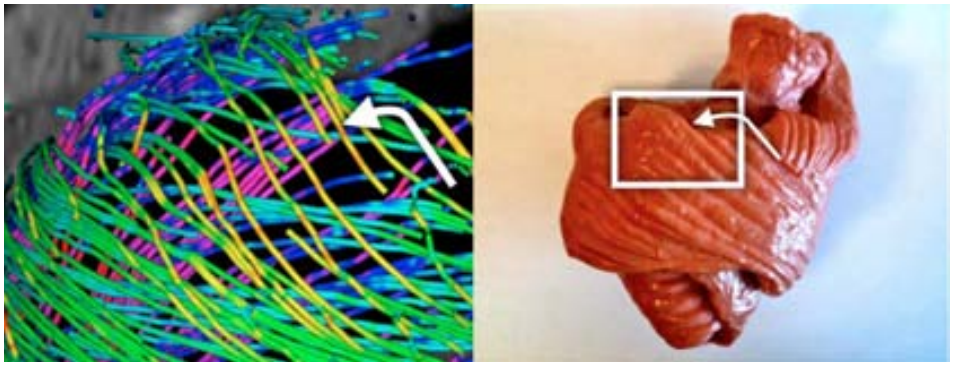

Figure 5.12: Tractographic reconstruction and rubber-silicon mould for the Right Segment validation.

5.7.1.2 B) Left segment

The previous pattern is reproduced along the left segment. At the end of this segment we can notice that the mentioned folding ends at the point where the streams get into the endocardium (Fig. 5.13).

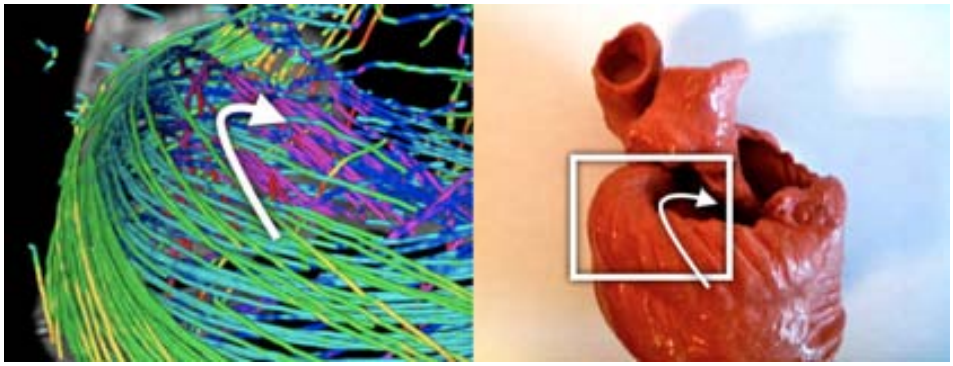

Figure 5.13: Tractographic reconstruction and rubber-silicon mould for the Left Segment validation.

5.7.1.3 C) Descendent Segment

From an anterior view (Fig. 5.14) we can clearly distinguish a spiral-descendent organization of the endocardium population of streams across the septum. This structure

continues to the apex and most of these streams continue on the right segment. Behind this endocardial structure it is also easy to notice an ascendent structure that we will analyze in the following section from another visualization point of view.

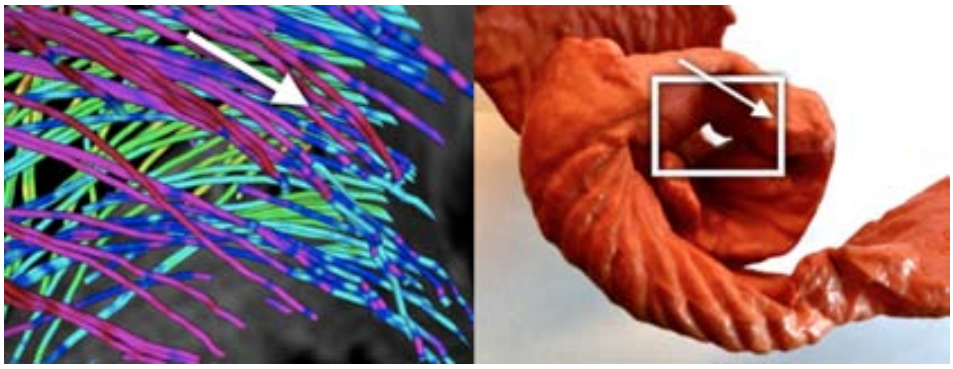

Figure 5.14: Tractographic reconstruction and rubber-silicon mould for the Descendent Segment validation.

5.7.1.4 D) Ascendent Segment

The analysis of this segment is more complex due the cluttered view of several crossings of myocyte populations. With less streamlines than on the previous captures, Fig. 5.15 can show 3 populations where we can see that in this area streams coming from the apex start a noticeable ascend (fading from green to red coloration of the streams denoting an increase of the slope of this streams) below the two other populations that are the beginning of the right segment on its connection with the pulmonary artery.

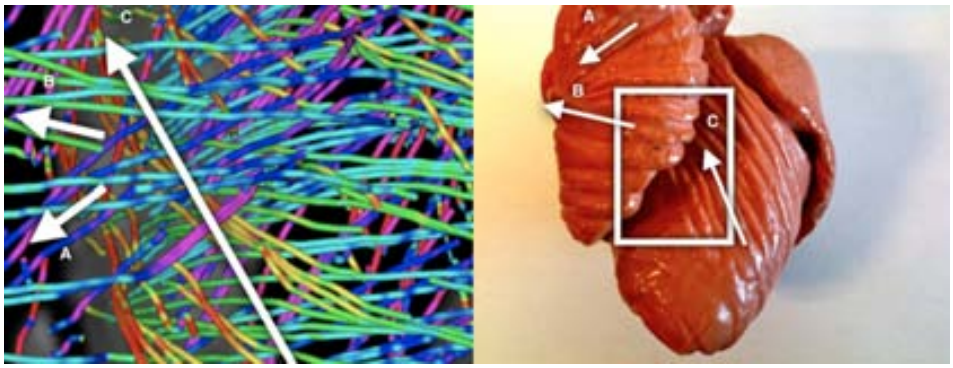

Figure 5.15: Tractographic reconstruction and rubber-silicon mould for the Ascendent Segment validation.

5.7.2 Heart anatomy analysis from multi-resolution tractography

Although our simplified models provide easier interpretation of global trends, they are still too complex for summarizing complex structures such as the Torrent-Guasp HVMB. To simplify the backbone myocardial fiber spatial orientation, we explored the geometry of the heart by looking for long paths that can represent connected regions on the DT-MRI tractography. The goal of this procedure was to provide a comprehensive reconstruction that allows interpretation at first sight by any possible observer. By manually picking seeds at the basal level we obtained continuous paths connecting both ventricles and wrapping the whole myocardium. Figure 5.16 shows 4 representative tracts of simplified models reconstructed from manually picked seeds located at basal level near the pulmonary artery. We observed that the tracts define a sample-wide coherent helical structure for all canine samples.

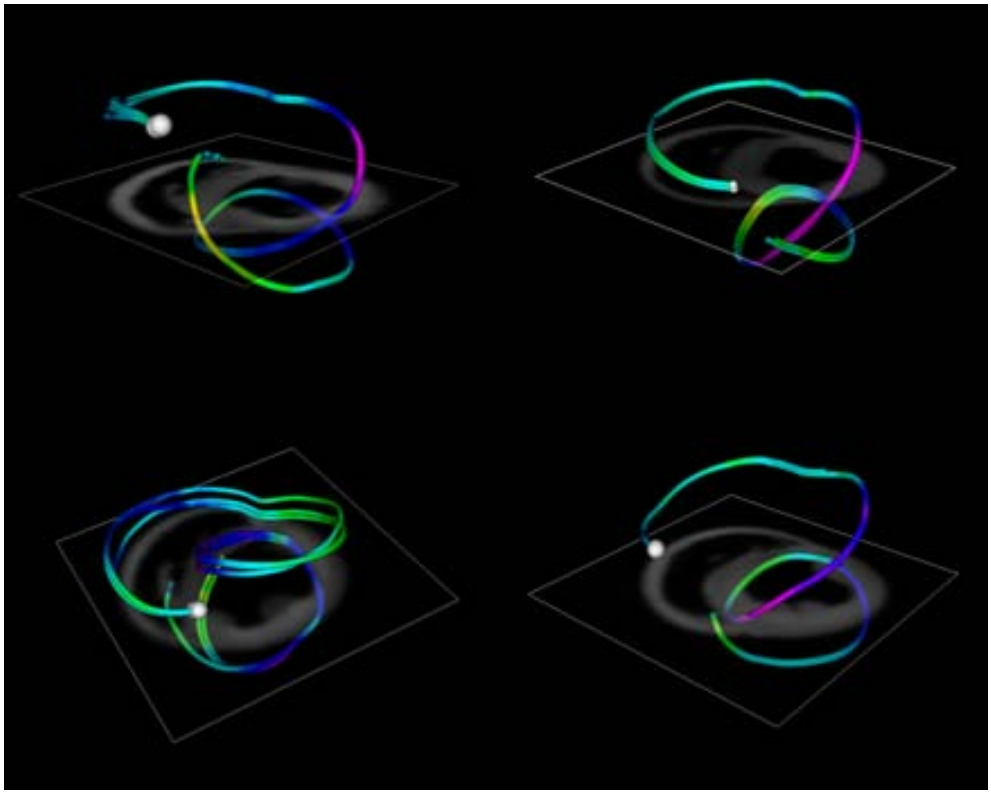

Figure 5.16: Example of tracts reconstructed with manually picked seeds (always chosen near the pulmonary artery) on four sample simplified tractographies.

The use of visualizations with single tracts changes the way in which this structure can be viewed. We compared such tracts to the proposed HVMB (Fig. 5.17). There is a clear similarity between the HVMB schematic model (Fig. 5.17, upper left) and

reconstructed paths (Figs. 5.17, upper right and bottom). In both models the main segments (labeled from A to G) of the helical architecture are clearly identified.

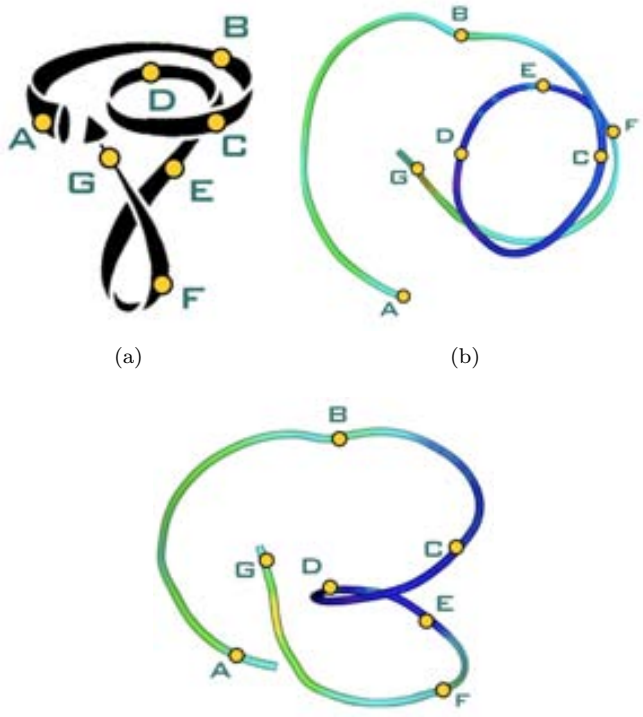

(a) (b)

(c)

Figure 5.17: Torrent-Guasp s HVMB theoretical model (a) compared to a tract reconstructed from a single manually picked seed on the DT-MRI volume with landmarks for comparison with the theoretical model. Top (b) and side (c) views.

Chapter 6

Conclusions and future work

Like statistics and statisticians, one must be skeptical of models and their makers. Models have the potential to lead reasoning, and they have the potential to mislead it as well.

John C. Crisicione, Filiberto Rodriguez, and D. Craig Miller
The Myocardial band: Simplicity can be a weakness
Letter to the Editor.
European Journal of Cardio-thoracic Surgery.
2005;28:363-4

6.1 Conclusions

The myocardium, unlike the rest of skeletal muscles, presents a complex microscopical formation. Its tissue is locally arranged in a discrete mesh of branching myocytes that have lead scientists to a vivid controversy in the comprehension of its gross architectural formation for more than 300 hundred years. There have been uncountable attempts to accurately describe this architecture of the heart from dissection or histological procedures. However, this studies have been repeatedly criticised by their lack of objectivity and reapeatibility. More recently, magnetic ressonance techniques such as Diffusion Tensor MRI have opened a new door into the study of the muscular architecture of the heart. Those techniques allow to provide a discrete characterization of the spatial arrangement of muscular cells. These techniques have been stablished as a new reference for measurement of the cardiac architecture because they usually better resolution than naked eye could achieve in a dissection procedure. Additionally, they offer a more coupled and repeatable methodology than series of destructive histological tests all over the anatomy. With this information, streamlining methodologies inherited from the study of fluids allowed to go further and retrieve fiber structure of the muscles for its visual study. However, the inherent complexity of the myocardial architecture, as well as other limitations of the methodologies to capture, reconstruct and represent this information still have not solved the controversy.

On this background, our main goal was to help cardiologists to obtain simplified, objective and validated representation of the myocardial architectecture to allow an easier interpretation of it. In order to achieve this goal, on the development of this thesis we have contributed to three main areas:

A Multi-resolution tractography

We introduced a multi-resolution schema adapted to the tractographic processing of DT-MRI to obtain simplified tractographic reconstructions. In the development of this methodology, also we studied several approaches for the generation of multi-resolution pyramids of data including basic Gaussian filtering, a novel structure preserving filter and also applying a Wavelet based solution searching for the more adequate alternatives to process DT-MRI data. Apart from that, we offered tools to achieve adequate deterministic fiber tracking techniques for the reconstruction of myoacardial data, as well as proposing new approaches for robust streamline seeding based on anatomical coherence of neighbouring biological structures. Further, we provided improvements in the visualization of anatomical structures on the muscular anatomy, including the settings to obtain effective representations of multi-resolution tractograpies that allowed to represent the power of anatomical abstraction introduced by this methodology.

B Validation framework

But all the previous developments would not be well founded without a validation methodology. We introduced a framework for the evaluation of effects of our preprocessing methodologies from low-level local anatomical structures to the geometrical evaluation of streamline reconstructions. This famework allowed us to provide comprehensive indicators of the confidence in our different approaches of construction of a multi-resolution model. Moreover, with the later geometrical evaluation methodology we also achieved confidence measures on generic tractographic reconstructions. These measures yield an important insight to evaluate anatomies both in full-scale and multi-resolution simplifications.

C Study of myocardial architecture

We have shown that this multi-resolution tractographic methodology can help to offer more abstract representations of the myocardial anatomy allowing an easier navigation and interpretation of its gross architecture. The results of those tractographic reconstructions where put in correspondence with the major theoretical approaches of myocardial architecture. In this study we showed an unequivocal ventricular fiber connectivity describing a continuous muscular structure forming the two ventricles arranged in a double helical orientation. This structure supports the Torrent-Guasp description of the HVMB.

6.2 Future work and lines of research

Further than the contributions presented by this work, we foresee the following lines of research and work that would extend our developments:

- **Broadening studies to different species and heart conditions**

  Most works relying in tractographic reconstructions of the heart muscle (including our own work) have a limited access to resources of DT-MRI data due to the current need to perform DT-MRI studies on ex-vivo specimens. In our case, data only contemplates a canine specimens. During this work we iniciated the capture of new samples to expand this study. However, going one step further, we would like to achieve a representative database including several species and cardiac conditions. In this way we would be able to study the differences across species or the remodelations of the myocardial architecture suffers from health to disease. This studies may help to elucidate solutions to current enigmas in cardiologic treatment.

- **Computations in the scale-space**

  In this work we introduced multi-scale processing as an schema to provide architectural simplifications of tractographic reconstructions. In other words, we consider levels of detail as independent representations of data. But these models can also be exploited to perform computations across scales. Handling volumes at different scales at the same time would yield even more potential of these approaches to study the most stable anatomical structures.

- **Alternative points of view of the architecture**

  Inspired by the surgical unwarping of the HVMB, we think that unwarpings of tractographies may also help the visual inspection of such a complex architecture. In combination with the techniques presented in this work, alternative geometrical projections or a parametric modelling of the anatomy may allow to further reduce the dimensional complexity of the tangled nature of the myocardium.

- **Study and improvement of streamlining methodologies**

  Deterministic tractographies constitute a simple, yet effective reconstruction methodology. However, in this thesis we have seen that some assumptions of the integration method (as interpolation to achieve continuous spaces from discrete DT-MRI) could induce negative effects on ceirtain methodologies. Further development should bring new methodologies to cope with these issues.

- **Synthetic validation**

  The foundation on the evaluation methodologies presented in this thesis is set on measuring the coherence of neighbouring anatomical structures (ranging from voxels to fibers). However, this methodology is limited to characterize noise or other capturing artifacts. The introduction of synthetic datasets as a ground truth reference would help to deepen in that study.

- **Benchmarking tractographic reconstruction**

  Another open challenge is finding better ways to compare and evaluate tractographic methodologies. The measures presented in this thesis could be reconfigured to achieve such comparisons and evaluations.

- **Multi-resolution tractographies in other disciplines**

  The tractographic methodology we present in this thesis has been tailored to fit the needs of the architectural study of the heart. However, this methodology could also able to bring interesting insight about architectural structures on other disciplines as the study of the brain or fluid mechanics.

- **From in-vivo water diffusion characterization to clinical practice**

  Recent advances on magnetic ressonance are getting closer to reach characterization of water diffusion in *in-vivo* hearts. This will open a new door of opportunities in the applicability of tractographic reconstructions. In this environment, measures of confidence in the reconstructed fiber tracts will be of upmost importance in order to introduce tractographic reconstructions of the myocardium into the clinical practice.

- **From in-vivo water diffusion characterization to computer assisted intervention**

  Further than introducing these methodologies intro clinical practice, we can also think on specially interesting future applications. For instance, the augmentation superimposition of tractographic visualizations over real organs in order to provide computer assisted intervention for practitioners performing heart surgery.

Publications

Journals

- **F. Poveda**, D. Gil, E. Martí-Godia, A. Andaluz, M. Ballester, F. Carreras. Helical Structure of the Cardiac Ventricular Anatomy Assessed by Diffusion Tensor Magnetic Resonance Imaging Multi-Resolution Tractography. *Revista Española de Cardiología.*, To be published in October s issue, 2013.

- **F. Poveda**, D. Gil, E. Martí-Godia, M. Ballester, F. Carreras. Helical structure of ventricular anatomy by diffusion tensor cardiac MR tractography. *Journal of the American College of Cardiology: Cardiovascular Imaging*, 5(7):754-5, 2012.

Congress Contributions

- **F. Poveda**, D. Gil, E. Martí-Godia. Multi-resolution DT-MRI Cardiac Tractography. In book *Statistical Atlases and Computational Models of the Heart. Imaging and Modelling Challenges. International Conference on Medical Image Computing and Computer Assisted Intervention (MICCAI)*, 270-277, 2013.

- **F. Poveda**, D. Gil, T. Gurguí, E. Martí-Godia. Multi-resolution myocardial architecture study. In proceedings of *Congreso Español de Informática Gráfica*. 165-6, 2012.

- A. Hidalgo, **F. Poveda**, D. Gil, Enric Martí-Godia, M. Ballester, F. Carreras. Evidence of continuous helical structure of the cardiac ventricular anatomy assessed by diffusion tensor imaging magnetic resonance multiresolution tractography. In proceedings of *European Congress of Radiology: Insight into Imaging (Suppl. 1)*, 361-362, 2012.

- **F. Poveda**, D. Gil, A. Andaluz, E. Martí-Godia. Multiscale Tractography for Representing Heart Muscular Architecture. In proceerings of *Workshop on Computational Diffusion MRI, International Conference on Medical Image Computing and Computer Assisted Intervention (MICCAI)*, 2011.

- D. Gil, A. Borras, M. Ballester, F. Carreras, R. Aris, M. Vazquez, E. Martí-Godia, **F. Poveda**. MIOCARDIA: Integrating cardiac function and muscular

architecture for a better diagnosis. In proceedings of *14th International Symposium on Applied Sciences in Biomedical and Communication Technologies*, 2011.

- **F. Poveda**, J. Garcia-Barnés, D. Gil, E. Martí-Godia. Validation of the myocardial architecture in DT-MRI tractography. In proceedings of *Medical Image Computing in Catalunya: Graduate Student Workshop*, 29-30, 2010.

- **F. Poveda**, J. Garcia-Barnés, D. Gil, E. Martí-Godia. Heart structure study from DT-MRI tractography. *Achievements and New Opportunities in Computer Vision. CVC Workshop. CVCRD*, 2010.

Other contributions

- Cover image in the *Journal of the American College of Cardiology: Cardiovascular Imaging*, 5(7), 2012.

- Video-interview as the article of the month for the *Revista Española de Cardiología.*, To be published in October s issue, 2013.

Bibliography

[1] World health organization website.

[2] Juan Cosin Aguilar and Amparo Hernandiz Martinez. The band arrangement of myocardial fibres determines cardiac morphology and function. *Revista Española de Cardiologia*, 2013.

[3] D. C. Alexander, J. Gee, and Bajcsy R. Similarity measures for match- ing diffusion tensor images. In *British Machine Vision Conference BMVC99*, pages 93 102, 1999.

[4] R Anderson, S Ho, K Redmann, D Sanchez-Quintana, and Paul P Lunkenheimer. The anatomical arrangement of the myocardial cells making up the ventricular mass. *European journal of Cardiothoracic surgery*, 28(4):517 525, Oct 2005.

[5] R Anderson, M Smerup, D Sanchez-Quintana, M Loukas, and PP Lunkernheimer. The three-dimensional arrangement of the myocytes in the ventricular walls. *Clinical Anatomy*, 22:64 76, Jan 2009.

[6] ROBERT H. ANDERSON, SIEW YEN HO, DAMIAN SANCHEZ-QUINTANA, KLAUS REDMANN, and PAUL P. LUNKENHEIMER. Heuristic problems in defining the three-dimensional arrangement of the ventricular myocytes. *The Anatomical Record Part A: Discoveries in Molecular, Cellular, and Evolutionary Biology*, 288(6):579 587, 2006.

[7] P Basser, S Pajevic, C Pierpaoli, and J Duda. In vivo fiber tractography using dt-mri data. *Magnetic Resonance in Medicine*, 44(4):625 632, Oct 2000.

[8] R.V. Batista, J.L. Santos, N Takeshita, L Bocchino, P.N. Lima, and M.A. Cuhna. Partial left ventriculectomy to improve left ventricular function in endstage heart. *J Card Surg*, 11:96 97, 1996.

[9] T.E.J. Behrens, H. Johansen Berg, S. Jbabdi, Rushworth, and M.W. Woolrich. Probabilistic diffusion tractography with multiple fibre orientations: What can we gain? *NeuroImage*, 34:144 155, 2007.

[10] A. Bjorck. *Numerical Methods for Least Squares Problems.* SIAM, 1996.

[11] R. Brecheisen, B. Platel, B.M. Haar Romeny, and A. Vilanova. Illustrative uncertainty visualization of dti fiber pathways. *The Visual Computer*, 29(4):297 309, 2013.

[12] Gerald D. Buckberg. Nature is simple, but scientists are complicated. *European Journal of Cardio-thoracic Surgery*, 28:358 367, 2005.

[13] Gerald D Buckberg, Aman Mahajan, Bernd Jung, Michael Markl, Juergen Hennig, and Manel Ballester-Rodes. Mri myocardial motion and fiber tracking: a confirmation of knowledge from different imaging modalities. *European journal of cardio-thoracic surgery : official journal of the European Association for Cardio-thoracic Surgery*, 29(1):S165 77, Apr 2006.

[14] P Burt. Fast filter transform for image processing. *Computer Graphics and Image Processing*, 16(1):20 51, May 1981.

[15] Francesc Carreras, Manel Ballester, Sandra Pujadas, Ruben Leta, and Guillem Pons-Llado. Morphological and functional evidences of the helical heart from non-invasive cardiac imaging. *European journal of cardio-thoracic surgery : official journal of the European Association for Cardio-thoracic Surgery*, 29 Suppl 1:S50 5, Apr 2006.

[16] Francesc Carreras, Manel Ballester, Sandra Pujadas, Ruben Leta, and Guillem Pons-Llado. Morphological and functional evidences of the helical heart from non-invasive cardiac imaging. *Journal of Cardio-Thoracic Surgery*, 29(S):S50 S55, 2006.

[17] P.S. CHEN, Y.M. CHA, B.B. PETERS, and L.S. CHEN. Effects of myocardial fiber orientation on the electrical induction of ventricular fibrillation. *Am J Physiol*, 264:H1760 H1773, 1993.

[18] Wei Chen, Zi ang Ding, Song Zhang, A. MacKay-Brandt, S. Correia, Huamin Qu, J.A. Crow, D.F. Tate, Zhicheng Yan, and Qunsheng Peng. A novel interface for interactive exploration of dti fibers. *IEEE Trans Vis Comp Gra*, 15(6):1433 1440, Dec 2009.

[19] John B. Colby, Lindsay Soderberg, Catherine Lebel, vo D. Dinov, Paul M. Thompson, and Elizabeth R. Sowell. Along-tract statistics allow for enhanced tractography analysis. *NeuroImage*, 59:3227 3242, 2012.

[20] Isabelle Corouge, P. Thomas Fletcher, Sarang Joshi, Sylvain Gouttard, and Guido Gerig. Fiber tract-oriented statistics for quantitative diffusion tensor mri analysis. *Medical Image Analysis*, 10(5):786 798, Oct 2006.

[21] Kevin D. Costa, Yasuo Takayama, Andrew D. McCulloch, and James W. Covell. Laminar fiber architecture and three-dimensional systolic mechanics in canine ventricular myocardium. *Am J Physiol Heart Circ Physiol*, 276:H595 H607, 1999.

[22] John C. Criscione, Filiberto Rodriguez, and D. Craig Miller. The myocardial band: simplicity can be a weakness. *European Journal of Cardio-thoracic Surgery*, 28:358 367, 2005.

[23] J. Dejerine and A. Dejerine-Klumpke. *Anatomie des centres nerveux*. 1895.

[24] Zhaohua Ding, John C. Gore, and Adam W. Anderson. Case study: reconstruction, visualization and quantification of neuronal fiber pathways. In *Proceedings of the conference on Visualization '01*, VIS 01, pages 453 456, Washington, DC, USA, 2001. IEEE Computer Society.

[25] Frank Enders, Natasha Sauber, Dorit Merhof, Peter Hastreiter, Christopher Nimsky, and Marc Stamminger. Visualization of white matter tracts with wrapped streamlines. *IEEE Visualization*, pages 51 58, 2005.

[26] Eurostat. Health statistics.

[27] LC. Evans. *Partial Differential Equations*. Berkeley Math. Lect. Notes, 1993.

[28] F Torrent-Guasp F, M.J. Kocica, A Corno, M Komeda, J Cox, A Flotats, M Ballester-Rodes, and F Carreras-Costa. Systolic ventricular filling. *Eur J Cardiothorac Surg*, 25(3):376 386, 2004.

[29] F. Torrent-Guasp. *Anatomia Funcional del Corazón, La actividad ventricular diastólica y sistólica*, pages 62 68. Paz Montalvo, 1957.

[30] Erwin Fehlberg. Klassische runge-kutta-formeln vierter und niedrigerer ordnung mit schrittweiten-kontrolle und ihre anwendung auf warmeleitungsprobleme. *Computing (Arch. Elektron. Rechnen)*, 6:61 71, 1970.

[31] A Filler, J Tsurda, T Richards, and F Howe. Image neurography and diffusion anisotropy imaging. *US Patent 5,560,360*, Oct 1996.

[32] O Friman, G Farneback, and C.F. Westin. A bayesian approach for stochastic white matter tractography. *IEEE Transactions on Medical Imaging*, 25:965 978, 2006.

[33] C Frindel, J Schaerer, P Gueth, P Clarysse, Yue-Min Zhu, and M Robini. A global approach to cardiac tractography. *Biomedical Imaging: From Nano to Macro, 2008. ISBI 2008. 5th IEEE International Symposium on*, pages 883 886, Apr 2008.

[34] Changqing Gao, Kun Lu, Weihua Ye, Libing Li, and Liuquan Cheng. Reconstruction of the architecture of ventricular myocardial fibers in ex vivo human hearts. *The heart surgery forum*, 12(4):E225 9, Aug 2009.

[35] Changqing Gao, Weihua Ye, Libing Li, Tao Zhang, Chonglei Ren, Liuquan Cheng, and Junlan Yan. Investigation on the structure of ventricular mass using magnetic resonance diffusion tensor imaging. *The heart surgery forum*, 12(2):E85 9, Apr 2009.

[36] D. Gil, A. Hernandez-Sabate, M. Brunat, S. Jansen, and J. Martínez-Vilalta. Structure-preserving smoothing of biomedical images. *Pat. Rec.*, 44(9):1842 1851, 2010.

[37] Debora Gil, Jaume Garcia-Barnés, Aura Hernández-Sabaté, and Enric Martí. Manifold parameterization of the left lentricle for a statistical modeling of its complete anatomy. *Proceedings of the SPIE*, 7623:762304 762304 9, 2010.

[38] Stephen H. Gilbert, David Benoist, Alan P. Benson, Ed White, Steven F. Tanner, Arun V. Holden, Halina Dobrzynski, Olivier Bernus, and Aleksandra Radjenovic. Visualization and quantification of whole rat heart laminar structure using high-spatial resolution. *Am J Physiol Heart Circ Physiol*, 302:H287 H298, 2012.

[39] C Golgi. Sulla struttura della sostanza grigia del cervello. *Gazzetta Medica Italiana*, 33:244 246, 1873.

[40] Sylvain Gouttard, Casey B. Goodlett, Marek Kubicki, and Guido Gerig. Measures for validation of dti tractography. *Proc. SPIE 8314 Medical Imaging 2012: Image Processing*, Feb 2012.

[41] Robert Alan Granger. *Fluid mechanics*. Courier Dover Publications, Jan 1995.

[42] R P Grant. Notes on the muscular architecture of the left ventricle. *Circulation*, 32:301 8, Aug 1965.

[43] H. Gray and W.H. Lewis. *Anatomy of the Human Body*. Lea & Febiger, 1918.

[44] R A Greenbaum, SY Ho, DG Gibson, AE Becker, and RH Anderson. Left ventricular fibre architecture in man. *Br Heart J*, 45:248 63, 1981.

[45] M Grene. *Essays on the Philosophy and Science of René Descartes*, chapter The Heart and Blood: Descartes, Plemp, and Harvey. Oxford University Press, 1993.

[46] A. F. Grimm, K. V. Katele, and H.-L. Lin. Fiber bundle direction in the mammalian heart: an extension of the nested shells model. *Basic Res. Cardiol.*, (381-388), 1976.

[47] Francisco Torrent Guasp. La mecánica agonista-antagonista de los segmentos descendente y ascendente de la banda miocárdica ventricular. *Rev Esp Cardiol*, 54:1091 1102, 2001.

[48] KB Harrington, F Rodriguez, A Cheng, F Langer, Ashikaga H, GT Daughters, JC Criscione, NB Ingels, and DC Miller. Direct measurement of transmural laminar architecture in the anterolateral wall of the ovine left ventricle: new implications for wall thickening mechanics. *Am J Physiol Heart Circ Physiol*, 2588:H1324 H130, 2005.

[49] Tal Hasin, Yariv Gerber, Sheila M. McNallan, Susan A. Weston, Sudhir S. Kushwaha, Timothy J. Nelson, James R. Cerhan, and Veronique L. Roger. Patients with heart failure have an increased risk of incident cancer. *J Am Coll Cardiol*, 62(10):881 886, Sept 2013.

[50] Patrick Helm. *A Novel Technique for Quantifying Variability of Cardiac Anatomy: Application to the Dyssynchronous Failing Heart*. PhD thesis, Johns Hopkins University, Baltimore, Maryland, 2005.

[51] Patrick Helm, Mirza Faisal Beg, Michael I Miller, and Raimond L Winslow. Measuring and mapping cardiac fiber and laminar architecture using diffusion tensor mr imaging. *Ann N Y Acad Sci*, 1047:296 307, Jun 2005.

[52] Patrick A Helm, Hsiang-Jer Tseng, Laurent Younes, Elliot R McVeigh, and Raimond L Winslow. Ex vivo 3d diffusion tensor imaging and quantification of cardiac laminar structure. *Magnetic resonance in medicine : official journal of the Society of Magnetic Resonance in Medicine / Society of Magnetic Resonance in Medicine*, 54(4):850 9, Oct 2005.

[53] P. Hermosilla, R. Brecheisen, P.P. Vázquez, and A. Vilanova. Uncertainty visualization of brain fibers. In The Eurographics Association, editor, *CEIG: Spanish Computer Graphics Conference*, pages 31 40, 2012.

[54] A. Alexander Holmes, D.F. Scollan, and Raimond L. Winslow. Direct histological validation of diffusion tensor mri in formaldehyde-fixed myocardium. *Magnetic Resonance in Medicine*, 44:157 161, 2000.

[55] Hugues Hoppe. Efficient implementation of progressive meshes. Technical report, Microsoft Research, 1998.

[56] Debora il, Agnés Borràs, Ruth Aris, Mariano Vázquez, Pierre Lafortune, Guillaume Houzeaux, Jazmin Aguado, Manel Ballester, Chi Hion Li, and Francesc Carreras. What a difference in biomechanics cardiac fiber makes. In *Statistical Atlases and Computational Models of the Heart. Imaging and Modelling Challenges*, pages 253 260. Springer, 2013.

[57] Instituto Nacional de Estadística. Defunciones según la causa de muerte.

[58] R C Robb J S Robb. he normal heart. anatomy and physiology of the structural units. *Am Heart J*, 23:455 67, 1942.

[59] Fangxiang Jiao, Jeff M. Phillips, Jeroen Stinstra, Jens Kruger, Raj Varma, Edward Hsu, Julie Korenberg, and Chris R. Johnson. Metrics for uncertainty analysis and visualization of diffusion tensor images. In Lecture Notes of Computer Science, editor, *Medical Imaging Augmented Reality 2010*, volume 6326, pages 179 190. Springer, 2010.

[60] Heidi Johansen-Berg and Timothy E. J. Behrens. Just pretty pictures? what diffusion tractography can add in clinical neuroscience. *Curr Opin Neurol*, 2006.

[61] Johns Hopkins University. Public dtmri dataset. http://gforge.icm.jhu.edu/gf/project/dtmri_data_sets/, January 2011.

[62] D Jones. robabilistic fibre track- ing using the wild bootstrap with diffusion tensor mri. *IEEE Transactions on Medical Imaging*, 27:1268 1274, 2008.

[63] K.D. Keele. Leonardo da vinci, and the movement of the heart. *Proc R Soc Med*, 44(3):209 213, March 1951.

[64] Gordon Kindlmann. Superquadric tensor shapes. In O Deussen, C. Hansen, D.A. Keim, and D. Saupe, editors, *Joint Eurographics - IEEE TCVG Symposium on Visualization*, 2004.

[65] Mladen J Kocica, Antonio F Corno, Francesc Carreras-Costa, Manel Ballester-Rodes, Mark C Moghbel, Clotario N C Cueva, Vesna Lackovic, Vladimir I Kanjuh, and Francisco Torrent-Guasp. The helical ventricular myocardial band: global, three-dimensional, functional architecture of the ventricular myocardium. *European journal of cardio-thoracic surgery : official journal of the European Association for Cardio-thoracic Surgery*, 29 Suppl 1:S21 40, Apr 2006.

[66] L Krehl. Beitrage zur kenntnis der fullung und entleerung des herzens. *Abhandlungen der Mathematisch-Physischen Classe der Königlich Sächsischen Gesellschaft der Wissenschaften*, (17):340 374, 1891.

[67] M. Lazar and A. L. Alexander. White matter tractography using random vector (rave) perturbation. In *Proc. Intl. Soc. Mag. Reson. Med.*, 2002.

[68] I.J. LeGrice, Y. Takayama, and J.W. Covell. Transverse shear along myocardial cleavage planes provides a mechanism for normal systolic wall thickening. *Circ.*, 77:182 193, 1995.

[69] Karim Lekadir, Babak Ghafaryasl, Emma Munoz-Moreno, Constantine Butakoff, Corné Hoogendoorn, and Alejandro F. Frangi. Predictive modeling of cardiac fiber orientation using the knutsson mapping. In *Medical Image Computing and Computer-Assisted Intervention - MICCAI 2011*, pages 50 57, 2011.

[70] M Lev and C Simkins. Architecture of the human ventricular myocardium; technic for study using a modification of the mall-maccallum method. *Laboratory investigation*, 5(5):396 409, 1956.

[71] D. Loeckx, P. Slagmolen, F. Maes, D. Vandermeulen, and P. Suetens. Nonrigid image registration using conditional mutual information. *IEEE Transactions on Medical Imaging*, 29(1):19 29, Jan 2010.

[72] Herve Lombaert, Jean Marc Peyrat, Pierre Croisille, Stanislas Rapacchi, Laurent Fanton, Patrick Clarysse, Herve Delingette, and Nicholas Ayache. Statistical analysis of the human cardiac fiber architecture from dt-mri. *Proceedings of the 6th international conference on FIMH*, pages 171 179, 2011.

[73] Richard Lower. *Tractatus de Corde: Item de Motu Et Colore Sanguinis et chyli in eum transitu*. apud Danielem Elzevirium, 1669.

[74] Paul P. Lunkenheimer, Peter Niederer, Damian Sanchez-Quintana, Margarita Murillo, and Morten Smerup. Models of ventricular structure and function reviewed for clinical cardiologists. *J. of Cardiovasc. Trans. Res*, 6:176 186, 2013.

[75] Paul P. Lunkenheimer, Klaus Redmann, and Robert H. Anderson. Reply to criscione et al. *European Journal of Cardio-thoracic Surgery*, 28:358 367, 2005.

[76] Bertini M, Sengupta PP, and Nucifora G. Role of left ventricular twist mechanics in the assessment of cardiac dyssynchrony in heart failure. *J Am Coll Cardiol Img*, 2(12):1425 1435, 2009.

[77] J. Partridge M. Smerupa, , P. Agger, S. Ringgaard, M. Pedersen, S. Petersen, J.M. Hasenkam, P. Niederer, P.P. Lunkenheimer, and R.H. Anderson. A mathematical model of the mechanical link between shortening of the cardiomyocytes and systolic deformation of the left ventricular myocardium. *Technology and Health Care*, 21:63 79, 2013.

[78] J. B. MacQueen. Some methods for classification and analysis of multivariate observations. *Proceedings of 5-th Berkeley Symposium on Mathematical Statistics and Probability*, 1:281 297, 1967.

[79] Mahnaz Maddah, W.Eric L. Grimson, and Simon K. Warfield. Statistical modeling and em clustering of white matter fiber tracts. In *IEEE Intl Symp on Biomedical Imaging ISBI*, pages 53 56, 2006.

[80] Franklin P Mall. On the muscular architecture of the ventricles of the human heart. *American Journal of Anatomy*, 11(3):211 266, Jan 1911.

[81] J. Marcé-Nogué, G. Fortuny, M. Ballester-Rodés, F. Carreras, and F. Roure. Computational modeling of electromechanical propagation in the helical ventricular anatomy of the heart. *Computers in Biology and Medicine*, 43(11):1698 1703, 2013.

[82] Tony McLoughlin, Mark W. Jones, Robert S. Laramee, Rami Malki, Ian Masters, and Charles D. Hansen. Similarity measures for enhancing interactive streamline seeding. *IEEE Trans Vis Comp Gra*, 19(8):1342 1353, Aug 2012.

[83] Choukri Mekkaoui, Shuning Huang, Howard H Chen, Guangping Dai, Timothy G Reese, William J Kostis, Aravinda Thiagalingam, Pal Maurovich-Horvat, Jeremy N Ruskin, Udo Hoffmann, Marcel P Jackowski, and David E Sosnovik. Fiber architecture in remodeled myocardium revealed with a quantitative diffusion cmr tractography framework and histological validation. *J Cardiovasc Magn Reson*, 14(70), 2012.

[84] B Moberts, A Vilanova, and J.J van Wijk. Evaluation of fiber clustering methods for diffusion tensor imaging. *IEEE Visualization*, pages 65 72, Oct 2005.

[85] M E Moseley, Y Cohen, J Kucharczyk, J Mintorovitch, H S Asgari, M F Wendland, J Tsuruda, and D Norman. Diffusion-weighted mr imaging of anisotropic

water diffusion in cat central nervous system. *Radiology*, 176(2):439 45, Aug 1990.

[86] Abbas Nasiraei-Moghaddam and Morteza Gharib. Evidence for the existence of a functional helical myocardial band. *Am J Physiol Heart Circ Physiol*, 296:H127 H131, 2009.

[87] P. M. F. Nielsen, I. J. LeGrice, B. H. Smaill, and P. J. Hunter. Mathematical model of geometry and fibrous structure of the heart. *Am J Physiol*, 260:H1365 H1378, 1991.

[88] Emma Mu noz Moreno, Rube n Cárdenes, and Alejandro F. Frangi. Analysis of the helix and transverse angles of the muscle fibers in the myocardium based on diffusion tensor imaging. In *32nd Annual International Conference of the IEEE EMBS*, pages 5720 5723, Sept 2010.

[89] L J O Donnell, M Kubicki, M E Shenton, M H Dreusicke, W E L Grimson, and C F Westin. A method for clustering white matter fiber tracts. *AJNR Am J Neuroradiol*, 27(5):1032 6, 2006.

[90] Lauren J O Donnell, Carl-Fredrik Westin, and Alexandra J Golby. Tract-based morphometry for white matter group analysis. *NeuroImage*, 45(3):832 844, 2009.

[91] Sudhir Pathak. Brain art competition 2012 contestant, 2012.

[92] T Peeters, A Vilanova, G Strijkerst, and B ter Haar Romeny. Visualization of the fibrous structure of the heart. *Vision, modelling and visualization*, pages 309 316, 2006.

[93] J B Pettigrew. Structure of the heart of mammal. *Design in Nature, Longmans Green & Co.*, pages 506 18, 1908.

[94] J M Peyrat, M Sermesant, X Pennec, H Delingette, C Xu, E McVeigh, and N Ayache. A computational framework for the statistical analysis of cardiac diffusion tensors: Application to a small database of canine hearts. *IEEE Transactions on Medical Imaging*, 26(11):1500, Nov 2007.

[95] Basser PJ and Pierpaoli C. Microstructural and physiological features of tissues elucidated by quantitative-diffusion-tensor mri. *J Magn Reson*, 213(2):560 570, 1996.

[96] William H. Press, Saul A. Teukolsky, William T. Vetterling, and Brian P. Flannery. *Numerical Recipes 3rd Edition: The Art of Scientific Computing*. Cambridge University Press, New York, NY, USA, 2007.

[97] D.E. Roberts, L.T. Hersh, and A.M. Scher. Influence of cardiac fiber orientation on wavefront voltage, conduction velocity, and tissue resistivity in the dog. *Circ. Res.*, 44:701 712, 1979.

[98] Paulo Rodrigues. *Homogeneity based segmentation and enhancement of Diffusion Tensor Images: A white matter processing framework*. PhD thesis, Technische Universiteit Eindhoven, 2011.

[99] D Rohmer, A Sitek, and G Gullberg. Reconstruction and visualization of fiber and laminar structure in the normal human heart from ex vivo diffusion tensor magnetic resonance imaging (dtmri) data. *Investigative Radiology*, 42(11):777 789, Nov 2007.

[100] A. Rosenfeld and J. Pfalt. Distance functions on digital pictures. *Pattern Recognition*, 1(1):33 61, 1968.

[101] Marc D. Samsky, Chetan B. Patel, Tracy A. DeWald, Alastair D. Smith, G. Michael Felker, Joseph G. Rogers, and Adrian F. Hernandez. Cardiohepatic interactions in heart failure. *Journal of the American College of Cardiology*, 61(24):2397 2405, June 2013.

[102] Peter Savadjiev, Yogesh Rathi, Sylvain Bouix, Ragini Verma, and Carl-Fredrik Westin. Multi-scale characterization of white matter tract geometry. In *Medical Image Computing and Computer-Assisted Intervention–MICCAI 2012*, pages 34 41. Springer Berlin Heidelberg, 2012.

[103] Peter Schmid, Thomas Jaermann, Peter Boesiger, Peter F Niederer, Paul P Lunkenheimer, Colin W Cryer, and Robert H Anderson. Ventricular myocardial architecture as visualised in postmortem swine hearts using magnetic resonance diffusion tensor imaging. *European journal of cardio-thoracic surgery : official journal of the European Association for Cardio-thoracic Surgery*, 27(3):468 72, Mar 2005.

[104] T. Schultz, N. Sauber, A. Arwander, H. Theisel, and H.P. Seidel. Virtual klingler dissection: Putting fibers into context. *Computer Graphics Forum*, 27:1063 1070, 2008.

[105] D F Scollan, A Holmes, R Winslow, and J Forder. Histological validation of myocardial microstructure obtained from diffusion tensor magnetic resonance imaging. *Am J Physiol*, 275(6 Pt 2):H2308 18, Dec 1998.

[106] David Francis Scollan. *Reconstructing the heart: Development and application of biophysically-based electrical models of propagation in ventricular myocardium reconstructed from Diffusion Tensor MRI*. PhD thesis, Johns Hopkins University, Baltimore, Maryland, 2002.

[107] Jean Baptiste Sénac. *Traité de la structure du coeur, de son action et de ses maladies*. chez Briasson, 1749.

[108] David E Sosnovik, Ruopeng Wang, Guangping Dai, Timothy G Reese, and Van J Wedeen. Diffusion mr tractography of the heart. *J Cardiovasc Magn Reson*, 11(47), 2009.

[109] Daniel D. Streeter, Walter E Powers, and F Torrent-Guasp. Three-dimensional fiber orientation in the mammalian left ventricular wall. *Cardiovascular System Dynamics*, pages 73 84, 1978.

[110] Daniel D. Streeter, Henry M. Spotnitz, Dali P. Patel, John Ross, and Edmund H. Sonnenblick. Fiber orientation in the canine left ventricle during diastole and systole. *Circulation Research*, 24:339 347, 1969.

[111] D.D. Streeter. Gross morphology and fibre geometry of the heart. *The cardiovascular system.*, pages 61 112, 1979.

[112] B. Taccardi, R.L. Lux E. Macchi, and P.R. Ershler. Effect of myocardial fiber direction on epicardial potentials. *Circulation*, 90:3076 3090, 1994.

[113] F. Tezuka. Muscle fiber orientation in normal and hypertrophied hearts. *Tohoku J. Exp. Med.*, 117:289 297, 1975.

[114] F Torrent-Guasp. El ciclo cardiaco: Consideraciones críticas sobre la interpretación clásica y nuevas ideas sobre el mismo. *Diana, Madrid*, 1954.

[115] F Torrent-Guasp, Manel Ballester, Gerald D Buckberg, F. Carreras, A Flotats, I Carrio, A Ferreira, LE Samuels, and J Narula. Spatial orientation of the ventricular muscle band: physiologic contribution and surgical implications. *Journal of Thoracic and Cardiovascular Surgery*, (122):389 392, Aug 2001.

[116] F. Torrent-Guasp, J.M. Caralps-Riera, and M. Ballester. Cuatro propuestas para la remodelación ventricular en el tratamiento quirúrgico de la miocardiopatía dilatada. *Rev Esp Cardiol*, 1997.

[117] F F Torrent-Guasp, W F Whimster, and K Redmann. A silicone rubber mould of the heart. *Technol Health Care*, 5(1-2):13 20, Apr 1997.

[118] Francisco Torrent-Guasp, Mladen J Kocica, Antonio F Corno, Masashi Komeda, Francesc Carreras-Costa, A Flotats, Juan Cosin-Aguillar, and Han Wen. Towards new understanding of the heart structure and function. *European journal of cardio-thoracic surgery*, 27(2):191 201, Feb 2005.

[119] W Tseng, T Reese, and R Weisskoff .... Cardiac diffusion tensor mri in vivo without strain correction. *Magnetic ...*, Jan 1999.

[120] David S. Tuch, Timothy G. Reese, Mette R. Wiegell, Nikos Makris, John W. Belliveau, and Van J. Wedeen. High angular resolution diffusion imaging reveals intravoxel white matter fiber heterogeneity. *Magnetic Resonance in Medicine*, 48:577 582, 2002.

[121] M. Vázquez, R. Arís, G. Houzeaux, R. Aubry, P. Villar, J. Garcia-Barnés, D. Gil, and F. Carreras. A massively parallel computational electrophisiology model of the heart. *Int J Numer Meth Biomed Engng*, pages 1 32, 2010.

[122] C.-F. Westin, S. Peled, H. Gudbjartsson, R. Kikinis, and F. A. Jolesz. Geometrical diffusion measures for mri from tensor basis analysis. In *International Society for Magnetic Resonance in Medicine*, page 1742, Apr 1997.

[123] Lance Williams. Pyramidal parametrics. *Proceedings of SIGGRAPH*, 17(3):1 11, Jul 1983.

[124] Ramón y Cajal. *Textura del Sistema Nervioso del Hombre y de los Vertebrados.* Moya, Madrid, 1899.

[125] L Zhukov and A Barr. Heart-muscle fiber reconstruction from diffusion tensor mri. *Visualization, 2003. VIS 2003. IEEE*, pages 597 602, 2003.